LA-UR- 95-1785

Title: **INTERMEDIATE-BREAK LOCA ANALYSES FOR THE AP600 DESIGN**

Author(s): **B. E. Boyack**
J. F. Lime

Submitted to: **Frank Odar**
NRC

Los Alamos
NATIONAL LABORATORY

Form No. 836 R5
ST 2629 10/91

INTERMEDIATE-BREAK LOCA ANALYSES FOR THE AP600 DESIGN

B. E. Boyack and J. F. Lime
Los Alamos National Laboratory
Los Alamos, New Mexico 87545

CONTENTS

TABLES

FIGURES

NOMENCLATURE

1D	One dimensional
3D	Three dimensional
ACC	Accumulator
ACC-A	Accumulator connected to broken direct vessel injection line A
ACC-B	Accumulator connected to intact direct vessel injection line B
ADS	Automatic depressurization system
CMT	Core makeup tank
CMT-A	Core makeup tank connected to direct vessel injection line A
CMT-B	Core makeup tank connected to direct vessel injection line B
Cold Leg 1A	CL-1A
Cold Leg 1B	CL-1B
Cold Leg 2A	CL-2A
Cold Leg 2B	CL-2B
CV	Control valve
DEGB	Double-ended guillotine break
DVI	Direct vessel injection
DVI-A	Direct vessel injection line A
DVI-B	Direct vessel injection line B
ECC	Emergency core coolant
ECCS	Emergency core coolant system
Hot Leg 1	HL-1
Hot Leg 2	HL-2
IBLOCA	Intermediate-break loss-of-coolant accident
IRWST	In-containment refueling water storage tank
JAERI	Japan Atomic Energy Research Institute
LBLOCA	Large-break loss-of-coolant accident
LSTF	Large Scale Test Facility
NRC	United States Nuclear Regulatory Commission
PBL-A	Pressure balance line connected to cold-leg A
PBL-B	Pressure balance line connected to cold-leg B
PCCS	Passive containment cooling system
PRHRS	Passive residual heat removal system
PSIS	Passive safety injection system
PWR	Pressurized water reactor
RCP	Reactor coolant pump
RCS	Reactor coolant system
ROSA	Rig of Safety Assessment, AP600 integral test facility, Japan
S	Safeguards
SBLOCA	Small-break loss-of-coolant accident
Steam Generator 1	SG-1
Steam Generator 2	SG-2

INTERMEDIATE-BREAK LOCA ANALYSES FOR THE AP600 DESIGN*

B. E. Boyack and J. F. Lime
Los Alamos National Laboratory
Los Alamos, New Mexico 87545

ABSTRACT

A postulated double-ended guillotine break of a direct-vessel-injection line in an AP600 plant has been analyzed. This event is characterized as an intermediate-break loss-of-coolant accident (IBLOCA). Most of the insights regarding the response of the AP600 safety systems to the postulated accident are derived from calculations performed with the TRAC-PF1/MOD2 code. However, complementary insights derived from a scaled experiment conducted in the ROSA facility, as well as insights based upon calculations by other codes, are also presented. The key processes occurring in an AP600 during a IBLOCA are primary coolant system depressurization, inventory depletion, inventory replacement via emergency core coolant injection, continuous core cooling, and long-term decay heat rejection to the atmosphere. Based upon the calculated and experimental results, the AP600 will not experience a core heat up and will reach a safe shutdown state using only safety-class equipment. Only the early part of the long-term cooling period initiated by In-containment Refueling Water Storage Tank injection was evaluated. Thus, the observation that the core is continuously cooled should be verified for the latter phase of the long-term cooling period, the interval when sump injection and containment cooling processes are important.

EXECUTIVE SUMMARY

The AP600 is an advanced passive 600 MWe reactor design being developed by Westinghouse in conjunction with the US Department of Energy's Advanced Light Water Reactor Technology Program. The AP600 has been submitted to the United States Nuclear Regulatory Commission for design certification. In accordance with the design certification requirements of 10CFR52.47, advanced reactor applicants are required to submit neutronic and thermal-hydraulic safety analyses over a sufficient range of normal operation, transient conditions, and specified accident sequences.

A postulated double-ended guillotine break of a direct-vessel-injection (DVI) line in an AP600 plant has been analyzed. This event is characterized as an intermediate-break loss-of-coolant accident (IBLOCA). The postulated break disables one-half of the passive safety injection capacity of the AP600. The assumed break location is the nozzle joining one DVI line to the reactor vessel. The parameters of the TRAC calculation have been specified such that the calculation is a direct counterpart of a safety analysis calculation reported by Westinghouse. The Westinghouse code used for the calculation was NOTRUMP.

* This work was funded by the US Nuclear Regulatory Commission's Office of Nuclear Regulatory Research.

Most of the detailed insights regarding the response of the AP600 safety systems to the postulated IBLOCA are derived from calculations performed with the TRAC-PF1/MOD2 code. However, complementary insights derived from an IBLOCA experiment conducted in the ROSA facility, as well as insights based upon calculations by other codes, are also presented.

The TRAC code series was developed at Los Alamos to provide advanced, best-estimate predictions for postulated accidents in pressurized-water reactors. The TRAC model of the AP600 is finely-noded and contains 184 hydrodynamic components. The reactor vessel and In-containment Refueling Water Storage Tank (IRWST) are modeled with a total of three multidimensional components containing 1136 computational fluid cells. The remainder of the AP600 is modeled using 181 one-dimensional components containing 990 computational fluid cells. The plant model has undergone an independent quality-assurance check. The plant model reflects the AP600 design information available on November 15, 1994.

The key processes occurring in an AP600 during a IBLOCA are primary coolant system depressurization, inventory depletion, inventory replacement via emergency core coolant injection, maintenance of continuous core cooling, and long-term decay heat rejection to the atmosphere. With due consideration for these key processes, four periods have been selected to characterize the AP600 IBLOCA transient: (1) break-dominated depressurization, (2) depressurization via automatic depressurization system (ADS) discharge to the IRWST, (3) depressurization via ADS discharge to the containment, and (4) long-term cooling. The code calculation was terminated at the start of the long-term cooling period.

The first period of this transient is an interval of *break-dominated depressurization* initiated by a double-ended guillotine break in one of the two DVI lines. The reactor coolant system initially depressurizes rapidly as mass and energy are lost through the break, but the depressurization slows and then stalls as coolant flashes to vapor. The break dominated depressurization period ends when first-stage ADS is activated after the core makeup tank attached to the broken DVI line has drained sufficient inventory to generate the ADS actuation signal.

The second period is characterized by *depressurization via ADS discharge to the IRWST*. The period begins when the first-stage ADS is actuated and concludes when the fourth-stage is actuated, opening a controlled discharge path between the reactor cooling system and the containment. Opening the first-stage ADS, even with one train inoperable, discharges sufficient mass and energy from the system to cause a resumption of primary system depressurization. Emergency core coolant injection begins following ADS actuation when the reactor coolant system pressure decreases to the accumulator actuation pressure.

The third period is characterized by *depressurization via ADS discharge to the containment*. The period begins when the fourth-stage ADS is actuated and concludes when the IRWST injection begins. The rate at which reactor coolant system inventory is lost through the ADS continues to decrease throughout this period and eventually drops below the rate at which coolant is injected by the intact accumulator. When this occurs, the vessel begins to refill. After the intact accumulator empties, continuous draining of the intact core makeup tank begins to drain. At about the same time, the reactor coolant system pressure decreases below the static head of the IRWST pool and pool injection begins, marking the end of this period.

The *long-term cooling period* is initiated by IRWST injection. Draining of the IRWST is expected to take several days, after which water from the sump is recirculated indefinitely. Steam released to the containment through the fourth-stage ADS condenses on the inner surface of the steel containment structure, condenses, and is either collected in gutters and delivered to the IRWST or drains into the sump. This period continues indefinitely until recovery operations begin. Only the initial phase of the long-term cooling period initiated by IRWST injection was calculated. The interval of sump injection was not calculated. In addition, the containment cooling system, which functions as an integral part of the long-term cooling process, was not simulated.

The NRC has contracted with the Japan Atomic Energy Research Institute to perform AP600 confirmatory testing in the ROSA facility. In October 1994, a DVI line break IBLOCA experiment, AP-DV-01, was conducted in the ROSA facility. A core heatup did not occur. While the ROSA facility and test AP-DV-01 have not been modeled with TRAC, processes and phenomena observed in the experiment, and equivalent processes and phenomena calculated for the AP600 by TRAC were compared. In general, however, there is reasonable qualitative agreement regarding the processes occurring, trends, dominant phenomena, and the order in which events occurred.

In 1994, Westinghouse reported a revised proprietary analysis of a DVI-line IBLOCA performed with the NOTRUMP code. A core heatup did not occur. The NOTRUMP- and counterpart TRAC-calculated event times are similar. The areas of agreement between the NOTRUMP and TRAC results seem to indicate that the major features of both the codes and input models similarly represent AP600.

In 1995, the Idaho National Engineering Laboratory reported an analysis of a DVI-line IBLOCA performed with the RELAP5/MOD3 code. The RELAP5 calculation was an AP600 counterpart to ROSA test AP-DV-01. Given that the TRAC calculation was a counterpart to the Westinghouse calculation, there were still significant areas of similarity between the TRAC and RELAP5 calculations. In general, the order and timing of events were similar. There were significant areas of similarity regarding processes and phenomena. Neither code predicted a core heatup. Differences were also observed, the most significant being an early reduction in core liquid level predicted by RELAP5. Further effort will be required to identify the root causes for the differences.

Based upon the analyses and ROSA experiment performed for a DVI-line IBLOCA, the AP600 will not experience a core heatup and will reach a safe shutdown state using only safety-class equipment. An extensive amount of void is generated in the core as coolant is lost through the break. However, the core is effectively cooled throughout the accident. Only the early part of the long-term cooling period initiated by In-containment Refueling Water Storage Tank injection was evaluated. Neither the calculations nor the ROSA test simulated that portion of the long-term cooling period when sump injection is active. In addition, the containment cooling system, which functions as an integral part of the long-term cooling process, was neither simulated in ROSA nor modeled in the calculations. Thus, the observation that the core is continuously cooled does not apply to that phase of the long-term cooling period when sump injection and containment cooling processes are important.

1. INTRODUCTION

The AP600 is an advanced passive 600 MWe reactor design being developed by Westinghouse in conjunction with the US Department of Energy's Advanced Light Water Reactor Technology Program. The AP600 has been submitted to the United States Nuclear Regulatory Commission (NRC) for design certification. In accordance with the design

certification requirements of 10CFR52.47, advanced reactor applicants are required to submit neutronic and thermal-hydraulic safety analyses over a sufficient range of normal operation, transient conditions, and specified accident sequences. Review and confirmation of these analyses constitute an important activity in the NRC's AP600 design certification effort. In support of its design certification activities, the NRC performs audit calculations using best-estimate thermal-hydraulic codes. The NRC uses TRAC-PF1/MOD2,[1] a best-estimate code developed by Los Alamos National Laboratory, for analyzing AP600 large-break loss-of-coolant accident (LBLOCA). In addition, TRAC is being used to evaluate the AP600's response to an intermediate-break LOCA (IBLOCA) and certain asymmetric events such as a small-break LOCA (SBLOCA). This report analyzes the AP600 response to an IBLOCA event, a double-ended guillotine break (DEGB) of a direct-vessel-injection (DVI) line.

2. AP600 DESCRIPTION

The AP600 is a two-loop design with one hot leg, one steam generator, two reactor coolant pumps (RCP), and two cold legs in each loop. A pressurizer is attached to one of the hot legs. The reactor coolant pumps, a canned-motor design, are integrated into the outlet plena of the steam generator. The loop seal is eliminated with this design, an added safety feature in that core uncovery caused by the existence of water-filled loop seals is eliminated during a postulated SBLOCA The core is designed for a low-power density and consists of 145 fuel assemblies with an active fuel length of 12 ft. Each fuel assembly is a 17 x 17 array of fuel and control rods.

The AP600 incorporates passive safety systems that rely only on redundant/fail-safe valving, gravity, natural circulation, and compressed gas. There are no pumps, diesels, or other active machinery in these safety systems. During plant shutdown, all the passive safety features will be tested to demonstrate system readiness, flow, and heat removal performance. These systems are illustrated in an isometric view of the AP600 reactor design (Fig. 1), containment cutaway (Fig. 2), and schematic diagram of the reactor coolant system (RCS) and passive safety systems (Fig. 3). Two Passive Safety Injection System (PSIS) trains, each with an accumulator (ACC), Core Makeup Tank (CMT), and DVI line, connect directly to the reactor-vessel downcomer.

Depressurization of the primary system is an essential process required to ensure long-term cooling of the AP600. For example, the accumulators inject coolant into the RCS only after the primary pressure has dropped to 4.83 MPa (700 psia). Coolant injection from large, safety-class water pools, specifically the In-containment Refueling Water Storage Tank (IRWST) and sump, can occur only after the RCS pressure decreases enough so that the gravitational head of each pool is sufficient to force coolant into the DVI line. An Automatic Depressurization System (ADS) ensures the needed RCS pressure reduction. The ADS has four stages. Each of the first three stages consists of two trains providing redundant flow paths between the top of the pressurizer and the IRWST. The RCS inventory discharged to the IRWST through spargers is condensed and accumulated for later injection into the RCS. The actuation signal for first-stage ADS is a reduction in the coolant inventory of one CMT to 67% of its initial value. The second ADS stage is actuated 70 s after first-stage actuation. The third ADS stage is actuated 120 s after second-stage actuation. The actuation signal for fourth-stage ADS is a reduction in the inventory of one CMT to 20% of its initial value and an interval of 120 s following third-stage ADS actuation. The fourth-stage ADS consists of two trains, one connecting the top of the pressurizer hot leg (loop 1 in this report) and the containment, and the other connecting the loop-2 hot leg and the containment. A direct discharge path to the containment is needed to ensure that the RCS pressure will equilibrate with the containment

pressure so that the head-driven IRWST and sump injection can proceed. The ADS actuation logic is summarized in Fig. 4.

After the accumulators are depleted and the primary system has depressurized sufficiently, IRWST injection begins. The CMT may also inject and empty during the early phase of IRWST injection. The IRWST empties after several days. Provisions are also made for recirculating coolant from a sump. IRWST and sump recirculation may occur at the same time for some transients.

The AP600 containment plays an essential role in the long-term cooling of the primary via the Passive Containment Cooling System (PCCS). Steam entering the containment, through either a break in the RCS or ADS operation, condenses on the inside of the steel containment shell. The condensate drains downward, and a large fraction is delivered via gutters to either the IRWST or the sump. Heat transfer on the outside of the containment steel shell is by evaporation of liquid sprayed near the top of the steel reactor containment dome by the PCCS, and by convection to an air stream induced by buoyancy-driven flow. The air stream enters a high-elevation inlet, flows downward to an elevation near the bottom of the cylindrical portion of the steel reactor containment structure, passes upward through the annular gap between the steel reactor containment structure and the concrete shield building, and is exhausted to the atmosphere near the top of the concrete shield building. The PCCS spray inventory is eventually depleted. However, by the time this happens, the decay heat has decreased sufficiently that the buoyancy induced air flow can remove the core decay heat.

For non-LOCA accidents, long-term heat removal is provided by the Passive Residual Heat Removal System (PRHRS), which removes core heat through buoyancy-induced circulation. Isolation valves on the PRHRS lines open upon receipt of the safeguards (S) signal and a buoyancy-induced flow transports primary coolant through the PRHRS. The PRHRS receives water from the top of the hot leg to which the pressurizer is connected. The single PRHRS line connected to the hot leg divides into two lines, each feeding one of the two PRHRS heat exchangers immersed in the IRWST. The two PRHRS discharge lines then rejoin and connect to the outlet plenum of the steam generator outlet in the same loop. When functioning as the heat sink for the PRHRS heat exchangers, the IRWST has sufficient water volume to remove decay heat for two hours before the tank inventory reaches saturation temperature. Subsequently, the IRWST heat exchangers begin to uncover as the IRWST inventory boils off, although days are required to empty the IRWST. The PRHRS also removes heat during LOCA events. However, continued operation of the PRHRS is interrupted if sufficient voiding occurs in the hot leg at the connection to the PRHRS inlet piping to terminate the natural circulation flow. Thus, the PRHRS is ineffective for LBLOCAs, has a limited interval of effectiveness for IBLOCAs, and has an extended period of effectiveness for SBLOCAs.

3. TRAC CODE DESCRIPTION

The TRAC-PF1/MOD2 code,[1] Version 5.4, was used for this calculation. The TRAC code series was developed at Los Alamos to provide advanced, best-estimate predictions for postulated accidents in pressurized water reactors (PWRs). The code incorporates four-component (liquid water, water vapor, liquid solute, and noncondensible gas), two-fluid (liquid and gas), and nonequilibrium modeling of thermal-hydraulic behavior. TRAC features flow-regime-dependent constitutive equations, component modularity, multidimensional fluid dynamics, generalized heat structure modeling, and a complete control systems modeling capability. The code also features a three-dimensional (3D),

stability-enhancing, two-step method, which removes the Courant time-step limit within the vessel solution. Earlier versions of the continually evolving TRAC-PF1 code have been assessed using data from a variety of experimental facilities, and applied to a number of pressurized light and heavy water reactor systems.

Code adequacy must be addressed when first applying a computer code to a new reactor type, e.g., AP600. One such approach is to (1) identify representative AP600 transient and accidents sequences; (2) identify the key systems, components, processes, and phenomena associated with the sequences; (3) conduct a bottom-up review of the individual TRAC models and correlations; (4) conduct a top-down review of the total or integrated code performance relative to the needs assessed in steps 1 and 2; and (5) correct significant identified deficiencies. The bottom-up review determines the technical adequacy of each model by considering its pedigree, applicability, and fidelity to separate-effects or component data. The top-down review determines the technical adequacy of the integrated code by considering code applicability and fidelity to integral test facility data. A review of the TRAC-PF1/MOD2 code, such as that just described, is planned to assess code adequacy for the AP600 LBLOCA application. TRAC-PF1/MOD2 is an NRC confirmatory analysis tool for this application. For the IBLOCA application, TRAC use to support confirmatory analyses will depend, in part, upon the significance of multi-dimensional phenomena during the transient. At present, the role of TRAC is complementary to other NRC analysis tools. Thus, the determination of adequacy for the IBLOCA application will rest largely on the similarity of processes and phenomena occurring in the AP600 during LBLOCA and IBLOCA events.

4. TRAC MODEL DESCRIPTION

The TRAC model of the AP600 is a finely noded, multidimensional model of 184 hydrodynamic components [three vessel components and 181 one-dimensional (1D) components] encompassing 1136 3D and 990 1D computational fluid cells, and 55 heat-structure components. The plant model has undergone an independent quality-assurance check.

4.1. Plant Model Data Base

Westinghouse has changed several features of the AP600 design since it was first submitted for design certification. The TRAC AP600 plant model reflects the AP600 design information available on November 15, 1994. Although a large fraction of the plant design information needed for the model was available, there were some gaps in the data base. When data base deficiencies were encountered, the model was based on documented assumptions or on data embedded in a RELAP5 AP600 plant model[2] of the AP600, if possible. A summary of the data base sources for the TRAC plant model is provided in Table I.

4.2. Reactor Vessel

The reactor vessel is modeled in 3D cylindrical coordinates, with 4 radial rings, 8 azimuthal sectors, and 17 axial levels. An isometric view of the reactor vessel model is shown in Fig. 5. Elevation and plan views of the reactor vessel model are also shown in Figs. 6 and 7, respectively. Two TRAC vessel components are used to model the reactor vessel in order to preserve the elevations of the hot-leg, cold-leg, and PSIS connections to the vessel. Otherwise, there would have to be a compromise in modeling the true vessel geometry. The elevation differences of these piping connections to the reactor vessel are clearly seen in Fig. 6.

The central vessel component models the lower plenum, core, upper plenum, and upper head. The core region is modeled with the first two radial rings. The third radial ring models the reflector region. The fourth radial ring is used in the lower plenum and in the upper head, but is a null model in the axial levels of the core and upper plenum. The outer vessel component models the downcomer annulus and is noded into 2 radial rings, 12 azimuthal sectors, and 13 axial levels. Radial ring 1 is a null ring and ring 2 is used to model the downcomer. Where possible, the same axial-level noding heights are used in both vessel components. The two vessel components are connected together by short 1D pipe components. Other 1D pipe components are used to model the fuel-assembly guide tubes, upper-head cooling spray flow, and core bypass flow.

A total of 32 TRAC heat structure components are used to model the core and reactor vessel structure, as shown in Fig. 8. The fuel rods are combined and modeled as 16 lumped assemblies, each with the same number of fuel rods, one for each of the 16 active core sectors shown in Fig. 7. The fuel-rod modeling is accomplished with one powered, segmented heat structure. Supplemental hot-rod components are also modeled that represent the maximum-power fuel rods. The thermal responses of the supplemental rods are evaluated using the same thermal-hydraulic conditions obtained for the average-powered rods. The core decay power is calculated using reactivity feedback coefficients. Control-rod and reactivity feedback coefficients are from a 15 x 15-fuel large-break US/Japanese PWR model.[3] Insufficient reactivity information for the AP600 design was available at the time the input model was developed. Westinghouse specifications for the reactivity feedback coefficients have since been obtained, but they were not incorporated for the present calculation. Adiabatic conditions are assumed for the outer surfaces of the remaining heat structures. The reflector-block heat structure also models 2.6% of the total core power during steady state. When the reactor is scrammed, the reflector-block power is reduced to zero. Conduction through the core barrel between the downcomer annulus and the core region is modeled.

4.3. Loop Components

Figures 9 and 10 are overviews of the reactor coolant loops. Loop 1 is modeled with 33 hydro components and 181 1D computational cells. The pressurizer is connected to the hot leg of loop 1. The PRHRS and one train of the fourth-stage ADS are also connected to loop 1; the PRHRS inlet line is connected to the loop-1 hot leg and the return line is connected to the steam generator outlet plenum in the same loop (see Fig. 3). Loop 2 has 32 components and 162 1D cells. The core makeup tank pressure balance lines connect to the cold legs.

The reactor-coolant pump homologous performance curves are from a Westinghouse COBRA/TRAC model. The steam generator model reflects the AP600 Δ75 design, which is similar to the current Westinghouse Model F design, but has a taller tube bundle and redesigned secondary-side risers and separators. Where specific AP600 component design data were unavailable, components from a pre-existing Westinghouse three-loop plant were used, specifically the feedwater lines, steam lines, and control systems. All external piping wall structures are modeled with an outer adiabatic boundary assumed.

4.4. Passive Safety Systems

Figure 11 is a modeling overview of the AP600 passive safety systems, the PSIS, ADS, PRHRS, and IRWST. These systems are modeled with 57 1D hydro components, 10 heat-structure components, and one 3D hydro component. There are two separate

trains for the PSIS, ADS, PRHRS, and IRWST discharge lines, and each of the trains are modeled separately. One CMT, one IRWST discharge line, and one ACC are connected to each of two DVI lines that connect to the downcomer via a nozzle. A venturi in each nozzle reduces the vessel-side discharge area for a DVI-line break.

Both PSIS trains are orificed to delivered the same steady-state flow even though the piping geometry of the two trains is different. Separate stand-alone cases of both PSIS trains were used to calibrate the ACC and CMT flows to Westinghouse-specified values.

The ADS is modeled using the TRAC pipe and valve components. ADS stages 1-3 connect the top of the pressurizer and the IRWST. The two trains of the fourth-stage ADS connect each hot leg to the containment. The ADS actuation logic is shown in Fig. 4. The fractions of the total ADS discharge area for ADS stages 1–4 are 0.038, 0.171, 0.171, and 0.62, respectively.

The geometry of each PRHRS train is modeled as shown on Westinghouse piping and instrumentation diagrams. Because there is no indication that the two PRHRS trains are orificed to ensure the same amount of steady-state flow, we have not orificed the lines. As a consequence, the steady-state flows in the two trains are different. During the transient, flow differences between the two trains are magnified (see Section 5.1).

The IRWST is modeled with a multidimensional vessel component (Fig. 12a-c). With the multidimensional model, spatial temperature distributions arising from PRHRS heat exchanger and ADS heat rejection can be simulated. The IRWST is modeled in Cartesian coordinates. We attempted to model the IRWST in cylindrical coordinates to more closely approximate the true geometry of the tank. However, we experienced difficulties with the code and were unable to complete this modeling effort. The adequacy of the multidimensional IRWST model is not presently known but could be evaluated using experimental data generated in the AP600 program.

4.5. Features Specific to the IBLOCA Model

A DEGB of DVI-line A (DVI-A) at the nozzle connecting DVI-A to the reactor vessel is assumed (Fig. 3). The vessel-side break area is constricted by a nozzle. The DVI-line-side of the break is the pipe cross-sectional area. The nozzle orifice area is 5.1% of the total ADS discharge area. The DVI-line area is 15.7% of the total ADS discharge area. This break disables one-half of the passive safety injection capacity of the AP600. A constant containment pressure of 0.31 MPa (45 psia) is assumed.

5. IBLOCA ANALYSIS

An analysis of a postulated IBLOCA in the Westinghouse-designed AP600 plant has been performed. The accident analysis is supported by figures displaying significant calculational results. In some cases, the figure legends identify components with alphabetic or numeric descriptors, for example, DVI-A or CMT-B. Figure 3, a schematic of the AP600 and its passive safety systems, shows the relationships between the plant components and the TRAC input model labels. With reference to Fig. 3, loop 1 contains hot leg 1 (HL-1) and cold legs 1A and 1B (CL-1A and -1B). The pressurizer is connected to HL-1. The PRHRS is connected between HL-1 and the outlet plenum of steam generator 1 (SG-1). One train of the fourth-stage ADS attaches to the PRHRS inlet line, which is in turn connected to HL-1. Loop 2 contains HL-2, CL-2A, and -2B. The PSIS has two trains that feed coolant directly to the downcomer through DVI lines A (DVI-A) and B (DVI-B). Connected to DVI-A are core makeup tank A (CMT-A), accumulator A (ACC-A), and a IRWST drain line. Connected to DVI-B are core makeup tank B (CMT-

B), accumulator B (ACC-B), and a second IRWST drain line. DVI-A is connected to CL-2A by pressure balance line A (PBL-A). DVI-B is connected to CL-2B by pressure balance line (PBL-B). One train of the fourth-stage ADS connects directly to HL-2.

The accident is initiated by a DEGB in DV-A. This postulated break disables one-half of the passive safety injection capacity of the AP600. The assumed break location is the nozzle joining DVI-A to the reactor vessel (Fig. 3). ACC-A and a CMT-A are connected to DVI-A. These two components are also called the broken ACC and broken CMT in this document. The reactor is at 100% power at the time of the break. For this analysis it is assumed that only safety-class systems respond to the initiating event to bring the reactor to a safe shutdown condition. Several failures in the safety-class equipment responding to the accident are assumed. First, stage 1 of ADS train A is inoperative. Thus, only one of two ADS first-stage trains responds to the accident. Second, stage 3 of ADS train B is inoperative. Thus, only one of two ADS third-stage trains responds to the accident. These failures in safety-class equipment responding to the postulated break were selected so that the present analysis would conform to an earlier analysis by Westinghouse.[4]

The primary source of information used in preparing the description of the IBLOCA is a calculation performed with TRAC-PF1/MOD2. The features of this code are briefly described in Section 3. A finely noded model of the AP600 plant originally prepared for calculation of AP600 LBLOCA was used for this calculation. The features of the AP600 input model are described in Section 4.

Several secondary sources of information were also examined in preparing the IBLOCA description. The NRC is conducting a confirmatory testing program in the Rig of Safety Assessment (ROSA), a 1/40 scale test facility of the AP600 reactor. An IBLOCA experiment, AP-DV-01[5] was recently conducted in ROSA. This experiment simulated a DEGB in one of the AP600 DVI lines and, therefore, is directly related to the analysis described in this report. The ROSA facility and the results from experiment AP-DV-01 are summarized in Section 6. A qualitative comparison of the experimental and TRAC-calculated results is also provided in that section. The results of other AP600 IBLOCA analyses prepared by Westinghouse[4, 6] and the INEL[7] are presented in Sections 7 and 8, respectively.

The key processes occurring in an AP600 during an IBLOCA are primary coolant system depressurization, inventory depletion, inventory replacement via emergency core coolant (ECC) injection, maintenance of continuous core cooling, and long-term decay heat rejection to the atmosphere. With due consideration for these key processes, four periods have been selected to characterize the AP600 IBLOCA transient: (1) break-dominated depressurization, (2) depressurization via ADS discharge to the IRWST, (3) depressurization via ADS discharge to the containment, and (4) long-term cooling. These periods are not unique; others could have been defined. However, the selected periods do provide a rational partitioning of the IBLOCA sequence on the basis that system depressurization is required to bring the AP600 to a safe shutdown condition.

The first period of this transient is an interval of *break-dominated depressurization* initiated by a DEGB in DVI-A. This period begins at the time of the DVI-line break. The RCS initially depressurizes rapidly as mass and energy are lost through the break but the depressurization slows and then stalls as coolant flashes to vapor, first in the hottest components of the primary system and then in the colder components. The break dominated depressurization period ends when first-stage ADS is activated after the CMT in the broken DVI line has drained sufficient inventory to generate the ADS actuation signal.

The second period is characterized by *depressurization via ADS discharge to the IRWST.* The period begins at 172.6 s when the first-stage ADS is actuated, opening a controlled discharge path to the IRWST. This period concludes at 482.7 s when the fourth-stage ADS is actuated, opening a controlled discharge path between the RCS and the containment. At the end of the previous period, primary system depressurization had stalled as the core-generated decay heat released to the primary, and energy removed from the primary via the break and the PRHRS were roughly in balance. Opening of the first-stage ADS, even with one train inoperable, discharges sufficient mass and energy from the system to cause a resumption of primary system depressurization.

The third period is characterized by *depressurization via ADS discharge to the containment.* The period begins when the fourth-stage ADS is actuated at 482.7 s and concludes when the IRWST injection begins at 631 s. The rate at which RCS inventory is lost through ADS stages 1–4 continues to decrease throughout this period and eventually drops below the rate at which coolant is injected by the intact ACC. When this occurs, the vessel begins to refill. After the intact ACC empties and the RCS pressure decreases below the static head of the IRWST pool, IRWST injection begins, marking the end of this period. CMT and IRWST injection may occur simultaneously during the early part of the period.

The *long-term cooling period* is initiated by IRWST injection. Draining of the IRWST is expected to take several days, after which water from the sump is recirculated indefinitely. Steam released to the containment through the fourth-stage ADS condenses on the inner surface of the steel containment structure, condenses, and is either collected in gutters and delivered to the IRWST, or drains into the sump. This period continues indefinitely until recovery operations begin.

The response of the IBLOCA to a DEGB of a single DVI line is presented in Figs. 13–50. The sequence of events is presented in Table II.

5.1 Period 1 - Break-Dominated Depressurization

Overview

The first period of this transient is an interval of *break-dominated depressurization* initiated by a DEGB in DVI-A. The RCS rapidly depressurizes as mass and energy are lost through the break (Fig. 13). The vessel-side break flow rapidly diminishes as fluid near the break flashes, increasing the resistance to flow through the break. As coolant flashes to vapor in the hotter parts of the RCS, the rate of primary depressurization rapidly slows and then stalls. However, coolant discharge from the vessel-side of the DEGB continues, causing a further reduction in RCS inventory and contributing to voiding in the higher elevations of RCS. The postulated break disables one-half of the PSIS capability, specifically the A train. The inventories of ACC-A, CMT-A, and the coolant delivered by one IRWST discharge line are lost through the break and discharged into the containment. Coolant recirculation begins immediately after the CMT isolation valves are opened following receipt of the S signal 9.2 s after break initiation. The recirculating fluid moves from the cold legs, through the cold-leg PBLs, through the CMTs, and is discharged into the vessel downcomer through the DVI lines. During the recirculation mode, CMTs remain full. The intact CMT (CMT-B) continues to recirculate throughout this period and thus does not drain. However, the recirculation period of CMT -A lasts only a few seconds, after which it begins to drain as coolant is lost through the break at a faster rate than can be replenished through PBL-A, which feeds CMT-A. The break dominated depressurization period ends at 172.6 s when the first-stage ADS is activated following the reduction of the inventory of CMT-A to the inventory setpoint (67% of initial inventory) at which the ADS actuation signal is generated.

System Response

ADS:

The ADS is not activated. The start of the second period coincides with ADS stage-1 actuation at 172.6 s.

PCCS:

The containment response to the DVI line DEGB was not calculated. The description of PCCS response during this and subsequent periods is a qualitative assessment of the processes and phenomena occurring in the PCCS. Two-phase fluid is discharged through the vessel-side break (Fig. 14) into the containment where the small liquid fraction flashes to steam. Steam migrates to the cooler walls of the steel containment where it begins to condense and drain downward to gutters, which collect the condensate and deliver it to the IRWST. For most of the first period, liquid is discharged through the DVI-line-side of the break. Because the ECC in the ACCs and CMTs are in thermal equilibrium with the containment prior to the accident, this liquid does not flash. It either collects in containment compartments or drains into the sump.

PRHRS:

The PRHRS is actuated early in the period at 10.4 s upon receipt of the S signal. The PRHRS isolation valves are opened, and buoyancy induced flow through the PRHRS heat exchangers is initiated (Fig. 15). Several large startup transition flow oscillations occur during the period; conditions for more stable operation are established by the end of the period. The calculated flows through the two heat exchangers are different. The differing flows arise from the modeling approach described in Section 4.4. Orificing was not introduced to compensate for differences in the piping layouts for the two trains. There is a large difference in the integrated flows through the two heat exchangers, as shown in Fig. 16. Void is generated at the hot-leg connections to the PRHRS shortly after break initiation (Fig. 17) and convected into the two PRHRS trains at different rates. Two-phase fluid is delivered to the PRHRS heat exchanger inlets for all but the first few seconds of the period. The differential convection of void alters the buoyancy potential which is, in turn, coupled to the flow. Although the calculated process seems plausible, design features, e.g., orificing to balance the flows, may already be in place to prevent or minimize the calculated processes. Although displaying the same large transitions as the PRHRS flow, the void fraction at the PRHRS heat exchanger inlets is generally increasing throughout the period. Steam in the mixture is condensed near the inlet of the PRHRS heat exchangers throughout the period and liquid returned to the steam generator outlet plenum is cooled to within 60 K of the initial IRWST pool temperature of 322 K. After PRHRS actuation, the average PRHRS energy removal rate is about 50 MWt. At the end of the period, the PRHRS energy removal rate is about 58 MWt and slowly decreasing. Energy removed from the RCS during this period by the PRHRS is compared with the core-generated decay heat in Fig. 18. For the final third of period 1, the decay heat and the PRHRS energy removal are approximately the same.

PSIS:

Because the initiating break occurs in only one of the DVI lines, the two PSIS trains go through markedly different transients during the IBLOCA. ECC from the broken train, i.e., DVI-A, is discharged into the containment and is, therefore, unavailable for core cooling until sump injection begins during the long-term cooling period. Discharges from both the ACC and CMT in the broken line (ACC-A and CMT-A) begin early (Fig. 19), accumulator injection begins shortly after break initiation, and CMT draining begins shortly after the CMT isolation valves are opened. Shortly before the end of the first period, the pressures in DVI-A and in the accumulator equilibrate, causing accumulator injection to be terminated. Accumulator injection does not restart until late in the second period. The ACC-A liquid level and CMT-A volume fraction are shown in Figs 20 and 21, respectively. The ACC in the intact PSIS line, ACC-B, does not actuate during the first period as the primary pressure remains above the actuation pressure of 4.83 MPa (700 psia). Coolant recirculation through CMT-B begins immediately after the CMT isolation valves are opened at 10.4 s (Fig. 22). However, CMT-B remains liquid full (Fig. 21) because the liquid entering the DVI line is replaced by liquid entering the top of the CMT through PBL-B. Energy deposition in the intact CMT during this period is shown in Fig. 18.

Primary Coolant System:

Break flow. With respect to the RCS, the break is one-sided and only the vessel-side break will be discussed. The maximum vessel-side break flow occurs immediately following break initiation (Fig. 23). Flashing occurs near the break exit plane and the increase in vapor fraction (Fig. 14) is accompanied by a decrease in mass flow through the break. After a decline from a maximum of about 575 kg/s, the vessel-side break flow remains at about 250 kg/s for the remainder of the period.

RCPs. The RCPs continue to operate until 25.4 s when they are tripped and begin to coast down. The pump speeds reduce to less than 10% of their steady-state value within 15 s. The RCP inlets remain liquid full throughout the period.

Cold legs. The cold-leg flows remain near their steady-state value until the RCPs are tripped (Fig. 24) and then rapidly decrease, generally following the pump coastdown but also displaying several modest flow oscillations, each oscillation lasting approximately 50 s. The cold-leg flows are small at the end of the period. With the exception of a brief interval of voiding beginning at about 90 s, the cold-legs remain liquid full throughout the period.

Hot legs. The hot-leg flows remain near their steady-state value until the RCPs are tripped (Fig. 25) and then rapidly decrease, generally following the pump coastdown but also displaying two modest flow oscillations, each oscillation lasting approximately 50 s. The flows are small at the end of the period. Void appears in the hot legs immediately after the RCPs are tripped at 25.4 s. As a consequence, the PRHRS inlet connected to the pressurizer hot leg receives two-phase flow. The hot-leg liquid fraction is near 40% at the end of the period.

Pressurizer. The pressurizer inventory flashes immediately following break initiation. Vapor generation forces the pressurizer inventory into the surge line and hot leg. The pressurizer is vapor filled by 35 s (Fig. 26).

Steam generators. As the end of RCP coastdown is reached, approximately 50 s following break initiation, the primary side of the steam generators void beginning at the top of the u-

tubes and progressing downward. The downflow legs of the u-tubes are fully voided by the end of the period. Two-phase liquid remains in the lower portions of the upflow legs of the u-tubes at the end of the period.

Reactor System:

An overview of vessel vapor fractions, specifically the portion of the upper head, upper plenum, core outlet, heated core, core inlet, lower plenum, and downcomer filled with vapor as a function of time, is presented in Fig. 27.

Control rods. A reactor trip signal is generated at 8.3 s on low pressurizer pressure. The control rods are rapidly inserted and reactor power rapidly decreases to decay heat levels (Fig. 28). The control rods maintain the reactor in a shutdown condition and are not moved until recovery operations begin to terminate the long-term cooling period. The control rods will not be discussed further for the remaining periods of the accident.

Lower plenum. The lower plenum remains liquid full (Fig. 29). The multidimensional flow conditions induced in the upper portions of the downcomer by the flow to the break through DVI-A are largely nonexistent in the lower plenum.

Core region. Throughout this period, the coolant at the core inlet is single-phase liquid (Fig. 30). Two-phase conditions first arise in the core at about 30 s following break initiation (Fig. 31). Early vapor generation is primarily due to flashing, with the decay heat addition to the coolant playing a secondary role. However, by 35 s, the hottest portions of the RCS have reached saturation conditions and the resultant vapor generation causes the RCS pressure to remain nearly constant at about 6 MPa. The amount of vapor existing at the core exit is small compared with the liquid flow (Fig. 32). Therefore, the increasing vapor fraction in the core thereafter is caused by boiling heat transfer. At the end of the period, the core exit vapor fraction is about 30%. Early in the transient, heat transfer between the fuel rods and the coolant is by forced convection to a single-phase fluid. Subsequently, nucleate boiling begins at the top of the core and progresses downward until heat transfer throughout the entire core is by nucleate boiling.

Upper plenum. Flashing of the upper plenum inventory begins shortly after upper head flashing and the liquid inventory begins to decrease (Fig. 33). At the end of the period, the vapor fraction in the upper plenum is about 40%.

Upper head. Flashing of the upper head inventory begins about 17 s following break initiation and the liquid in the upper head is exhausted by 115 s (Fig. 33).

Downcomer. The downcomer remains liquid full until 65 s and then begins to decrease (Fig. 29). Multidimensional flow and thermal conditions exist in the downcomer during this period. The vessel-side break flow is drawn from the downcomer through the DVI-A nozzle. ECC enters the downcomer through the DVI-B nozzle. The ECC entering the downcomer through the DVI-B nozzle is in excess of 200 K colder than the primary coolant. However, the azimuthal temperature difference at the junction of the downcomer and lower plenum is generally less than 20 K.

Fuel rods. Although two-phase boiling conditions exist in the core for most of this period, the fuel rods remain cooled and they do not experience any temperature excursion (Fig. 34).

Steam Generator System-Secondary Side:

The feedwater control valves are closed about 17 s following break initiation. The main steam isolation valves start to close at 18.9 s. Thus, primary-to-secondary energy transport continues for only a brief interval following break initiation (Figs. 35, 36), at which time the primary and steam-generator secondary equilibrate. The primary pressure decreases below the steam-generator secondary pressure shortly before the end of the period (Fig. 13), initiating secondary-to-primary heat transfer. However, the tubes in the steam-generator primary are mostly vapor filled by this time, and the energy transferred is small.

5.2 Period 2 - Depressurization Via ADS Discharge to the IRWST

Overview

The second period of this transient is characterized by *depressurization via ADS discharge to the IRWST*. The period begins when the first-stage ADS is actuated at 172.6 s and concludes when the fourth-stage ADS activates at 482.7 s to open a controlled discharge path between the RCS and the containment. Each of the first three ADS stages consist of two trains, which discharge primary system mass and energy into the IRWST. Two ADS failures are assumed as previously identified. First-stage ADS actuation releases sufficient mass and energy to restart primary system depressurization, even with one train inoperable (Fig. 13). The rate of depressurization is moderate but increases further when the second-stage ADS starts to open at 242.7 s, a preset 70 s interval following first-stage ADS actuation. The second-stage ADS discharge area is approximately ten times greater than that of the single operative first-stage ADS and, therefore, an observable increase in the rate of depressurization follows second-stage ADS actuation. The RCS pressure soon decreases to 4.83 MPa (700 psia), initiating coolant injection from the intact ACC. The accumulator flow rate increases as the primary pressure continues to decrease. The increasing accumulator flow gradually terminates draining of the intact CMT attached to the same DVI line. Draining of the intact CMT does not resume until the ACC empties at the end of the third transient period. One train of the third-stage ADS starts to open at 362.7 s, a preset 120 s interval following ADS stage-2 actuation. One train of the third-stage ADS has one-half the discharge area of the two ADS stage-2 trains.

Throughout this period the balance of mass discharges (inventory losses through the ADS valves and vessel-side of the break), and mass injections (inventory gains via CMT draining and accumulator injection) vary. At the start of the period, the vessel-side break flow dominates the RCS inventory loss, being nearly an order of magnitude greater than the inventory gain via CMT draining. The first-stage ADS flow is a small contributor to inventory loss, approximately the same magnitude as the CMT draining flow. At the end of the period, the downcomer liquid level has drained below the level of the DVI nozzle, reducing the vessel-side break discharge to nearly zero. The second- and third-stage ADS flows are the dominant contributors to the continuing loss of RCS inventory. The maximum ADS mass flow through stages 1–3 is reached by 350 s at the time both trains of ADS stage 2 fully open. The total ADS flow is rapidly decreasing at the end of the period. The intact accumulator flow, however, continues at a near-constant flow rate, setting the stage for refilling the vessel early in the next period of the transient. The period of RCS depressurization via discharge through ADS stages 1–3 to the IRWST ends at 482.7 s when fourth-stage ADS is activated following the reduction of the inventory of CMT-A to 20%, the volume fraction at which the fourth-stage actuation signal is generated.

System Response

ADS:

The second IBLOCA period begins with ADS actuation, by definition. The precondition for ADS actuation is draining of the inventory of one CMT to 67% of its initial liquid-full state. This occurs in CMT-A at 152.5 s (Fig. 21). Train B of ADS stage 1 activates 20 s later at 172.6 s (Fig. 37). CMT-B remains in the recirculation mode and liquid-full at the time the inventory in CMT-A drains to the ADS stage-1 actuation set point. By assumption, the A-train of ADS-1 fails to operate (Fig. 38), reducing the available ADS stage-1 discharge area by 50%. The B-train of ADS stage 1 opens over an interval of 25 s (Fig. 37). The ADS-1 discharge flow increases in a nearly linear manner as the valve opens, attains a maximum flow of 20 kg/s once the valve is fully opened, and slowly decreases thereafter (Fig. 39). ADS stages 2 and 3 are actuated at timed intervals following stage-1 actuation. ADS stage 2 is actuated 70 s after stage 1, and ADS stage 3 is actuated 120 s after stage 2. Both trains of ADS stage 2 begin to open at 242.7 s; the stage-2 valves take 105 s to open (Figs. 38, 37). The discharge area of each stage-2 train is about nine times larger than the single-train stage-1 area, so the flow is much larger (Figs. 39, 40). The A-train of ADS stage 3 begins to open at 362.7 s. The stage-3 valves take 105 s to open. The single operating train of stage-3 ADS has one-half the discharge area of the two stage-2 ADS trains. The ADS stage-3 discharge flow is shown in Fig. 40. Actuation of ADS stages 1-3 is effective in reducing the RCS pressure as shown in Fig. 13. The maximum ADS mass flow is reached by 350 s at the time both trains of ADS stage 2 fully open (Fig. 41).

PCCS:

The description of PCCS response is a qualitative assessment of the processes and phenomena occurring in the PCCS; the components and processes are not included in the TRAC model. For most of this period, two-phase fluid is discharged through the vessel-side break (Fig. 14) into the containment where the small liquid fraction flashes to steam. By the end of the period, the break flow is entirely vapor. Steam continues to migrate to the cooler walls of the steel containment where it condenses and drains downward to gutters that collect the condensate and deliver it to the IRWST. Liquid not collected by the gutters drains into various containment compartments and the sump. For most of this period, two-phase fluid is injected into the containment from the DVI-line-side of the break. However, once broken-line ACC injection resumes at 327 s, liquid is again injected into the containment. Because the ECC in the accumulators and CMTs are in thermal equilibrium with the containment prior to the accident, this liquid does not flash. It either collects in containment compartments or drains into the sump.

PRHRS:

Flow continues to circulate through the PRHRS (Fig. 15), removing energy from the RCS and rejecting it to the IRWST pool. The energy removal rate is approximately 58 MWt at the beginning of the period and 14 MWt at the end of the period (Fig. 18). As the void fraction in the pressurizer hot leg increases throughout this the period, the vapor content of the two-phase flow entering the PRHRS heat exchangers also increases (Fig. 17). Steam in the flowing two-phase mixture is condensed in the PRHRS heat exchangers throughout the period, and the liquid returned to the steam generator outlet plenum is cooled to within 60 K of the initial IRWST pool temperature of 322 K. The core-generated decay heat and PRHRS energy removal remain approximately equal until 275 s, after which the PRHRS energy removal decreases. This occurs when the PRHRS inlet void fraction becomes very high (Fig. 17), degrading the energy transport to the PRHRS heat exchangers.

PSIS:

ECC from the broken train, i.e., DVI-A, is discharged into the containment and is, therefore, unavailable for core cooling. CMT-A continues to discharge until its inventory is depleted at about 340 s (Fig 21). Inventory discharge from the ACC-A stopped near the end of the first period and does not resume until 330 s, late in period 2 (Fig. 19). The IRWST also begins to drain into DVI-A at approximately 330 s (Fig. 42). Prior to the restart of ACC-A and IRWST injection, DVI-A was nearly vapor filled with only a small liquid flow from CMT-A. Over the next 60 s, the flows from ACC-A and the IRWST refill DVI-A. Refilling DVI-A increases the flow resistance through the line. As the IRWST head remains constant, at 390 s the IRWST discharge flow adjusts to a lower flow rate (Fig. 42) consistent with the increased DVI-A flow resistance. At 465 s, the IRWST discharge flow again adjusts, this time to the discharge of the ACC-A cover gas. Although the cover gas discharge process will occur, some of the calculated behavior is related to the TRAC model for the accumulators. Once the liquid level crosses the boundary of the bottom node of the model, a two-component mixture is discharged. This effect can be observed in both an alteration of the rate at which the ACC-A liquid level decreases (Fig. 20) and the effect of the gas discharge on the IRWST discharge flow (Fig. 42).

Following ADS stage-1 actuation, CMT-B begins to drain into the intact DVI line (Fig. 21). The draining is induced by voiding at the highest elevation of the cold-leg PBL (Fig. 43). This is caused by voiding in the cold leg to which PBL-B is connected (Fig. 45). However, once the primary pressure decreases to 4.83 MPa (700 psia) at 225.7 s, the accumulator flow, which increases with decreasing primary pressure, increases and eventually causes CMT-B draining to terminate. In fact, a slow refilling of the CMT by reverse flow coming upward through the bottom of the CMT is calculated (Figs. 21 and 22). The predicted refilling may be an artifact of the check valve modeling. As modeled in the TRAC input deck, a pressure difference exceeding 2.75 KPa (0.4 psi) is required before the check valve will close. The calculated pressure difference across the check valve did not exceed this value during the refilling of CMT-B. Approximately 20% of the intact accumulator's coolant inventory is injected during the period. CMT-B does not resume draining until the inventory in the intact ACC is depleted during period 3.

The thermal response of the IRWST pool is illustrated in Fig. 46. The temperature change in a stack of cells containing sparger A (Fig. 12b) is shown. The trace for Z=1, is at the bottom of the IRWST pool, and the Z=6 is at the last liquid-filled cell at the top of the pool. The sparger injects into the cell at Z=5. The discharge flow through the first-stage ADS beginning at 172.6 s is small, and the temperature increase in the pool is also small. However, following second-stage ADS actuation at 242.7 s, the liquid temperatures in the cells immediately above the sparger rapidly increase. The hotter fluid mixes with colder liquid in the upper levels of the IRWST. The hot liquid rising near the sparger is replaced by cooler liquid below the sparger and promotes buoyancy-induced natural circulation in the pool. As ADS injection continues, the thermal front progresses downward and the lower parts of the pool begin to heat. At about 450 s, the ADS flow begins an extended decline (Fig. 41), and the diminished energy addition to the pool is reflected in the temperature response of the liquid above the sparger. Circulation is also promoted by heat rejected to the IRWST through the PRHRS heat exchangers. The thermal response of a stack of fluid cells located between the A and B heat exchangers is shown in Fig. 47. temperatures of the liquid near the heat exchangers begin to increase immediately following PRHRS actuation. The heating of the pool to progressively lower levels is clearly shown.

Primary Coolant System:

Break flow. At the beginning of the period, a high vapor-fraction, two-phase flow is exiting the RCS through the vessel-side break (Fig. 14). As vessel coolant inventory depletion continues, the liquid level in the downcomer decreases and approaches the DVI nozzles. The liquid fraction in the break flow further diminishes, and by 300 s only vapor is passing through the break. The flow through the DVI-line side of the break is best understood by considering the contributions to that flow from the attached CMT and ACC (Fig. 19). At the start of the period, CMT-A drains and the broken-line ACC does not discharge. The broken-line ACC resumes discharging at 327.7 s. Two-phase fluid is discharged through the break while it is being supplied by CMT draining only. Once the broken-line ACC resumes discharging, the break flow transitions to fully liquid discharge (Fig. 14).

RCPs. The RCPs completed their coastdown from steady-state conditions during the previous period. The pumps have little or no influence on the course of the transient during this or subsequent periods of the IBLOCA. They continue to freewheel at a low speed and increase the resistance of the small cold-leg flows existing during this period.

Cold legs. The cold-leg flows are extremely small during this period and the remaining periods of the IBLOCA transient. The cold legs are liquid full at the beginning of the period but nearly vapor-filled at the end of the period (Figs. 44 and 45). The source of small loop-1 cold-leg flows and associated coolant is the PRHRS discharge into the loop-1 steam-generator outlet plenum. Other than providing a conduit for returning the PRHRS flow to the downcomer, the loop-1 cold legs have little or no influence on this or subsequent periods of the IBLOCA transient. Voiding in the loop-2 cold-leg piping (Fig. 45) does affect the course of the transient as it creates a vapor path through the loop-2 PBL line with the resultant initiation of CMT-B draining.

Hot legs. The hot-leg vapor fraction continues to increase throughout this period. The PRHRS operation is affected by the increasing void in the PRHRS inlet line connected to the loop-1 hot leg. As the PRHRS inlet line void fraction increases (Fig. 17), the buoyancy-induced flow through the PRHRS is reduced, and the effectiveness of the PRHRS heat exchangers is compromised. There is essentially no flow through the loop-2 hot leg (Fig. 25). However, there is an ongoing flow through the loop-1 hot leg, which is induced by actuation of ADS stages 1-3, which are connected to the top of the pressurizer connected to loop 1.

Pressurizer. The pressurizer is vapor filled at the beginning of the period. However, following ADS stage-1 actuation, fluid is drawn into the pressurizer from the loop-1 hot leg and discharged to the IRWST. Thus, the liquid inventory of the pressurizer increases (Fig. 26).

Steam generators. Following tripping of the RCPs during the first transient period, most of the coolant inventory of the steam generators drained into the loops. Draining of the down leg of the u-tube bundles was completed during the first transient period. A small amount of liquid remained in the up legs of the u-tube bundles, but this inventory diminished during period 2 and is insignificant by the end of the period. Heat transfer between the primary and secondary is insignificant during this and subsequent periods of the transient because the tube bundles are filled with vapor.

Reactor System. RCS inventory depletion through the vessel-side break (Fig. 23) is about one order of magnitude greater than the ECC flow delivered to the downcomer through the intact DVI line (Fig. 22) at the start of the period. In addition, actuation of the ADS

provides a path for the discharge of primary coolant to the containment (Figs. 39, 41). Injection by the intact accumulator (ACC-B) begins about 55 s after the start of the period but the increased ECC flow from the ACC remains less than the ADS and break flows, even at the end of the period. The net RCS coolant loss is reflected in the core collapsed liquid level (Fig. 29).

Lower plenum. A small amount of vapor appears in the lower plenum beginning at about 350 s. The lower plenum serves as a conduit for the ECC delivered to conduit through DVI-B.

Core region. Reduction of the core liquid inventory continues throughout the period because the loss of RCS inventory through the break and ADS stages 1-3 is larger than the ECC delivered to the vessel through the intact DVI line throughout the period (Fig. 31). Transfer of core decay heat to the core coolant occurs via several mechanisms including subcooled nucleate boiling and nucleate boiling. Heat transfer throughout the entire core is via nucleate boiling during the entire period.

Upper plenum. Reduction of the upper plenum liquid inventory continues throughout the period, as the loss of RCS inventory through the break and ADS stages 1–3 is larger than the ECC delivered to the vessel through the intact DVI line throughout the period (Fig. 33).

Upper head. The upper head remains vapor filled throughout this and subsequent periods of the transient.

Downcomer. Reduction of the downcomer liquid inventory continues throughout the period, as the loss of RCS inventory through the break and ADS stages 1–3 is larger than the ECC delivered to the vessel through the intact DVI line throughout the period. However, as the downcomer liquid level decreases to the elevation of the DVI nozzles, the flow delivered to the break contains an ever higher fraction of vapor. Thus, inventory lost through the vessel-side break diminishes throughout the period and is very small by the end of the period (Fig. 23).

Fuel rods. Although two-phase boiling conditions exist in the core throughout this period, the fuel rods remain cooled and do not experience any temperature excursion (Fig. 34).

Steam Generator System-Secondary Side:

The feedwater and main steam isolation valves were closed during period 1, shortly after break initiation. The primary-side steam generator tube bundles are vapor filled, minimizing heat transfer between the steam-generator primary and secondary sides.

5.3 Period 3 - Depressurization Via ADS Discharge to the Containment

Overview

The third period of this transient is characterized by *depressurization via ADS discharge to the containment.* Each of two fourth-stage ADS lines connect to the top of a separate hot leg and exhaust directly to the containment. The objective of the fourth-stage ADS is to complete the depressurization of the primary system by reducing the RCS pressure below a level at which the IRWST pool head is sufficient to induce injection. The period begins when the fourth-stage ADS is actuated at 482.7 s, and concludes when the IRWST injection begins at 631 s. About 80 s after fourth-stage ADS actuation, the RCS pressure approaches the containment pressure (Fig. 13), establishing the precondition for IRWST discharge into the intact DVI line once the ACC attached to same line empties.

The fourth-stage ADS discharge area is approximately 62% of the total ADS system discharge area. At the time of fourth-stage ADS actuation, the hot-leg piping contains only a little liquid and, therefore, RCS depressurization continues with only a moderate additional loss of coolant inventory over a period of approximately three minutes. After the discharge flow is established following opening of the ADS fourth stage, the rate of RCS inventory loss through fourth-stage ADS oscillates, but generally decreases as the period progresses. Inventory discharges through ADS stages 1–3 continue to diminish throughout the period and are small at the end of the period. Eventually, the rate at which coolant is injected by the intact ACC exceeds the coolant loss through all stages of the ADS and the vessel-side break. This occurs at about 535 s, and the core begins to refill (Fig. 29). The intact ACC empties at 623 s. Draining of the intact CMT resumes shortly before the intact ACC empties. IRWST draining through the intact DVI line begins shortly after the intact ACC empties at 631 s, marking the end of the period.

System Response

ADS:

By definition, this period begins with fourth-stage ADS actuation. The preconditions for ADS actuation are draining of the inventory of one CMT to 20% of its initial liquid-full state, which occurs at 255.2 s, and a delay of 120 s after the third-stage valves open at 362.7 s. Therefore, fourth-stage ADS valves begin to open at 482.7. The sequencing of the fourth-stage ADS valves is shown in Figs. 38 and 37. The discharges from valve stages 4A and 4C, which are connected to HL-1 (Fig. 3), and valve stages 4B and 4D, which are connected to HL-2, are shown in Figs. 48 and 49. The total fourth-stage ADS discharge is presented in Fig. 50. The discharges generally increase while the fourth-stage valves are opening, with the peak discharge attained at the time all fourth-stage valves are fully opened (533 s). Although the fourth-stage discharge flows fluctuate until the remaining liquid inventory of the hot legs is depleted, they generally decrease once all fourth-stage valves are fully opened.

ADS stages 1-3 continue to discharge to the IRWST throughout the period (Fig. 41). However, the discharge decreases from 135 kg/s at the start of the period to about 25 kg/s at the end of the period.

By 540 s, the discharges from ADS stages 1-4 have decreased sufficiently that the discharge from the intact ACC exceeds both the ADS and vessel side break discharges. At this time, the core inventory begins to recover (Fig. 29).

PCCS:

The description of PCCS response is a qualitative assessment of the processes and phenomena occurring in the PCCS; the components and processes are not included in the TRAC model. Throughout this period, vapor is discharged through the vessel-side break (Fig. 14) into the containment. Steam migrates to the cooler walls of the steel containment where it condenses and drains downward to gutters that collect the condensate and deliver it to the IRWST. Liquid not collected by the gutters drains into various containment compartments and the sump. Throughout this period, two-phase fluid is injected into the containment from the DVI-line-side of the break. Because the ECC in the ACCs and CMTs are in thermal equilibrium with the containment prior to the accident, the liquid-phase discharge does not flash. It either collects in containment compartments or drains into the sump. The vapor-phase discharge migrates to the cooler walls of the steel containment where it condenses and is collected for delivery to the IRWST.

PRHRS:

The PRHRS and one set of ADS stage-4 valves are connected to HL-1 by a common offtake pipe. Actuation of ADS valve 4A temporarily induces large flow oscillations in the PRHRS heat exchangers (Fig. 15). However, the PRHRS inlet flow generally decreases thereafter and is small at the end of the period. The PRHRS inlet flow is highly voided throughout the period (Fig. 17), and the PRHRS energy removal averages about 8.5 MWt during the period. Energy removal by the PRHRS diminishes immediately following fourth-stage ADS actuation and is small throughout this period (Fig. 18).

PSIS:

ECC from the broken train, i.e., DVI-A, is discharged into the containment and is, therefore, unavailable for core cooling. CMT-A emptied during the previous period. The broken-line ACC empties near the end of the period at approximately 625 s (Fig. 20). The IRWST continues to drain into DVI-A throughout the period (Fig. 42).

The intact-line accumulator, ACC-B, empties during this period (Fig. 22). The ACC-B flow rate begins to rapidly decrease at approximately 580 s. ACC-B empties at about 623 s (Fig. 20). The near linear decrease in ACC-B flow rate between 580 and 623 s is an artifact of the model. Once the calculated liquid level decreases below the top of the bottom node in the ACC-B model, the code considers the accumulator discharge to be a two-phase mixture. The decreasing flow rate as the last node of the ACC-B model empties is a reflection of this two-phase discharge. In reality, the ACC would continue to discharge liquid until it emptied. The reverse flow from the DVI-line refills CMT-B shortly after the start of the period (Fig. 21). See the PSIS discussion of period-2 phenomena for additional information about the reverse flow. The reverse flow continues after CMT-B has refilled. It continues until the predicted flow from ACC-B into the DVI line rapidly diminishes as the accumulator discharges the last of its liquid (Fig. 22). At this time, the CMT-B check valve closes, and the reverse flow into CMT-B terminates. Forward flow through CMT-B begins as ACC-B empties, shortly before the end of the period. Thus, the period ends with complete flow discharge of CMT-B, the flow restart of intact-line CMT, and preconditions established for the start of IRWST injection into the intact-DVI line.

Primary Coolant System:

Break flow. The vessel-side break discharge is pure vapor throughout the period (Fig. 14), and the mass flow is negligible (Fig. 23).

Flow through the DVI-line side of the break is also small (Fig. 23), but its makeup is more complex. From the start of the period until approximately 516 s, ACC-A discharges a mixture of coolant and noncondensible gas into the DVI line. The mixture discharge begins shortly before the end of the second period when the decreasing accumulator liquid level enters the bottom computational cell of the ACC-A model. The predicted period of mixed noncondensible and liquid discharge may be an artifact of the computational model. Once ACC-A empties, the IRWST flow adjusts slightly (increases) and the DVI-line discharges stabilizes with respect to both void fraction (Fig. 14) and flow rate (Fig. 23).

RCPs. The pumps have little or no influence on the course of the transient. They continue to freewheel at a low speed and increase the resistance of the small cold-leg flows existing during this period.

Cold legs. The cold-leg flows are essentially stagnant throughout the period (Fig. 24). The cold legs are vapor-filled with the exception of a few intervals when a small amount of liquid appears in CL-2B.

Hot legs. HL-1 has a small flow at the start of the period but becomes stagnant midway through the period (Fig. 25). HL-2 is stagnant throughout the period. Each hot leg contains a high void-fraction fluid at the start of the period and is vapor filled at the end of the period.

Pressurizer. As the amount of liquid in the hot legs decrease and as the flows through ADS stages 1-3 decrease, the amount of entrained liquid in the pressurizer decreases (Fig. 26). The pressurizer is vapor filled at the end of the period.

Steam generators. Heat transfer between the primary and secondary is insignificant during this period of the transient because the tube bundles remain filled with vapor.

Reactor System:

At the start of this period, loss of vessel inventory continues (Fig. 29). However, by 535 s, ECC injection into the vessel downcomer through the intact DVI line exceeds the inventory loss through the vessel-side break and the ADS.

Lower plenum. A small amount of vapor continues to reside in the lower plenum throughout the period. The lower plenum serves as a conduit for the ECC delivered to conduit through DVI B.

Core region. At about 535 s, the core begins to refill (Fig. 29) as the ECC flow entering the downcomer from the intact DVI line is greater than the flow loss through the vessel-side break and the ADS. Transfer of core decay heat to the core coolant occurs by several mechanisms including subcooled nucleate boiling and nucleate boiling. Heat transfer throughout the entire core is by nucleate boiling during the entire period.

Upper plenum. The liquid fraction in the upper plenum is slightly more than 20% throughout the period (Fig. 33).

Upper head. The upper head remains vapor filled throughout the period (Fig. 33).

Downcomer. The downcomer liquid inventory fraction stabilizes at about 40% early in the period (Fig. 29) as ECC delivered to the downcomer through the intact DVI line exceeds the RCS inventory loss through the vessel-side break and the ADS.

Fuel rods. Although two-phase boiling conditions exist in the core throughout this period, the fuel rods remain cooled and they do not experience any temperature excursion (Fig. 34). Once the primary coolant pressure attains equilibrium with the containment pressure, the coolant saturation temperature also stabilizes. The core cladding temperatures stabilize slightly above the coolant saturation temperature.

Steam-Generator System-Secondary Side:

The steam-generator secondaries are isolated. The primary-side steam-generator tube bundles remain vapor filled, minimizing heat transfer between the steam-generator primary and secondary sides.

5.4 Period 4 - Long-Term Cooling

Overview

The TRAC-PF1/MOD2 calculation results presented in this document do not cover the entirety of the long-term cooling period. Thus, the descriptive information provided for the long-term cooling period is based upon other AP600 PIRT activities,[8] other discussions of long-term cooling processes and phenomena at several recent NRC-sponsored meetings as typified by Ref. 9, and information appearing in quick-look reports documenting tests in the ROSA facility as typified by Ref. 5.

The long-term cooling period begins with IRWST actuation and continues indefinitely. IRWST injection begins at 631 s. Draining of the IRWST is expected to take several days, after which water from the sump is recirculated indefinitely. Water from the IRWST passes to the vessel downcomer through the DVI lines. The injected water is heated in the core, a portion evaporates establishing a two-phase liquid level in the core, and the steam generated in the core is discharged to the containment through the fourth-stage ADS. The passive containment cooling system plays an important role during the long-term cooling period. Steam released into the containment through either the break or fourth-stage ADS condenses on the inner surface of the steel containment shell and drains downward either to gutters that return the condensed liquid to the IRWST or the sump. Heat transfer on the outside of the steel containment shell is by evaporation of water and buoyancy induced circulation of air until the PCCS water supply is exhausted. Thereafter, the buoyancy induced air flow is sufficient to remove the decay heat released into the containment.

The AP600's long-term cooling period behavior is believed to be similar for many accidents because the end state of events such as a large-break LOCA, small-break LOCA, main steam line break, and steam-generator tube rupture are similar.[8] Specifically, the primary is depressurized, emergency core coolant enters the primary from the IRWST and sump, there is boiling in the core, and there is a direct path for releasing RCS mass and energy to the containment through the fourth-stage ADS. Some differences in phenomena occurring during the late phase of various accidents are expected but these differences are not expected to have a major impact on the late-period course of the sequences.

Because the TRAC IBLOCA calculation was terminated shortly after the start of the long-term cooling period, the calculation data base needed to describe the detailed system and component responses is unavailable. Detailed descriptions of AP600 performance during the long-term cooling phase are provided in Ref. 9.

6. IBLOCA Insights from ROSA IBLOCA Test AP-DV-01

The NRC has contracted with the Japan Atomic Energy Research Institute (JAERI) to perform AP600 confirmatory testing in the JAERI's Large Scale Test Facility (LSTF). This facility was previously used in a multinational test program to simulate SBLOCA behavior in PWRs. Within the United States, the LSTF has been called the ROSA facility and this name will be used in this report. The ROSA facility was modified from its earlier scaled representation of a PWR to better simulate the system response of the AP600 reactor. ROSA is not a perfect representation of the AP600 reactor, and numerous geometric distortions exist that must be considered when projecting the ROSA response to the AP600.[5] For example, AP600 has two cold legs per loop. AP600 has two cold-leg PBLs, each connecting to one cold leg of the same loop. ROSA, however, has only a single cold leg per loop. Both the NRC and JAERI have concluded that while ROSA is not

an exact scale model of the AP600, it is sufficiently similar to reproduce the most important thermal-hydraulic phenomena associated with AP600.

In October, 1994, an IBLOCA experiment, AP-DV-01, was conducted in the ROSA facility .[5] This experiment simulated a DEGB in one of the AP600 DVI lines. Thus, one-half of the PSIS injection capability was disabled. Specifically, the unavailability of the discharge from one ACC, one CMT, and one of the IRWST discharge lines was simulated. In an AP600, the coolant from the broken DVI line would have been discharged into the containment. This process is not simulated in ROSA.

A TRAC-PF1/MOD2 model of ROSA has not been developed, thus, test AP-DV-01 has not been simulated with TRAC. The degree to which TRAC would simulate the processes and phenomena of test AP-DV-01 in ROSA is unknown. However, the test results have been reviewed with the objective of highlighting areas of similarity and dissimilarity between the ROSA AP-DV-01 data and the TRAC-calculated results for the same postulated accident in AP600. It should be noted that the TRAC DVI-line IBLOCA is a direct counterpart to the Westinghouse calculation of an AP600 DVI-line IBLOCA.[4] ROSA experiment AP-DV-01 conditions differ in some respects. For example, the ROSA break location is located ~6.8 m from the reactor vessel nozzle, which is equivalent to about 8.3 m from the reactor vessel nozzle in AP600. The break location for the TRAC DVI-line IBLOCA was at the reactor vessel nozzle. The ADS is fully functional in the ROSA test. One stage of the first- and third-stage ADS is assumed to fail in the TRAC calculation. A single heat exchanger and fluid train simulates the AP600 PRHRS in ROSA. Both AP600 PRHRS trains are simulated in the TRAC model. Other than the differences noted, the TRAC calculation is a reasonable counterpart to ROSA experiment AP-DV-01. A comparative assessment of the areas of similarity and dissimilarity between the TRAC DVI-line IBLOCA calculation and the sequence of events, processes, and phenomena in the ROSA experiment AP-DV-01 are summarized in the following.

The following *similarities* between the ROSA test results and TRAC calculated results were identified.

Overall. With the exceptions presented in the tabulation that follows, the sequence of events occurring during the ROSA experiment and in the AP600 calculation are similar.

Pressurizer. The pressurizer empties early because of flashing associated with the initial RCS depressurization. The pressurizer collapsed liquid level recovers following the opening of the first-stage ADS.

RCS Depressurization. Depressurization stalls prior to ADS actuation when the hottest portions of the RCS saturate.

Accumulator. The broken-line ACC discharges for an interval, but terminates before ADS stage-1 initiation. The accumulator discharge resumes after the RCS pressure once again decreases below the accumulator injection pressure. The intact-loop ACC remains inactive until the pressure drops below the actuation pressure.

CMT. The broken loop CMT drains fairly rapidly into the broken DVI line and thence out the break. The intact-loop CMT has an initial period of recirculation, followed by a brief period of draining that is terminated following accumulator injection. CMT injection does not resume until the ACC is empty. CMT and IRWST injection proceed simultaneously after the ACC empties.

Cladding temperatures. Temperatures follow saturation pressure. There is no core cladding heatup.

The following *dissimilarities* between the ROSA test results and TRAC calculated results were identified.

Pressurizer. The data show that recovery of collapsed liquid level continues through fourth- stage ADS actuation. TRAC calculated a much shorter period of liquid level recovery.

RCS depressurization. The ROSA data shows a shorter-duration primary pressure plateau following RCS saturation. The PRHRS transfers sufficient energy from the RCS to the IRWST that RCS pressure begins to decrease before ADS stage-1 operation. The TRAC-calculated RCS pressure plateau persists until ADS stage 1 is actuated.

Accumulator. The ROSA data show the RCS pressure decreases to the accumulator injection pressure immediately following first-stage ADS actuation. The more rapid pressure decrease in ROSA prior to ADS actuation is the consequence of energy removal from the RCS by the PRHRS. The TRAC-calculated RCS pressure decreases to the accumulator injection pressure after second-stage ADS actuation. As simulated in the TRAC model of AP600, the PRHRS appears to be removing less energy from the RCS. ROSA has a single PRHRS heat exchanger while two heat exchangers are present in the TRAC model. As discussed in Sections 4.4 and 5.1, asymmetries in the layouts of the two PRHRS trains result in different flows through the two heat exchangers, possibly reducing the total heat removal calculated by TRAC.

CMT. Following intact-loop accumulator injection in ROSA, CMT draining immediately terminates, recovers, and then terminates again as the accumulator flow increases with decreasing pressure. TRAC does not calculate the immediate termination and recovery for the AP600.

Cladding temperature. Saturation temperatures follow RCS depressurization in both the ROSA data and the TRAC calculation, but the cooldown rate differs because a faster depressurization transient occurred in ROSA than calculated by TRAC for AP600.

Another approach to examining the *similarities* and dissimilarities is to examine the sequence of events and phenomena that occur following break initiation. The sequence of events for experiment AP-DV-01 have been tabulated.[5] The AP-DV-01 test sequence is provided in Table III. The TRAC-calculated sequence for AP600 is shown in the second column of the table. The specific times are also provided for comparison.

The TRAC-calculated IBLOCA is in general agreement with respect to the important systems, components, processes and phenomena occurring in ROSA test AP-DV-01. The primary area of disagreement relates to the system pressure response and related processes and phenomena. To fully explore the causes of the differences, it would be necessary to simulate ROSA test AP-DV-01 with TRAC. Analysis of the resultant assessment calculation would lay the foundation for understanding whether the previously discussed scenario differences arise from ROSA atypicalities relative to AP600, assumptions in the TRAC input model for AP600 PRHRS, or code deficiencies. Los Alamos believes that the first inquiry should focus on whether the TRAC model of the PRHRS is adequate.

7. IBLOCA Insights from IBLOCA Analyses by Westinghouse

In 1992, an analysis of a DVI-line IBLOCA for an earlier version of the AP600 design was reported in the AP600 Standard Safety Analysis Report.[6] The Westinghouse analysis was based on a NOTRUMP calculation. NOTRUMP is a conservative methodology that follows the 10CFR50 Appendix K methodology. It is a 1D, general network code. The earlier design did not include the venturi present in the DVI-line nozzle of the current design. In addition, the design contained a pressurizer to CMT PBL. The double-ended nature of the DVI-line break means that there are effectively three break planes for this accident in the earlier design. They are: (1) downcomer to containment via the vessel-side break at the DVI nozzle, (2) cold leg to containment via the connections through the CMT and DVI line, and (3) pressurizer to containment through the pressurizer PBL. The vessel-side DVI-line-break discharge area in the earlier design was larger than in the current design. NOTRUMP calculated a core heatup when insufficient coolant remained in the core and upper plenum to sustain a core mixture level that would cool the core. The core cladding heatup began at about 60 s and peaked 60 s later when the intact-loop ACC started to inject. The peak core temperature increase was about 250 K. The cladding temperature excursion was terminated by 170 s when the last of the core quenched.

In 1994, Westinghouse reported a revised analysis of a DVI-line IBLOCA.[4] The report is Westinghouse proprietary. The reanalysis was performed to determine the impact of passive safeguards system changes reflected in the design of February 15, 1994. The most important of these changes were the addition of a DVI nozzle venturi to limit the vessel-side flow, ADS flow capacity and actuation logic, and PRHRS actuation logic. The pressurizer PBL remained in the design at the time of the reanalysis. It was subsequently removed. The analysis was once again based upon a calculation performed with the NOTRUMP code.

With the venturi modeled in the DVI nozzle, no core uncovery and cladding heatup is predicted to occur. This result is consistent with the TRAC-calculated result reported in Section 5. In addition, the NOTRUMP-calculated and TRAC-calculated event times for reactor trip, S signal, start of RCP coastdown, ADS stage-1 actuation, start of intact-loop accumulator flow, ADS stage-2 actuation, ADS stage-3 actuation, and ADS stage-4 actuation are similar. The calculated times for generating the reactor trip signal, S signal, and start of RCP coastdown are within about 1 s. The ADS actuation times are within 10 s, and the intact loop accumulator injection times are within 20 s. Differences between the NOTRUMP and TRAC calculations were also observed. These included a shorter duration RCS pressure plateau, slower upper head draining, recovery of the downcomer mixture level after ADS actuation, and lower ADS flow rates predicted by NOTRUMP for the transient. Some of the differences may be related to the Appendix K methodology incorporated in the NOTRUMP model. Others, such as the RCS pressure behavior following RCS saturation, may be due to the TRAC model of the PRHRS.

When code-to-code comparisons are made, three potential areas of cause must be explored. First, the same understanding of facility design and operation must be held by each team developing a code input model. Second, the input model must adequately represent the actual design and its operation. Third, code features or inadequacies may play a role. The areas of agreement between the NOTRUMP and TRAC results seem to indicate that the major features of both the codes and input models similarly represent AP600. However, there are also differences. An understanding of these differences can probably only be obtained by increasing the dialogue and/or communication between Westinghouse and Los Alamos regarding the DVI-line IBLOCA.

8. IBLOCA Insights from IBLOCA Analyses by the INEL

In 1995, INEL staff analyzed an AP600 DVI-line IBLOCA based on a RELAP5 calculation.[7] The objective of the effort was to provide a pretest AP600 counterpart calculation for ROSA DVI-line IBLOCA test AP-DV-01. Both baseline and sensitivity calculations were performed. Although the ROSA test has been conducted, a posttest calculation and analysis are to be done in the future. A brief assessment of the similarities and dissimilarities of the RELAP5 pretest and TRAC calculations of the DVI-line IBLOCA follows.

Several differences in the problem statement have been identified. These arise from differing objectives for the two AP600 DVI line LOCA. The objective of the TRAC calculation is to replicate the conditions of a Westinghouse analysis.[4] Thus, one train of the first-stage ADS is assumed to fail. One train of the third-stage ADS is also assumed to fail. All trains of the ADS are assumed to function in the ROSA counterpart calculation. Although the break location for each calculation is in the DVI line between the vessel and tee to the IRWST, the break location in the TRAC is closer to the vessel as discussed in Section 6. In both the TRAC and RELAP5 calculations, the DVI nozzle venturi was located in the vessel-side break path. In the INEL calculation, the containment is initially assumed to be at atmospheric pressure and is allowed to pressurize using a rudimentary containment model; in the TRAC calculation a constant, 45-psia containment pressure was assumed. In addition, there are modeling differences related to the codes themselves. The baseline RELAP5 calculation modeled the downcomer as a single axial stack of fluid volumes. A sensitivity study was performed in which eight cross-connected axial stacks were used to simulate the multidimensional character of the downcomer.

There are significant areas of similarity between the TRAC and RELAP calculations. In general, the order and timing of events are similar. For example, the calculated times of IRWST injection are within 15 s. ADS actuation is predicted to occur about 45 s earlier in TRAC. RELAP5 calculated an interval during which draining of the broken CMT stalled when subcooled liquid from the downcomer entered the CMT and condensed vapor in the CMT. Because the ADS actuation signal is generated on CMT liquid level, all ADS actuations calculated by RELAP5 were delayed relative to the TRAC-calculated times. There are significant areas of similarity regarding processes and phenomena. Similarities are observed in the behavior of the accumulator and CMT attached to the broken DVI line. The behaviors of the intact ECC trains are similar. Except for the early core liquid level reduction and subsequent reduction calculated by RELAP5, the inventory trends of the downcomer and core calculated by the two codes are similar. Both codes predict that the core remain cooled throughout the accident.

Several significant phenomenological differences were calculated by the two codes. First, RELAP5 calculated a significantly larger early reduction of core coolant inventory than TRAC. The collapsed liquid level at 165 s was reduced to 15% of the steady-state value. The collapsed liquid level rapidly recovered shortly thereafter. During the same interval, the TRAC-calculated core liquid fraction decreased to 70%. A RELAP5 sensitivity calculation was performed with RELAP5 with the eight-stack model. The collapsed liquid level again decreased to the bottom of the active fuel but the duration of the core liquid level depression was reduced. The break flows calculated by the two codes immediately following the break are close: about 825 kg/s for TRAC, and about 870 kg/s for RELAP5. However, by 30 s, the vessel-side break flow calculated by TRAC has diminished to about 230 kg/s, and the flow rate remains near this value throughout the remainder of the period of *break dominated depressurization.* The corresponding RELAP5 flow at 30 s is about 335 kg/s. Although the flow subsequently increases to about 450 kg/s at 65 s and decreases to 190 kg/s at 120 s, a flow of 300–350 kg/s appears to be an average for the

remainder of the period. Thus, the difference in core collapsed liquid level calculated by the two codes between 80 and 180 s is consistent with the differences in the calculated break flows. Thus, the different break locations used in the two calculations may be significant. The vessel-side break flow calculated by RELAP5 was significantly altered in the sensitivity calculation with the eight-stack model. Additional comparative reviews of the two calculations, and possibly sensitivity calculations for the two break locations, would provide the basis for understanding the root causes for the calculated differences.

Second, following ADS actuation, RELAP5 calculates both more liquid in the pressurizer and a longer period during which the pressurizer retains liquid. The ADS failure specification in the TRAC calculation is a contributing factor, although it is not clear if this is the total explanation.

Third, the pressurization plateau interval during the blowdown period is shorter in the RELAP5 calculation. Los Alamos attributes the longer period of the pressure plateau in the TRAC calculation to be associated with a reduced amount of heat rejection to the PRHRS. Sensitivity studies could provide insights into the adequacy of the TRAC two-train PRHRS model.

Finally, The broken CMT drained several hundred seconds earlier in the TRAC calculation. RELAP5 calculated a 95-s interval during which condensation phenomena occurred in the CMT as subcooled liquid passed from the downcomer into the cold leg and then into the top of the intact CMT. The decrease in the RELAP5-calculated CMT liquid level stalled during this interval. The interruption of CMT draining by condensation-induced phenomena was not calculated by TRAC.

9. Issues Regarding Input Model Adequacy

As the calculation results were analyzed, several issues relating to input model adequacy were identified. Although each has been discussed in the body of the report, the modeling issues are summarized briefly in this section.

We have attempted to provide a geometrically correct model of the PRHRS by representing both heat exchanger trains. As the piping layouts for the two trains are not identical, the resistances of the two trains differ. Lacking any data base information stating that orificing is to be provided to balance the train resistances, the inherent resistances of the two trains in the present model differ. The differing resistances are reflected in both the steady-state and transient performance of the PRHRS (Section 5.1). Specifically, the calculated flows through train A are significantly larger than through train B (Fig. 16). Los Alamos will request that the NRC seek additional information regarding PRHRS train resistances from Westinghouse.

Lacking specific information regarding check valve performance, a pressure difference exceeding 2.75 KPa (0.4 psi) is required for the present TRAC model before the CMT check valve will close. As discussed in Section 5.2, the CMT refills during period 2. The flow through the check valve is insufficient to activate the check valve and prevent reverse flow. Los Alamos will request that the NRC seek additional information regarding check valve characteristics from Westinghouse.

The IRWST is currently modeled in Cartesian coordinates (Figs 12a-c). A more geometrically accurate representation of the IRWST is possible in cylindrical coordinates. However, code problems were encountered when the IRWST was modeled in cylindrical coordinates (see Section 10). A phenomena identification and ranking tabulation has

recently been completed for a LBLOCA scenario in the AP600.[10] The IRWST is assessed as a highly important component only during the long-term cooling period, which begins with IRWST injection. Los Alamos believes that the same ranking is appropriate for the IBLOCA. During the first three periods of the IBLOCA transient, the IRWST is not a component of high importance because it has little or no impact on either the fuel rod cladding temperature or the vessel coolant inventory. Therefore, we conclude that the current model of the IRWST in Cartesian coordinates is adequate.

Once the calculated liquid level decreases below the top of the bottom node in the accumulator model, the code considers the accumulator discharge to be a two-phase mixture. In reality, the accumulator would continue to discharge liquid until it either emptied or there was cover gas blowthrough. The calculated behavior is an inherent feature of the model discretization. The distortion could be minimized by using a finer noding near the bottom of the accumulator. However, we see no significant adverse outcomes of the calculation as performed. Therefore, no further action is recommended.

10. Insights Regarding TRAC-PF1/MOD2 Adequacy

Difficulties were encountered with code robustness at several points in the calculation. Generally, these were associated with ADS actuation and the resultant injection of steam into the IRWST pool. As the steam condensed, either the code failed to converge or the time step was reduced to such a small value that the calculation was essentially stopped. Because modification of the condensation model would require a significant effort, approaches to minimize the impacts were examined. Two approaches were found to be effective and permitted the calculation to be completed. First, the terminus node for the sparger was increased in size so that the injected steam had a larger cell volume in which to condense. The negative impact of this approach was that spatial resolution was diminished. However, because the IRWST is not considered to be a component of high importance during the first three periods of the transient (see Section 9), the more coarse noding was accepted. The second approach involved restarting the failed run from a restart dump and altering either the maximum allowed time step or the convergence criteria.

11. Summary Observations

The summary observations that follow are based upon information from four sources. Most detailed insights are based upon an analysis of the TRAC-calculated, DVI-line IBLOCA documented in this report. The TRAC-calculation-based insights are complemented by a scaled DVI-line IBLOCA experiment, test AP-DV-01, conducted in the ROSA facility.[5] They are further complemented by counterpart analyses based upon DVI-line IBLOCA calculations performed with other codes. The TRAC calculation documented in this report is a direct counterpart of a calculation performed by Westinghouse using NOTRUMP.[4] The INEL has performed a direct AP600 counterpart calculation to ROSA test AP-DV-01 using RELAP5/MOD3.[7]

Although similar processes, phenomena, and outcomes have been either calculated or observed in each source, uncertainties remain. As with any scaled experimental facility, atypicalities exist. Work underway at the INEL should help to characterize these atypicalities. Activities to demonstrate code applicability for AP600 LOCA processes are either in progress or planned. However, the uncertainty associated with TRAC and RELAP5 calculations of IBLOCA processes and phenomena have not been quantified to date.

The key processes occurring in an AP600 during a IBLOCA are RCS depressurization, inventory depletion, inventory replacement via ECC injection, maintenance of continuous core cooling, and long-term decay heat rejection to the atmosphere.

RCS depressurization is successfully accomplished by the ADS. The primary outcomes of ADS depressurization are accumulator injection beginning at 4.83 MPa (700 psia) and IRWST injection beginning when the RCS pressure equilibrates with the containment pressure, and the IRWST pool head is sufficient to inject coolant into the intact DVI line.

There are several sources of RCS inventory depletion. During the period of *Break Dominated Depressurization*, period 1, the vessel-side break is the only source of RCS inventory depletion. The vessel-side break is a significant contributor to inventory depletion for the first one-third of period 2, the period of *Depressurization Via ADS Discharge to the IRWST*. Discharges through the first three stages of the ADS are the dominant cause of RCS coolant loss during this period. This is particularly true after the vessel-side break flow diminishes when the downcomer liquid level drops below the downcomer connection to the broken DVI line. Some RCS coolant resides in the pressurizer following ADS stage-1 actuation, further reducing the circulating RCS coolant inventory. Following actuation of the fourth-stage ADS at the start of period 3, *Depressurization Via ADS Discharge to the Containment*, the fourth-stage ADS flow is the largest cause of RCS inventory reduction. However, the peak fourth-stage ADS flow is significantly lower than the peak flows through either the vessel-side break or ADS stages 1–3.

There are several sources of inventory replacement via ECC injection. Of course, the entire inventory of one ECC system train is lost as a direct result of the postulated DVI-line break. Thus, only the inventory of the intact ECC train is available for cooling the core. Intact-train accumulator injection begins following ADS actuation. Continuous draining of the intact-train CMT begins once the intact-train accumulator drains. IRWST injection into the intact DVI line begins following fourth-stage ADS actuation. Loss of RCS coolant inventory terminates once the ECC flow from the intact-train accumulator exceeds the RCS discharges through the vessel-side break, ADS stages 1–3, and ADS stage 4. This occurs at about 535 s, during period-3 depressurization via ADS discharge to the containment.

The core is continuously cooled. ECC coolant injection from the single intact train is sufficient to prevent core dryout.

We note, however, neither the calculations nor the ROSA test simulated that portion of the long-term cooling period when sump injection is active. In addition, the containment cooling system, which functions as an integral part of the long-term cooling process was neither simulated in ROSA nor modeled in the calculations. Thus, the conclusion that the core is continuously cooled does not apply to the period of sump injection. The absence of this conclusion regarding the latter phase of the long-term cooling period does not imply that continuous core cooling is suspect. It only means that the needed analytical and/or experimental confirmation of cooling is unavailable at the present time.

12. References

1. J. C. Lin, et. al., "TRAC-PF1/MOD2 Code Manual," Volumes 1-4, Los Alamos National Laboratory report NUREG/CR-5673, also LA-12031-M (1994).

2. R. J. Beelman, S. M. Sloan, and J. E. Fisher, "AP600 Quality Assured RELAP5 Input Model Description," Idaho National Engineering Laboratory report EGG-NRE-10824 (rough draft and proprietary) (Last revised: June 28, 1993).

3. P. R. Shire and J. W. Spore, "TRAC-PF1/MOD1 Analysis of a Minimum-Safeguards Large-Break LOCA in a US/Japanese PWR with Four Loops and 15x15 Fuel," Los Alamos National Laboratory report LA-2D/3D-TN-86-18 (December 1986).

4. "AP600 Design Change Description Report," Westinghouse Electric Corporation Proprietary Class 2C report (February 15, 1994).

5. R. Shaw, T. Yonomoto, and Y. Kukita, "Quick Look Report for ROSA/AP600 Experiment AP-DV-01," Draft Report, Thermohydraulic Safety Engineering Laboratory, Japan Atomic Energy Research Institute (December 1994).

6. Simplified Passive Advanced Light Water Reactor Plant Program, AP600 Standard Safety Analysis Report, Westinghouse Electric Corp document (June 26, 1992).

7. J. E. Fisher, "AP600 Double-Ended DVI Line Break ROSA Counterpart RELAP5/MOD3 Calculation," Lockheed Idaho Technologies Company DRAFT report (February 1995).

8. C. D. Fletcher, G. E. Wilson, C. B. Davis, and T. J. Boucher, "Interim Phenomena Identification and Ranking Tables for AP600 Small Break Loss-of-Coolant Accident, Main Steam Line Break, and Steam Generator Tube Rupture Scenarios," Idaho National Engineering Laboratory DRAFT report INEL-94/0061; Rev. 0 (November 1994).

9. G. E. Wilson, "Transmittal of AP600 T/H Consultants Meeting Minutes," Idaho National Engineering Laboratory letter J6008-GEW-09-95 to T. Lee (February 15, 1995).

10. B. E. Boyack, "AP600 Large-Break Loss-of-Coolant Accident Phenomena Identification and Ranking Tabulation," Los Alamos National Laboratory Draft document (January 3, 1995).

TABLE I

DATA BASE FOR TRAC MODEL

Component	TRAC Model Data Base
Reactor Vessel	
Vessel internal geometry	Westinghouse AP600 drawings.
Fuel-bundle geometry	Westinghouse AP600 drawings.
Fuel-rod reactivity coefficients	Assumption. Used USPWR plant model.[3]
Vessel flow and internal resistances	Westinghouse data.
Reactor Coolant System	
Hot- and cold-leg piping	Westinghouse AP600 drawings.
Reactor coolant pumps	Westinghouse rated values and COBRA/ TRAC homologous pump curves.
Steam generator	Internal geometry and thermal-hydraulic data from Westinghouse computer output.
Pressurizer and pressurizer surgeline	Westinghouse AP600 drawings.
Passive Safety Injection System	
CMT and accumulator tank geometry	Westinghouse dimensions and volumes.
Injection line piping	Westinghouse reduced-size AP600 drawings. Dimensions approximated for illegible values.
CMT pressure balance lines	Westinghouse AP600 drawings.
Check valves	0.4 psi to open, based on Westinghouse in-situ check-valve tests, -0.4 psi to close, assumed.
Flow resistances	Westinghouse, design-basis flows and resistances.

Control systems	Information provided by Westinghouse for some trips but not all.
Trips, set points, and delay times	
Pressurizer pressure and level control	These and other plant control systems adapted from a TRAC model of a Westinghouse three-loop plant.
Steam generator level control	
Automatic Depressurization System	
ADS valve piping geometry	Westinghouse drawings
ADS valve areas	Westinghouse specified
ADS spargers	Westinghouse drawings
Flow resistances	Westinghouse design-basis flows and resistances.
Passive Residual Heat Removal System	
Inlet and outlet piping geometry	Westinghouse drawings
Heat exchanger geometry	Westinghouse drawing and specified tube geometry
Flow resistances	Westinghouse-specified flow resistances
In-Containment Refueling Water Storage Tank	
Tank geometry, volume, and surface area	Westinghouse drawings and tabulated data.
Drain lines	INEL calculation sheets

TABLE II

IBLOCA SEQUENCE OF EVENTS

Time (s)	Event
0.0	Break occurs in DVI line A next to vessel.
8.3	Reactor trip on low pressurizer pressure
9.2	S signal on low pressurizer pressure. Steam generator feedwater control valves starts to close.
10.4	PRHRS isolation valve starts to open. CMT isolation valves start to open.
18.9	Main steam line isolation valves start to close.
25.4	Reactor coolant pumps trip.
152.5	67% liquid volume fraction reached in CMT-A (broken DVI line).
172.6	ADS stage 1 control-valve trip signal. Stage 1 of ADS train B starts to open. Stage 1 of ADS train A assumed to be inoperative and does not open. Stage 1 valve opening time: 25 s.
242.7	ADS Stage 2 control-valve trip signal. Stage 2 valves of both ADS trains start to open. Stage 2 valve opening time: 105 s.
255.2	20% CMT level signal. This signal, plus a 120-s delay after Stage 3 valves opens, allows actuation of ADS Stage 4 valves.
328	Flow through IRWST drain line-B (broken DVI line) begins.
337	CMT-A (broken DVI line) empties.
362.7	ADS Stage 3 control-valve trip signal. Stage 3 of ADS train A starts to open. Stage 3 of ADS train B assumed to be inoperative and does not open. Stage 3 valve opening time: 105 s.
482.7	ADS Stage 4a and 4c valves start to open. 85% valve area assumed. Valve opening time: 20 s.
512.7	ADS Stage 4b and 4d valves start to open. 85% valve area assumed. Valve opening time: 20 s.
516	Accumulator-A (broken DVI line) empties.
623	Accumulator-B (intact DVI line) empties.
631	Flow through IRWST drain line-A (intact DVI line) begins.

TABLE III

COMPARISON OF ROSA AND AP600 IBLOCA EVENTS

Test AP-DV-01 [time (s)]	Calculation for AP600 [time (s)]
Break initiated [0]	Break initiated [0]
Broken ACC injection begins [0+]	Broken ACC injection begins [0+]
Scram signal [12]	Scram signal [8.3]
S signal [14]	S signal [9.2]
CMT signal [14]	CMT signal [9.2]
Upper plenum saturation [15]	
RCPs begin to increase speed [17]	NA
Main feedwater terminated [17]	Main feedwater terminated [10.4]
CMT injection valves open [18]	CMT isolation valves start to open [10.4]
Natural circulation begins in PRHR [21]	Natural circulation begins in PRHR [11.1]
Actual initiation of power decay [36]	Initiation of power decay [8.3]*
Pressurizer empty [40]	Pressurizer empty [18]
Initiation of pump coastdown [50]	Initiation of pump coastdown [25.4]
Boiling in core [50]	Boiling in core [33]
Broken CMT liquid level decreasing [60]	Broken CMT liquid level decreasing [27.8]*
SG U-tubes empty [120]	SG U-tubes empty [150] down leg
Downcomer liquid level at cold legs [130]	Downcomer liquid level at cold legs [~200]*
ADS signal [160]	ADS signal [152.5]
Two-phase discharge at PSIS side of break [160]	Two-phase discharge at PSIS side of break [152.5]
Broken ACC discharge terminated (temporary) [170]	Broken ACC discharge terminated (temporary) [163]
ADS-1 valve opened [180]	ADS-1 valve starts to open [172.6]
Intact ACC injection begins [180]	Intact ACC injection begins [225]
ADS-2 valve opened, ADS-1 valve closed [250]	ADS-2 valve starts to open, ADS-1 remains open [242.7]
ACC discharge resumes [275]	Broken ACC discharge resumes [325]
Broken CMT empty [300]	Broken CMT empty [335]
Broken ACC empty [330]	Broken ACC empty [525]*
ADS-3 valve opened [375]	ADS-3 valve starts to open [362.7]
ADS-4 valves opened [505]	ADS-4 valves start to open [482.7]
Intact ACC empty [550]	Intact ACC empty [623]
IRWST injection started [600]	IRWST injection started [631]
Subcooling regained in lowest core [1500]	Calculation terminated at 700 s
Intact CMT empty [2700]	Calculation terminated at 700 s
Experiment terminated [3800]	

* Events for which the TRAC-calculated sequence for AP600 differs from AP-DV-01.

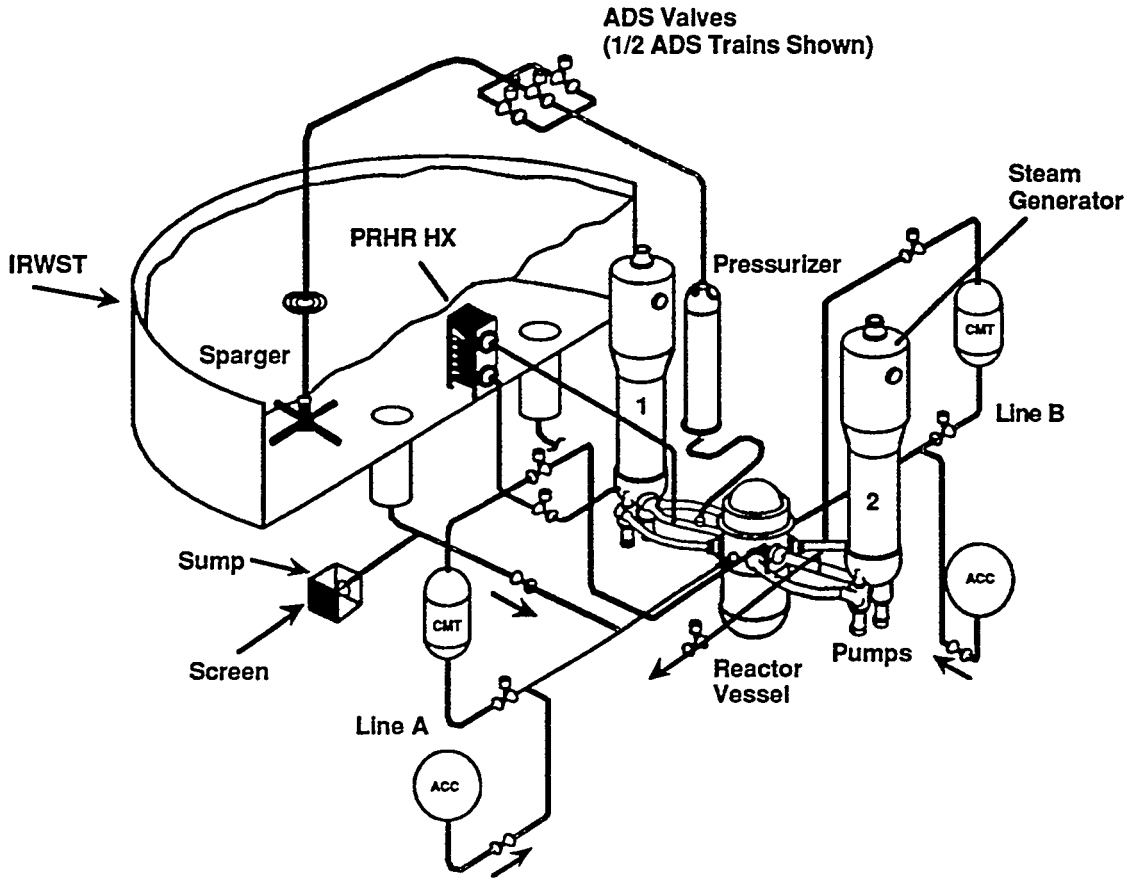

Fig. 1. AP600 plant isometric.

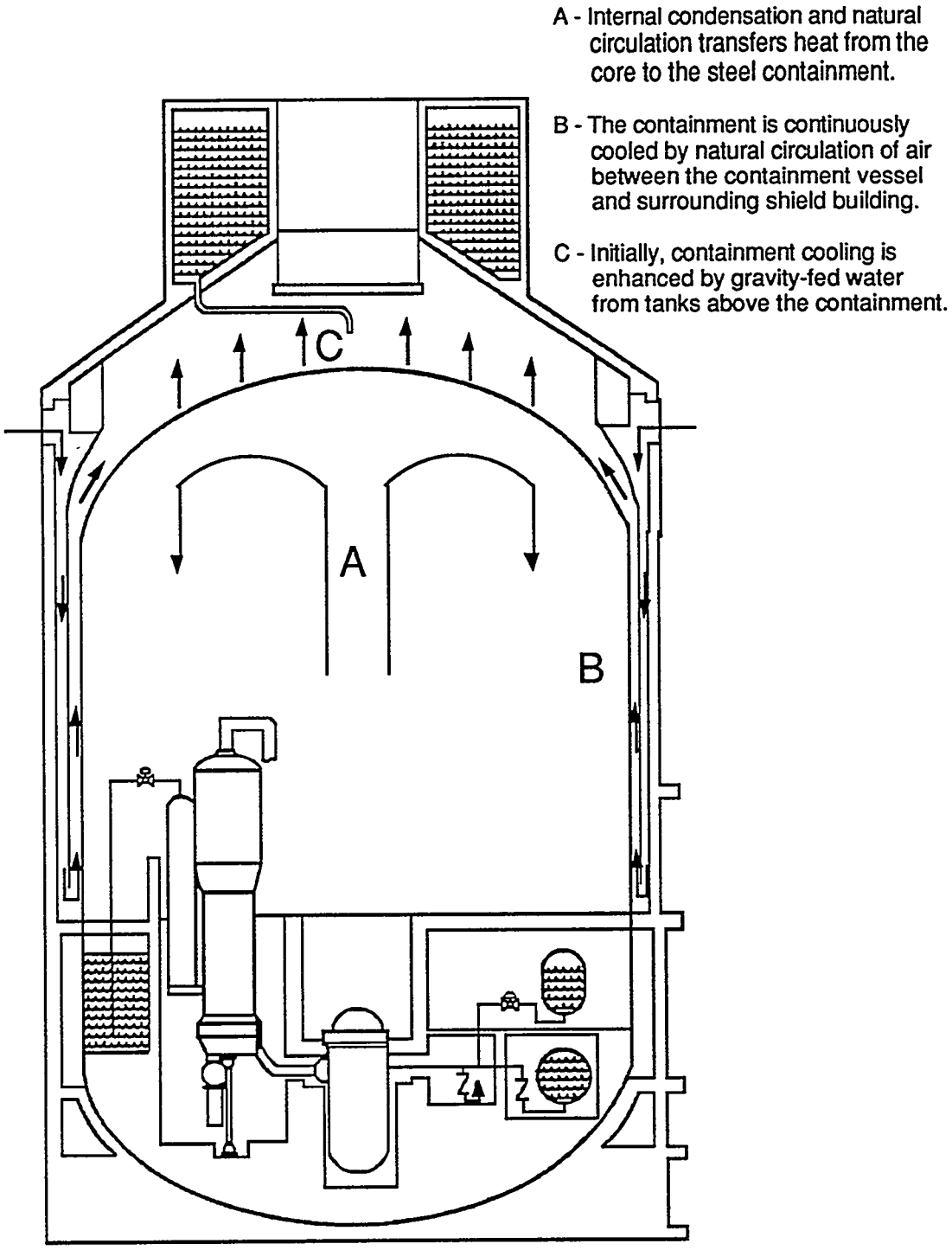

Fig. 2. AP600 containment cutaway view.

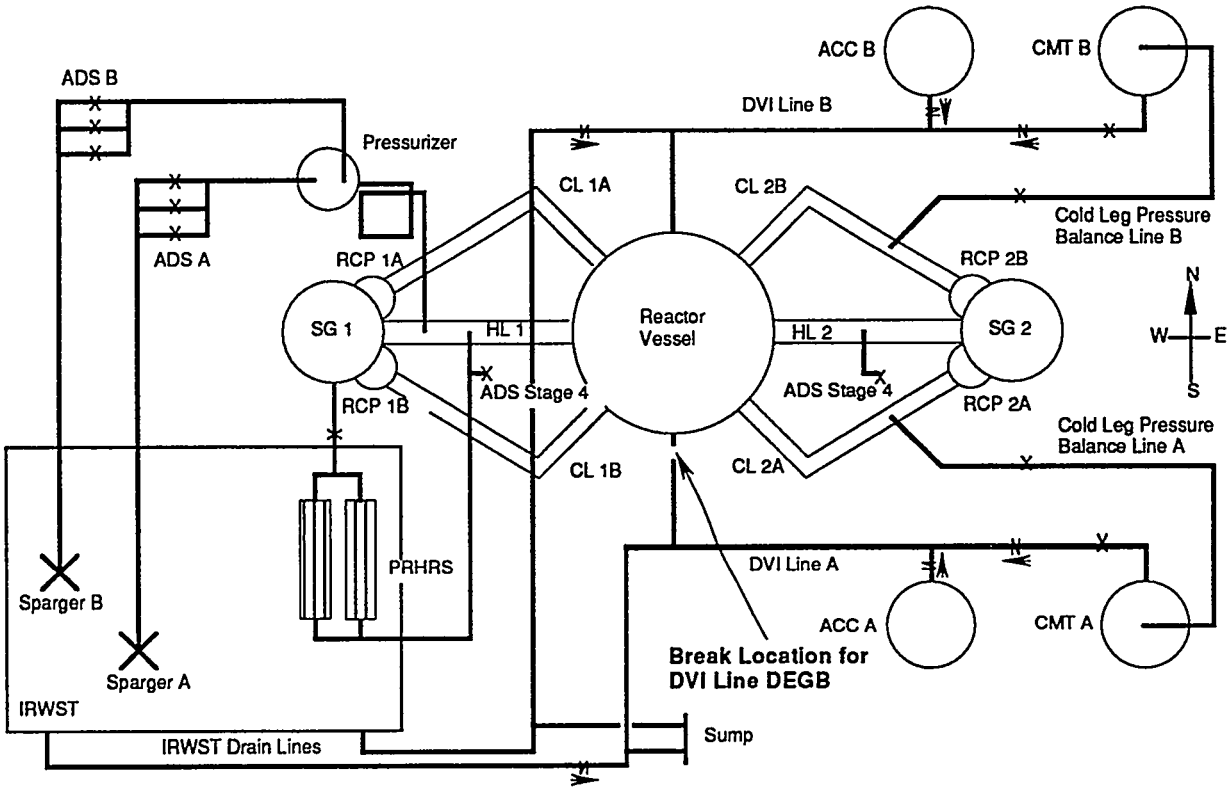

Fig. 3. Schematic of AP600 reactor coolant system and passive safety systems.

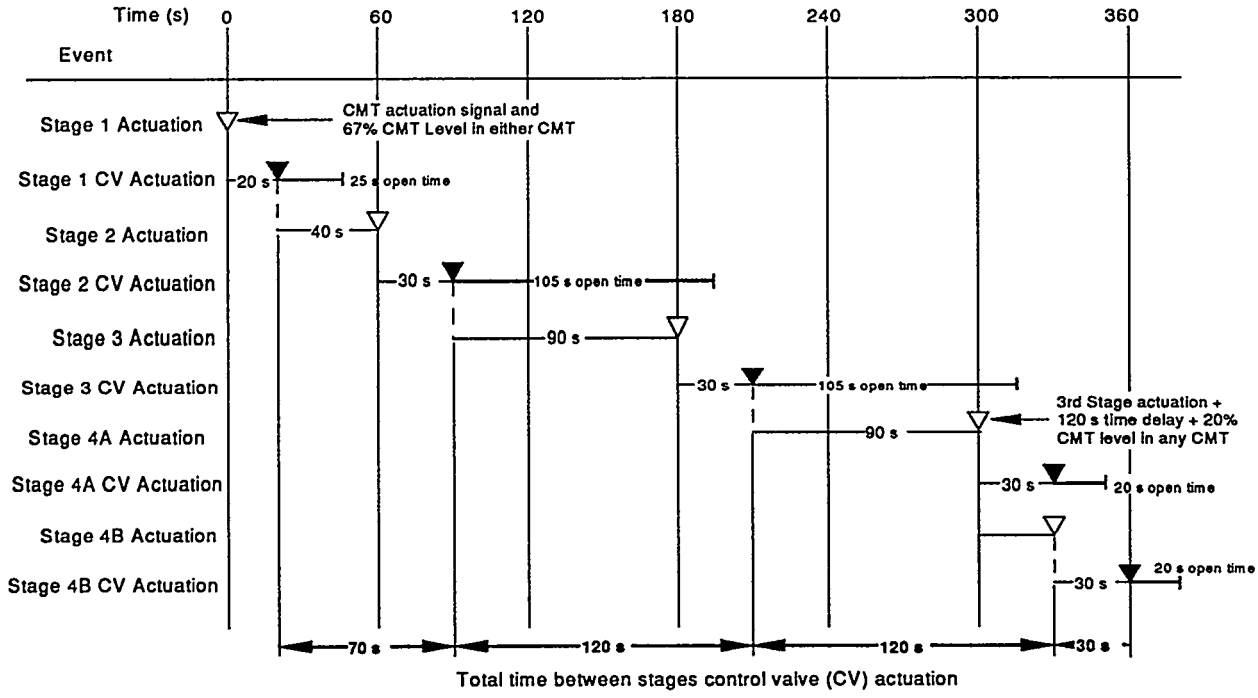

Fig. 4. ADS actuation logic.

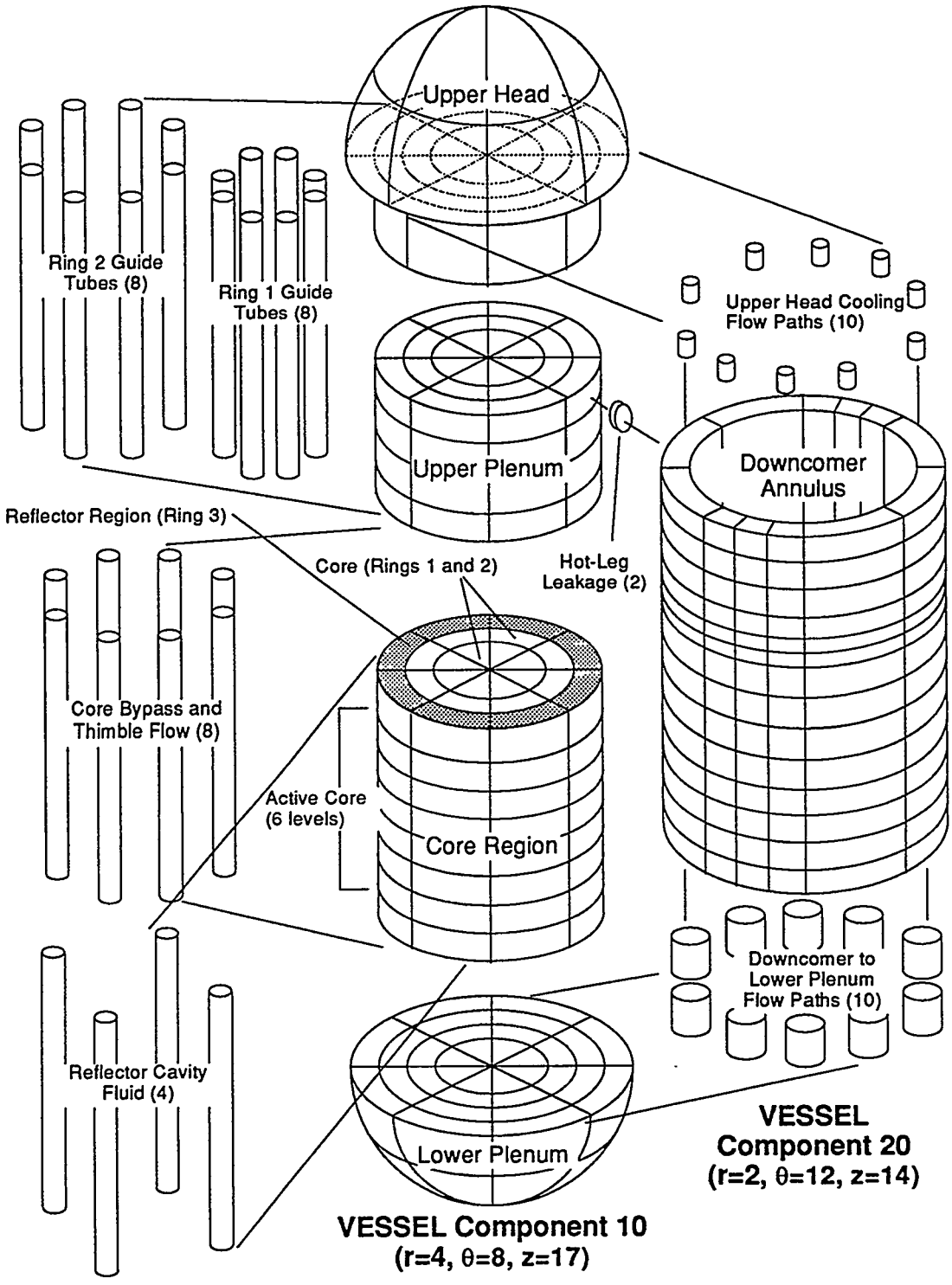

Fig. 5. Isometric view of reactor vessel model.

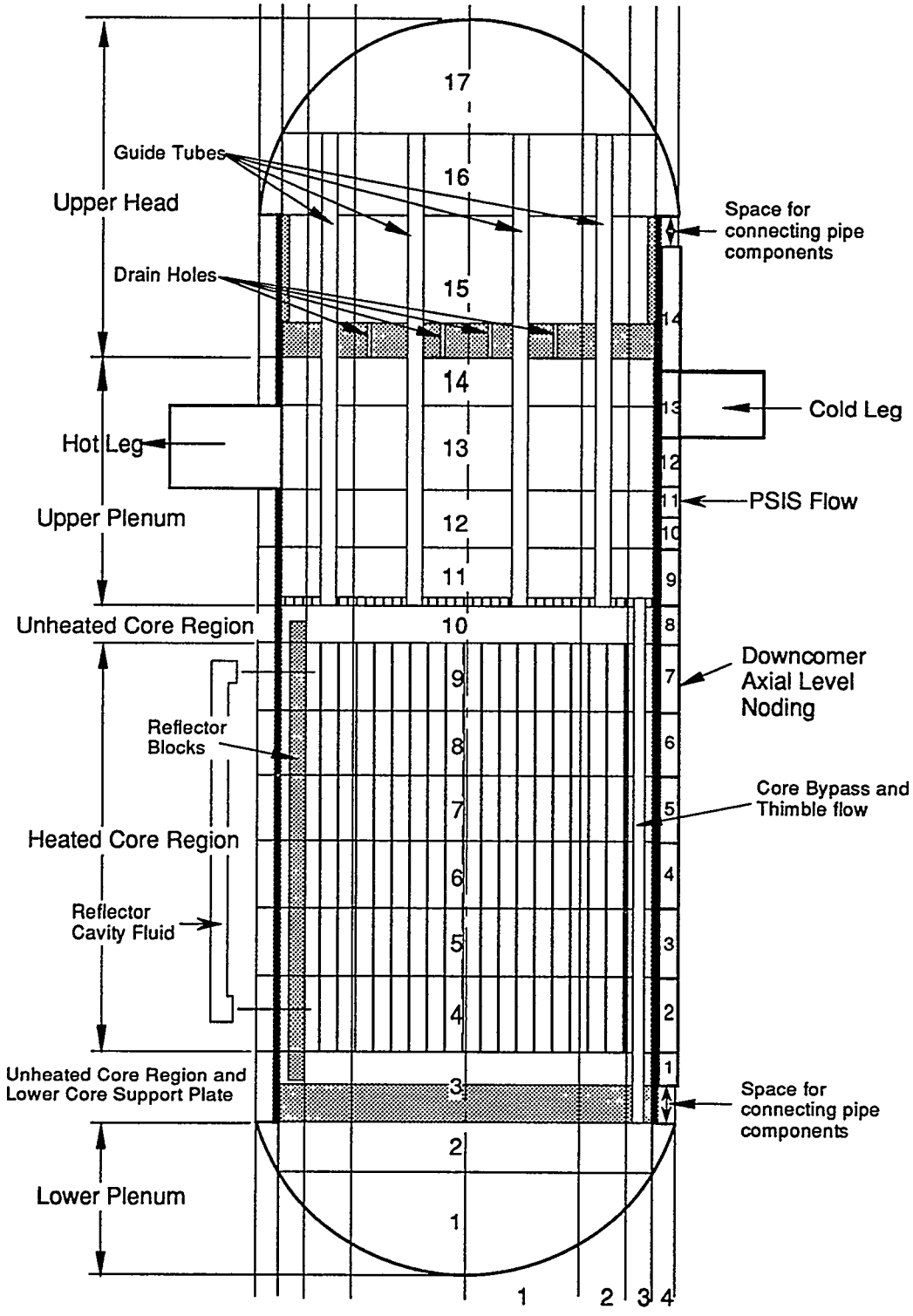

Fig. 6. Elevation view of reactor vessel model including downcomer noding.

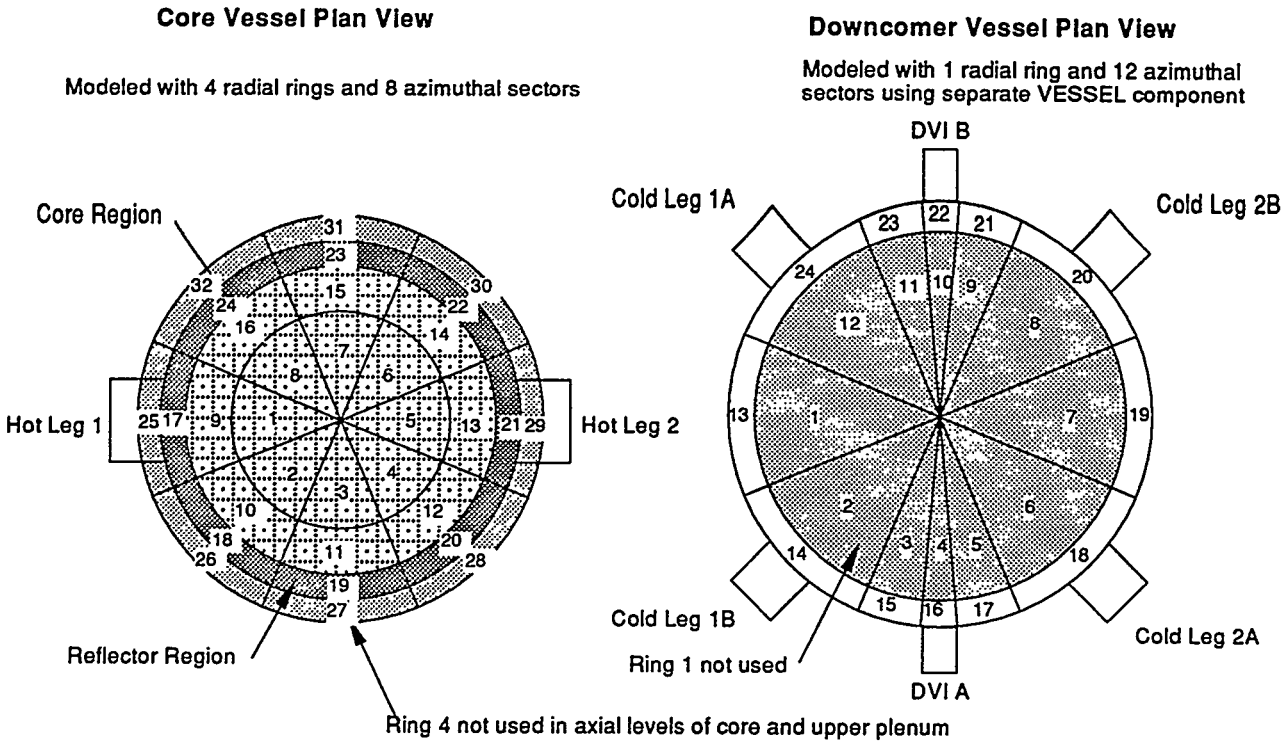

Fig. 7. Plan views of reactor vessel model.

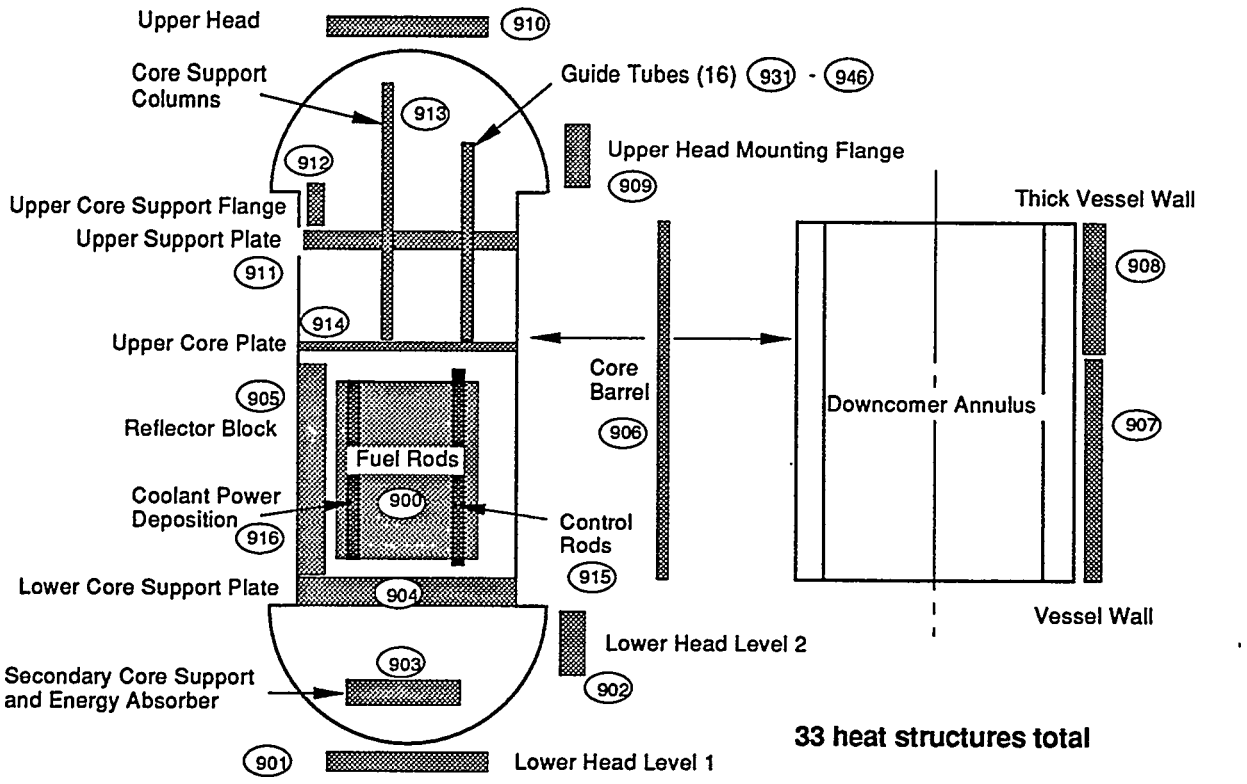

Fig. 8. Reactor vessel heat structures.

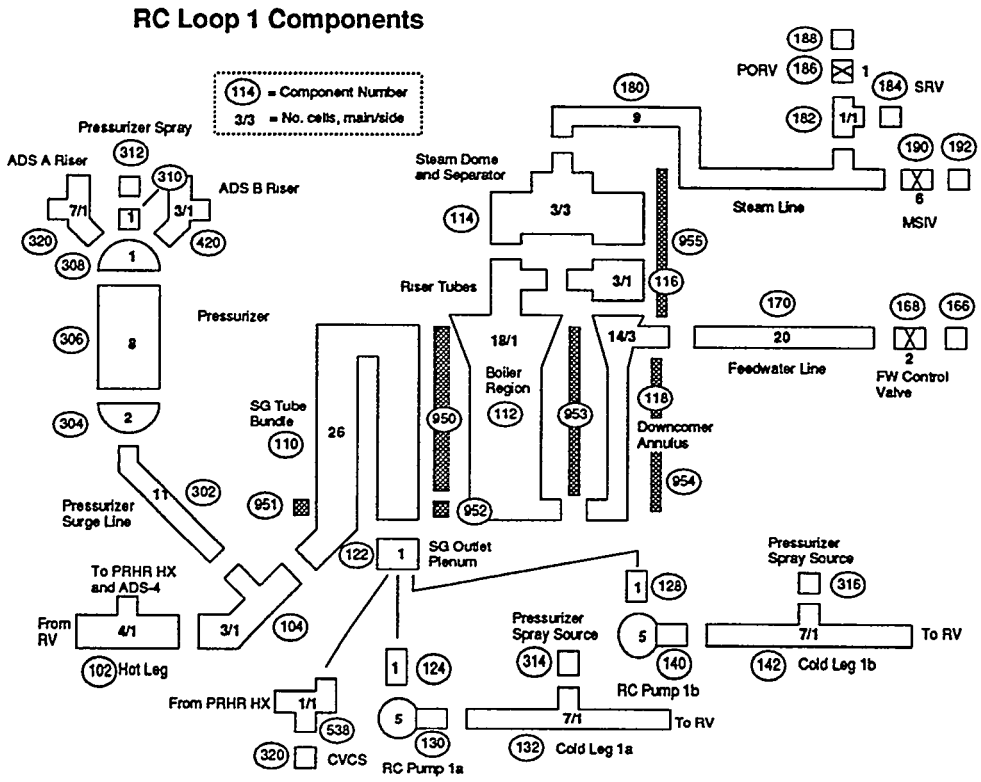

Fig. 9. Reactor coolant loop 1 model overview.

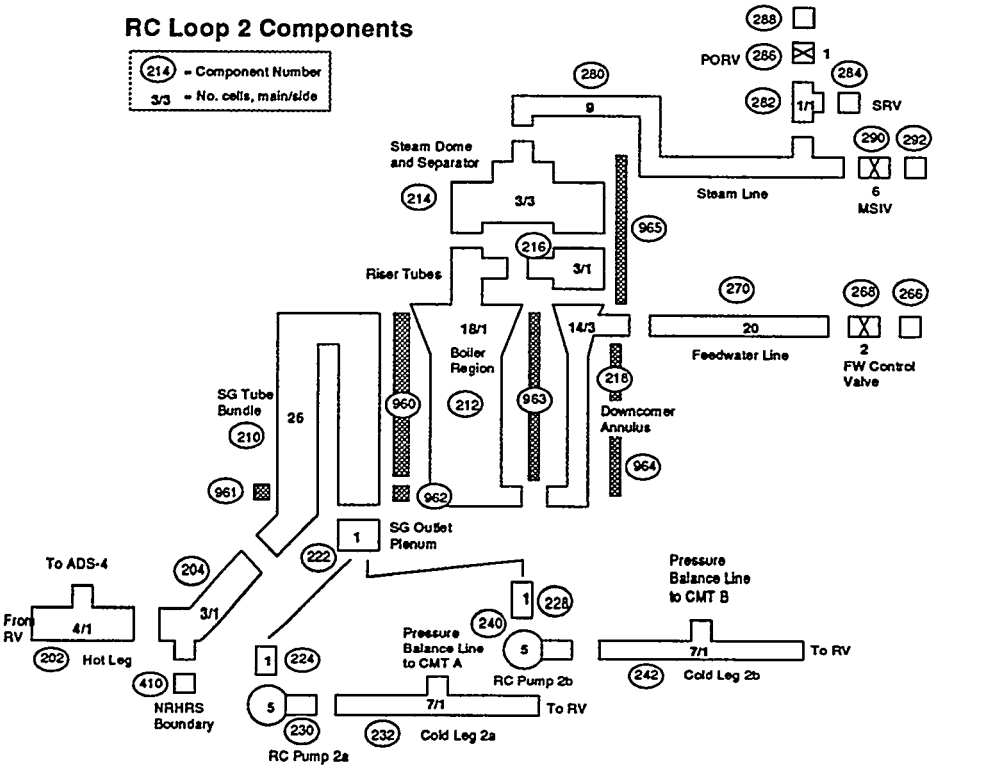

Fig. 10. Reactor coolant loop 2 model overview.

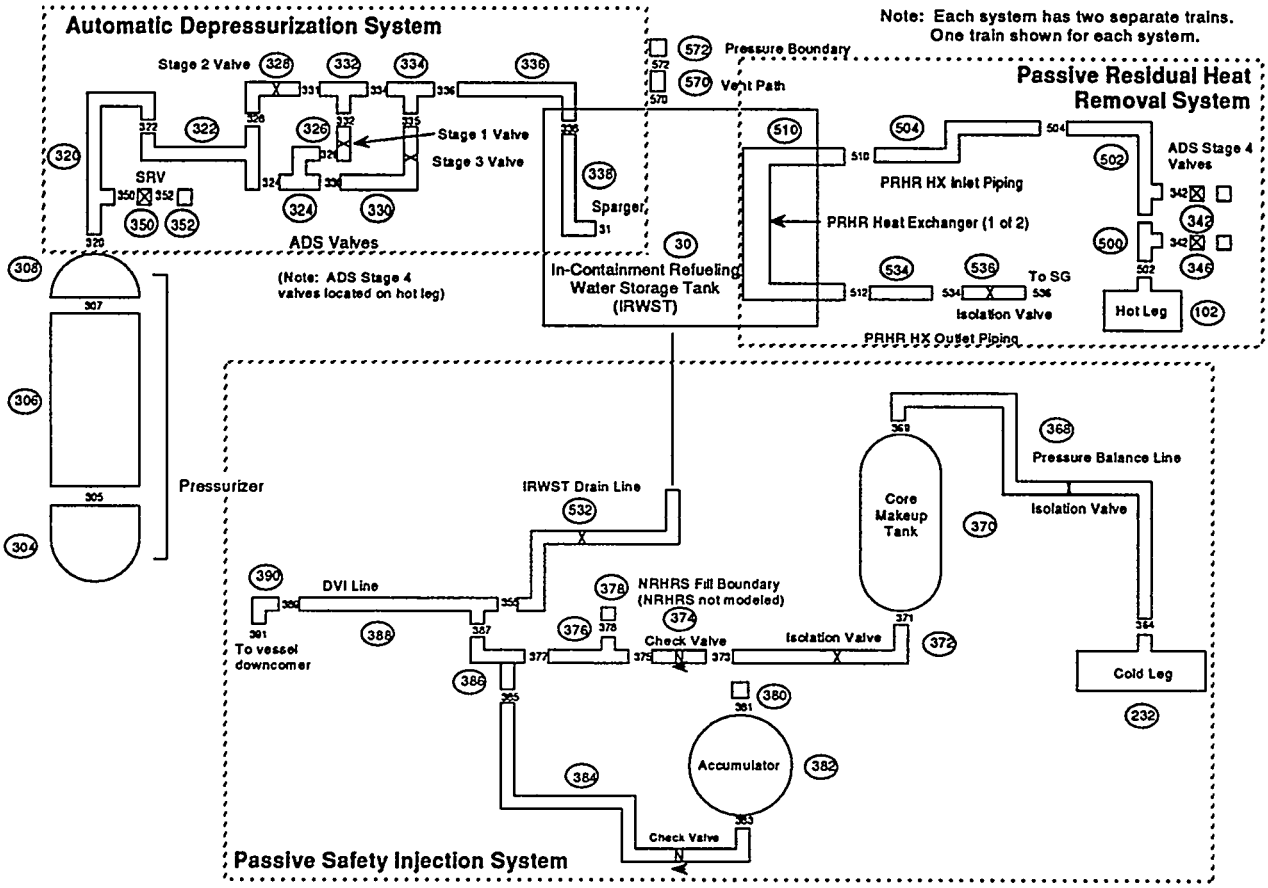

Fig. 11. Passive Safety Systems model overview.

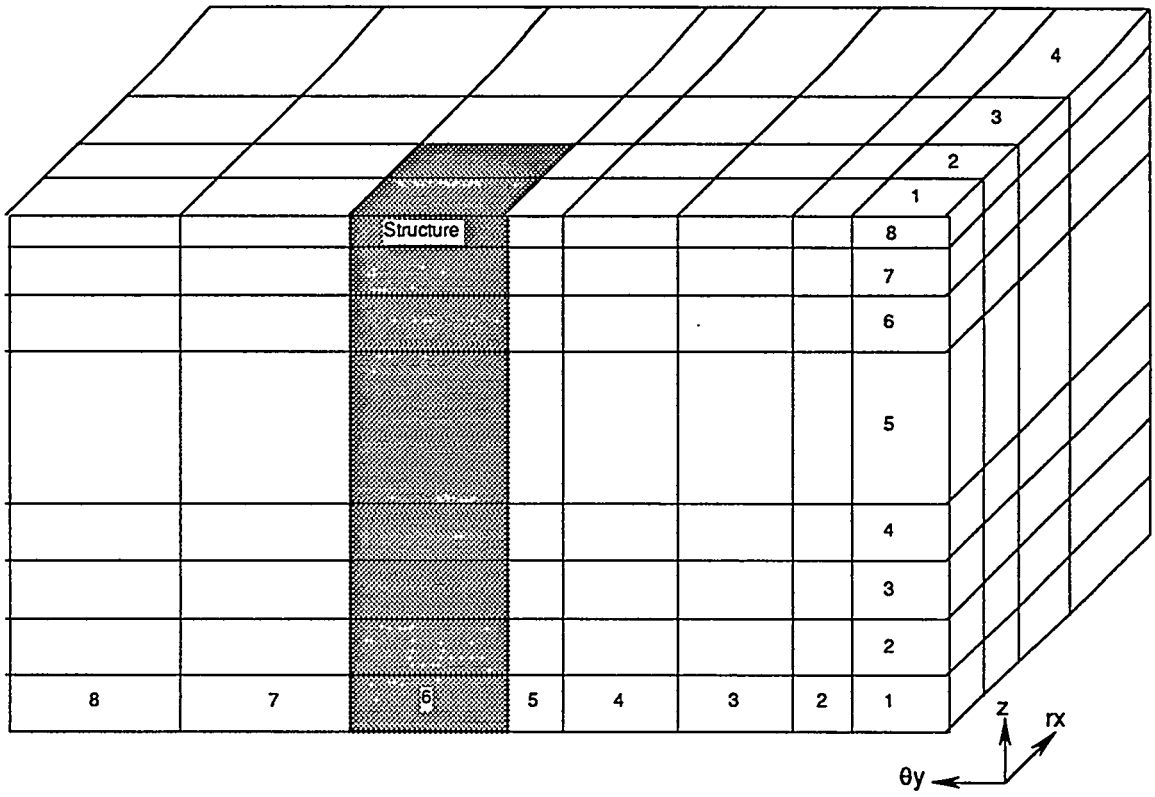

Fig. 12a. IRWST multidimensional model - overview.

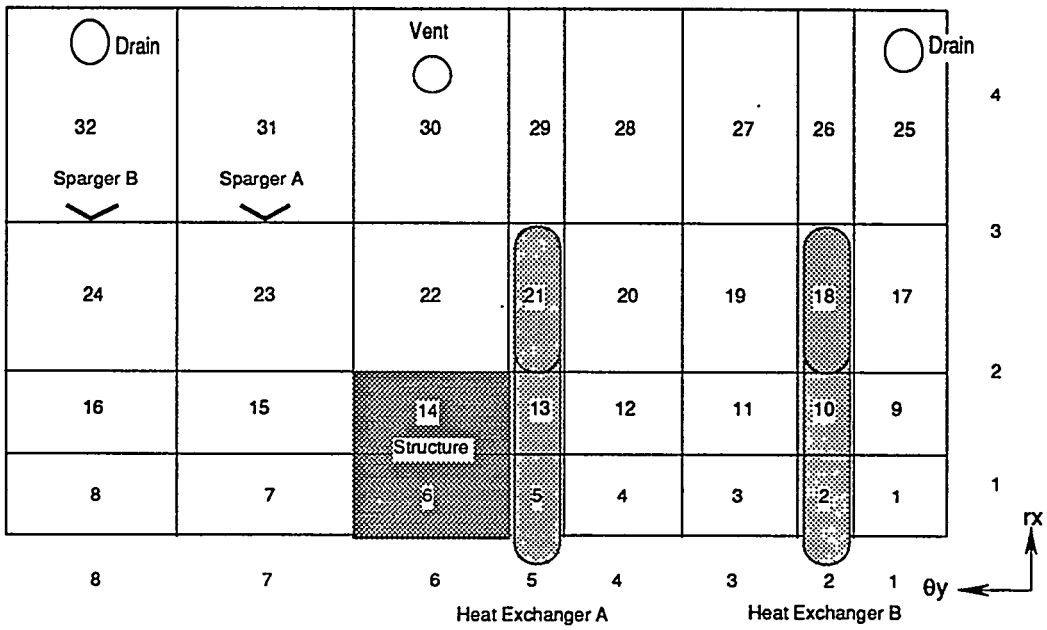

Fig. 12b. IRWST multidimensional model - top view.

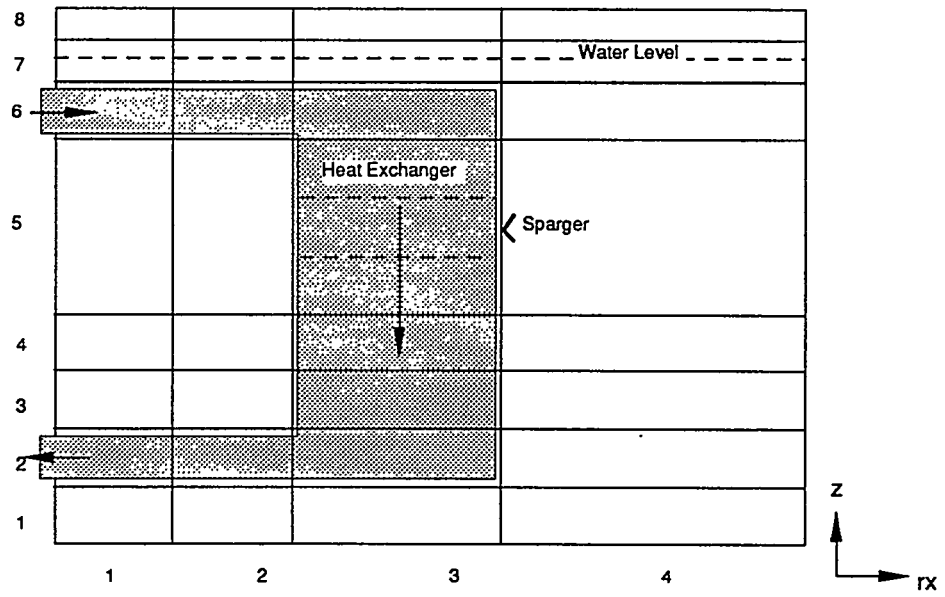

Fig. 12c. IRWST multidimensional model - side view.

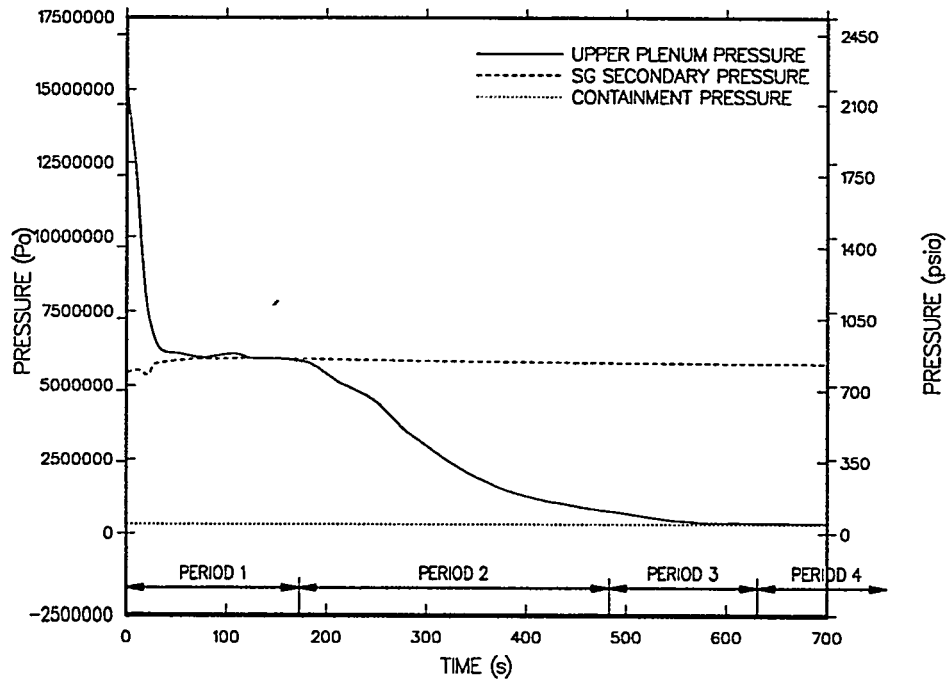

Fig. 13. Primary and secondary pressures.

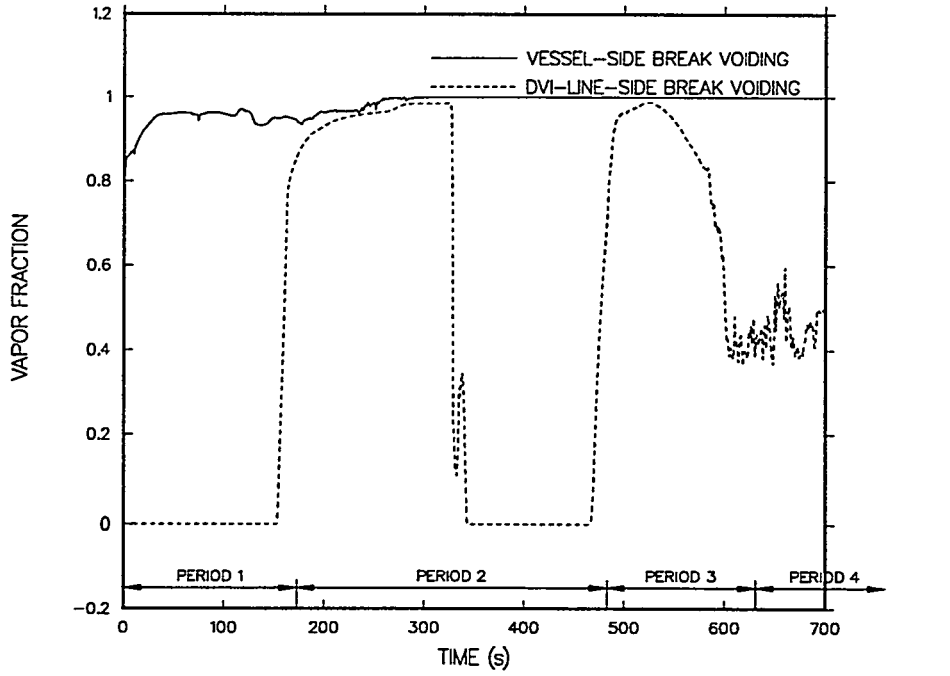

Fig. 14. Break exit voiding.

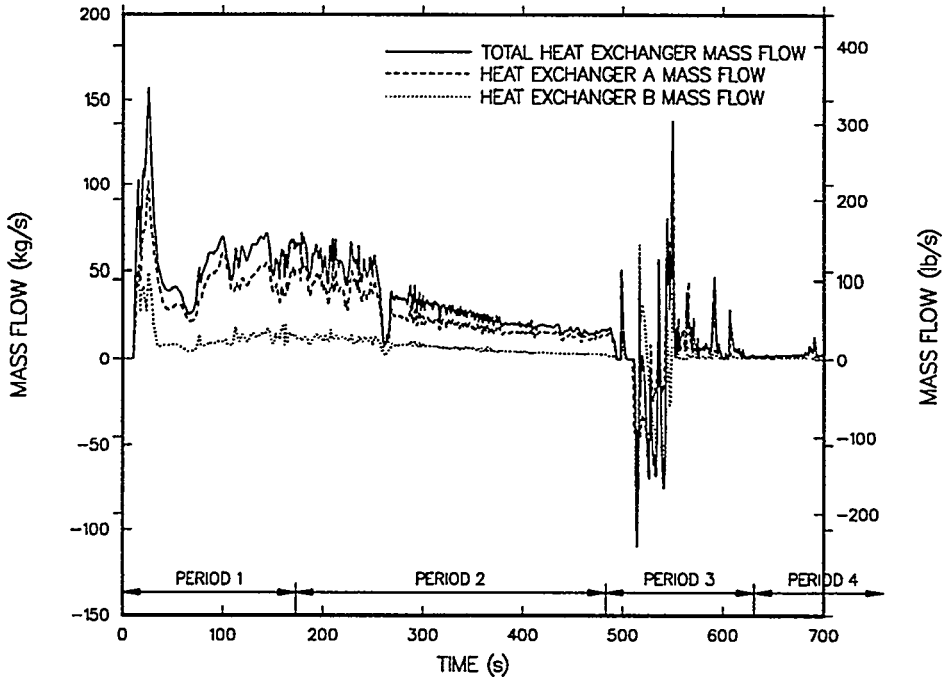

Fig. 15. PRHRS heat exchanger masss flows.

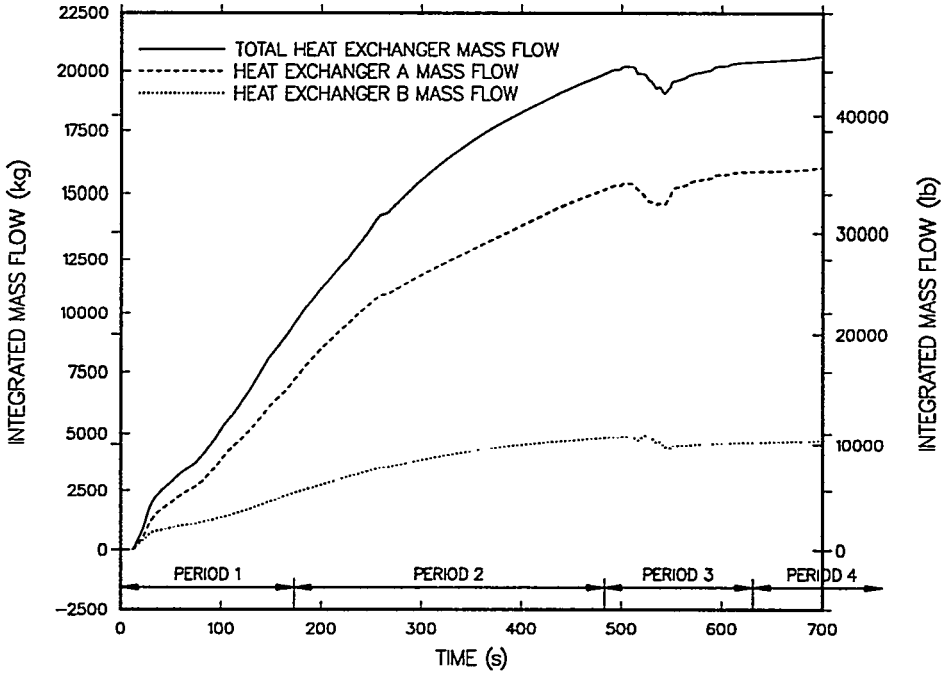

Fig. 16. PRHRS integrated heat exchanger mass flows.

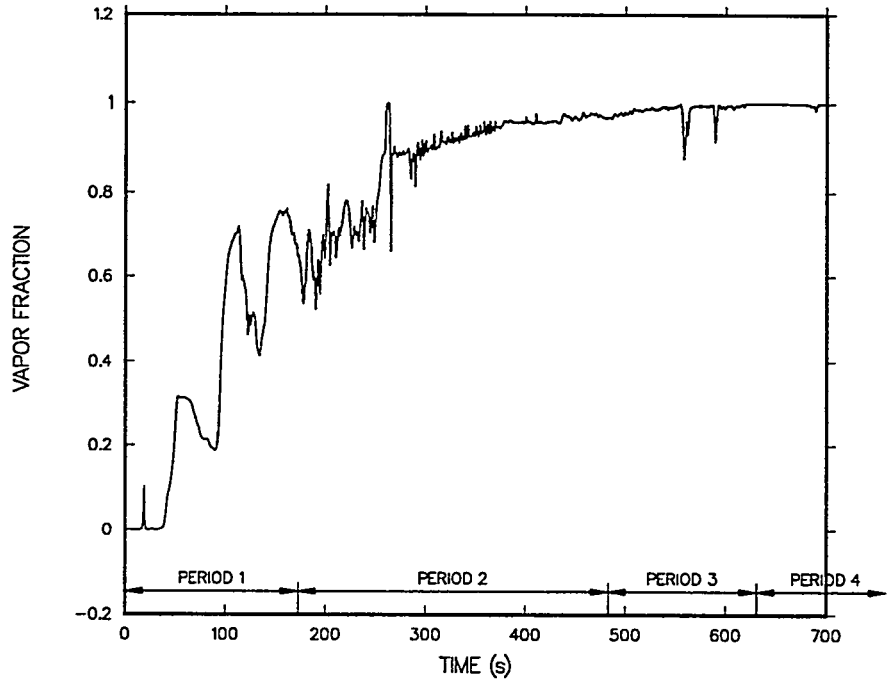

Fig. 17. PRHRS inlet line voiding.

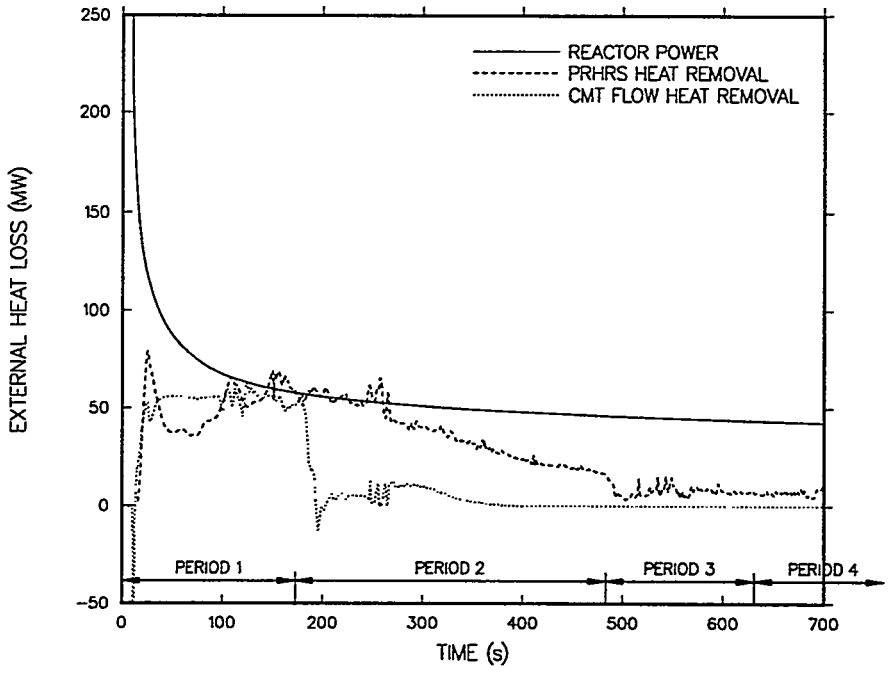

Fig. 18. Heat generation and removal rates.

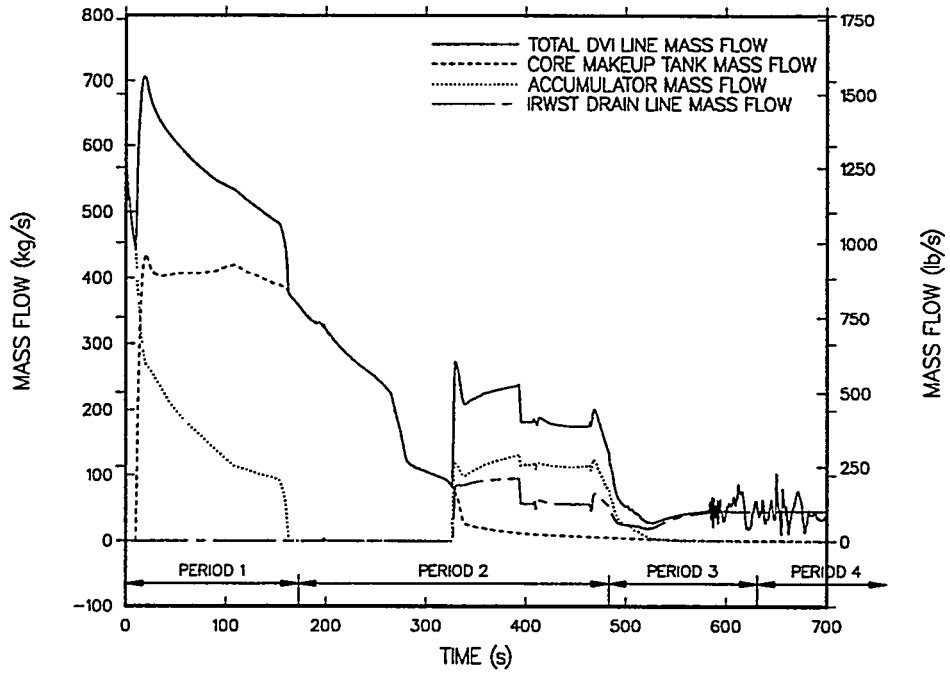

Fig. 19. Broken DVI line mass flows.

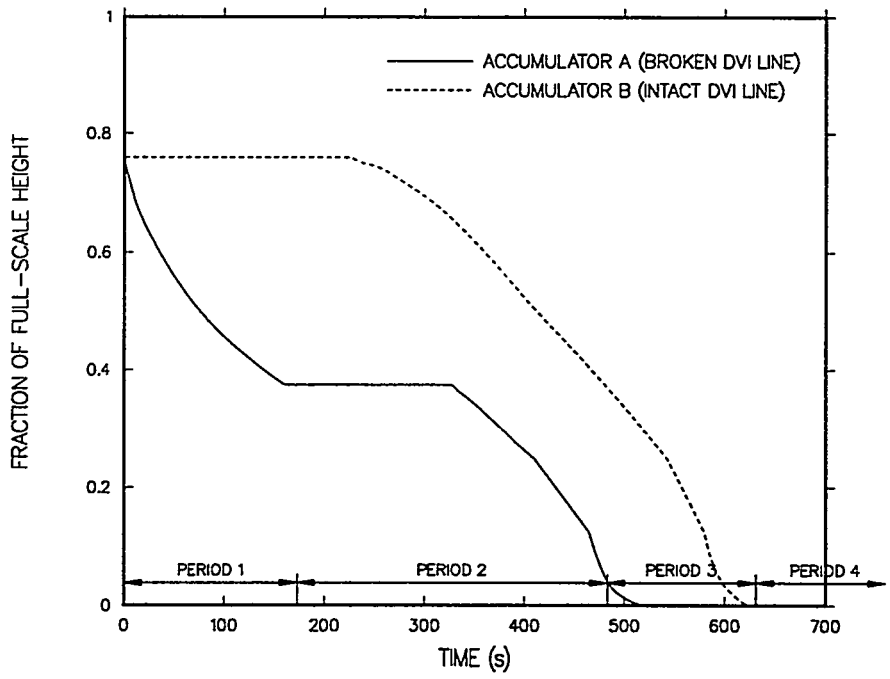

Fig. 20. Accumulator tank liquid levels.

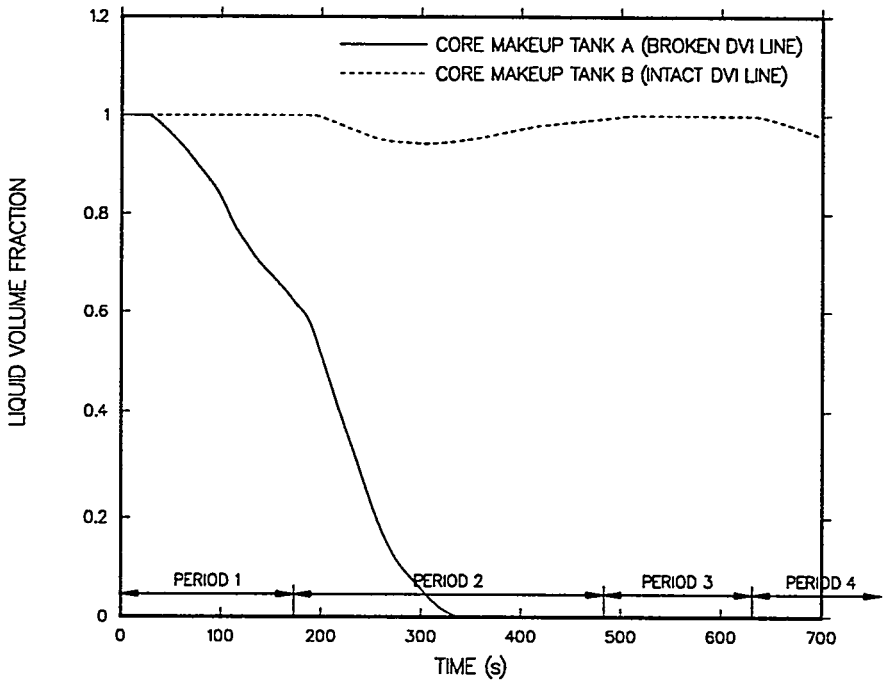

Fig. 21. CMT liquid volume fractions.

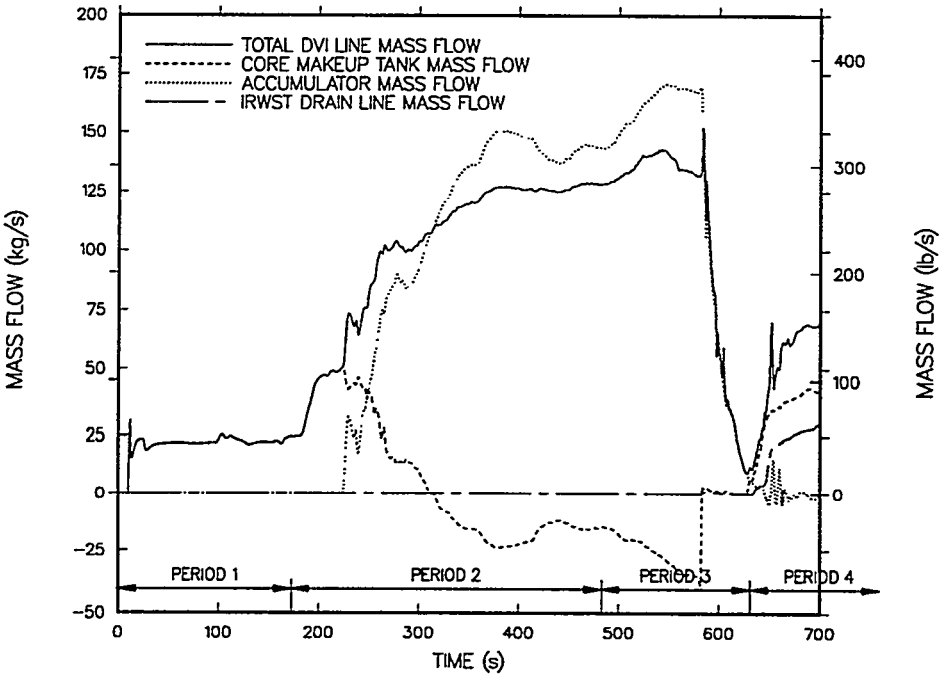

Fig. 22. Intact DVI line mass flows.

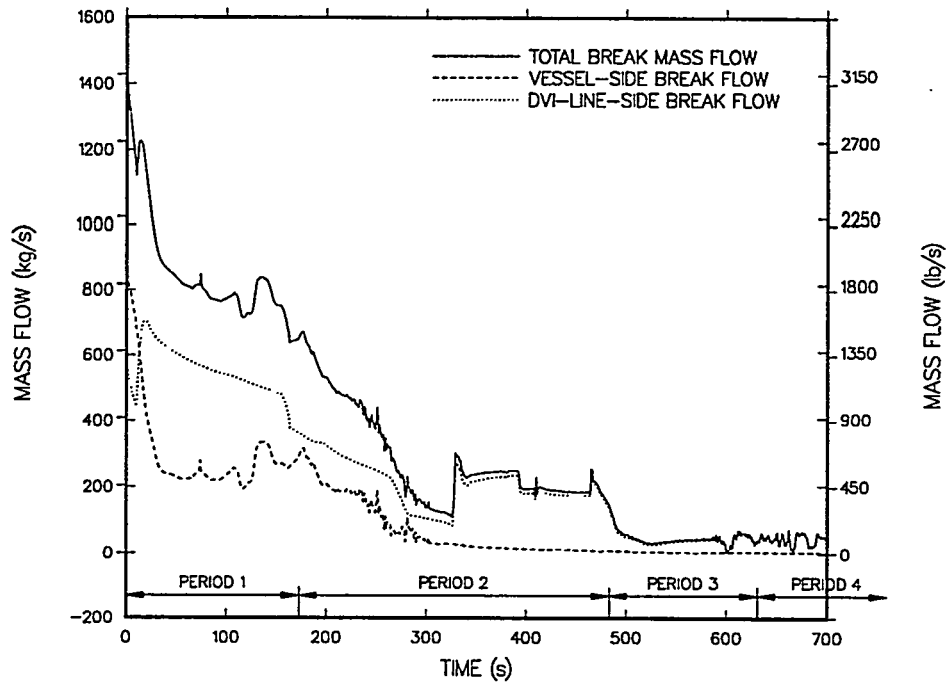

Fig. 23. Break mass flows.

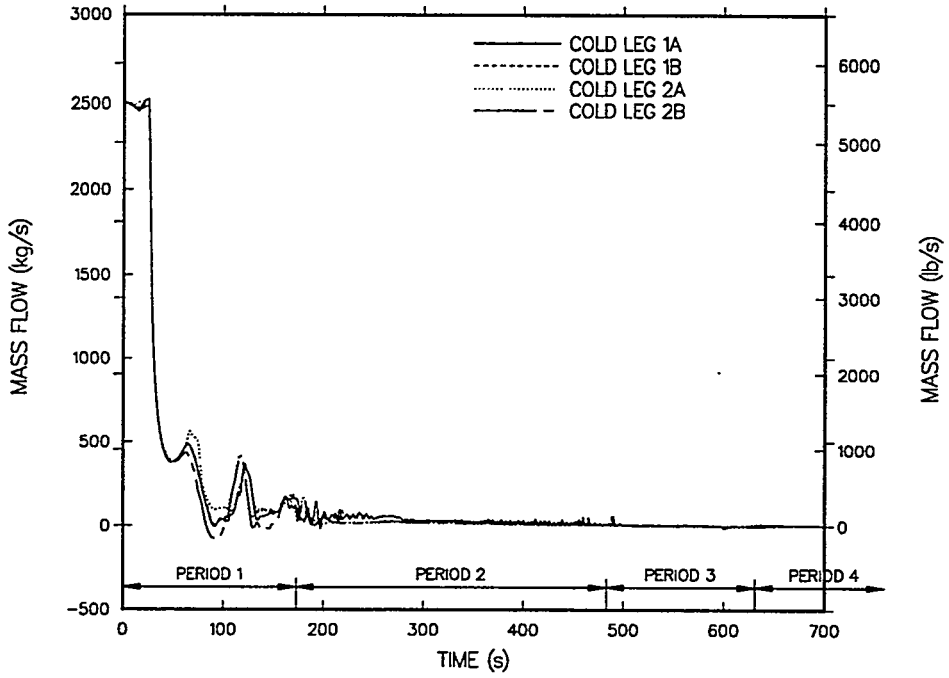

Fig. 24. Cold leg mass flows.

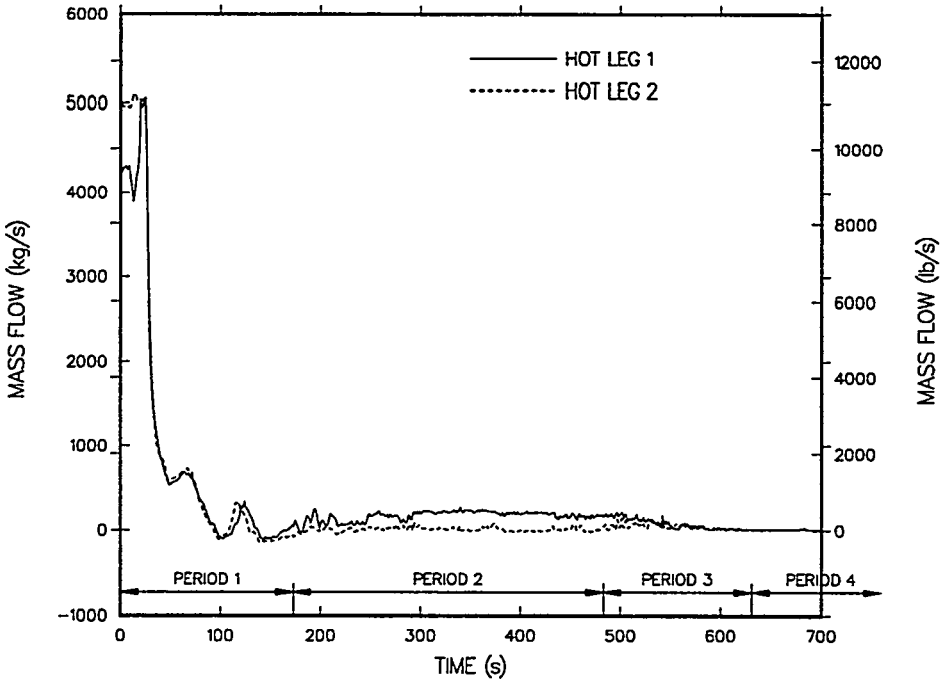

Fig. 25. Hot leg mass flows.

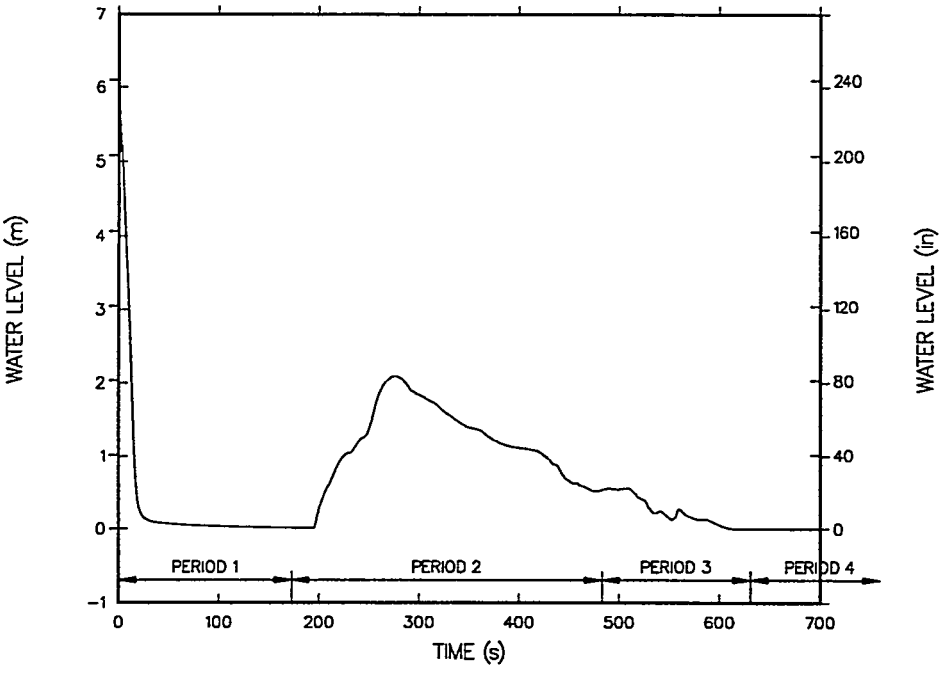

Fig. 26. Pressurizer collapsed liquid level.

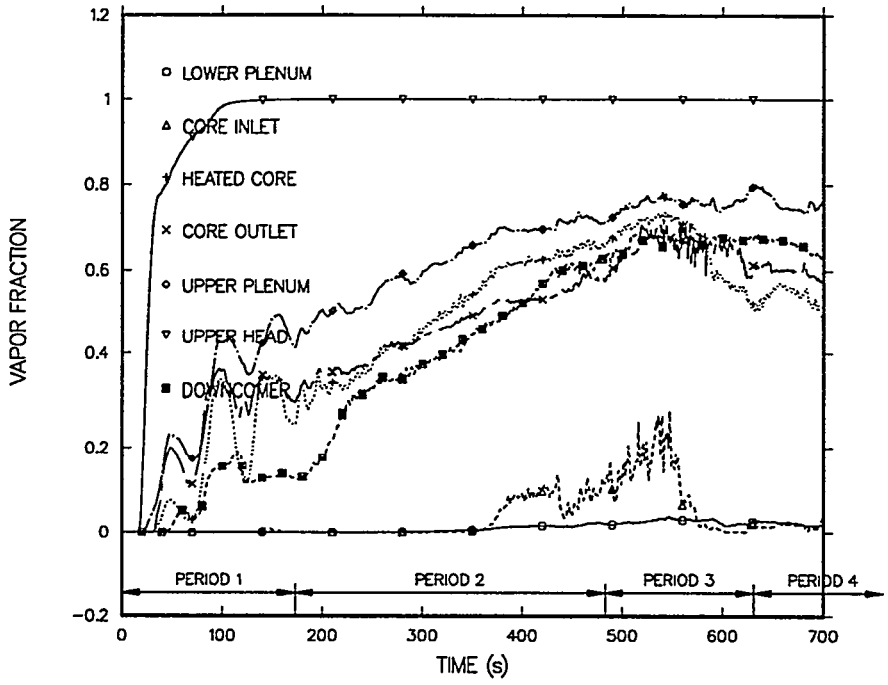

Fig. 27. Vessel vapor fractions.

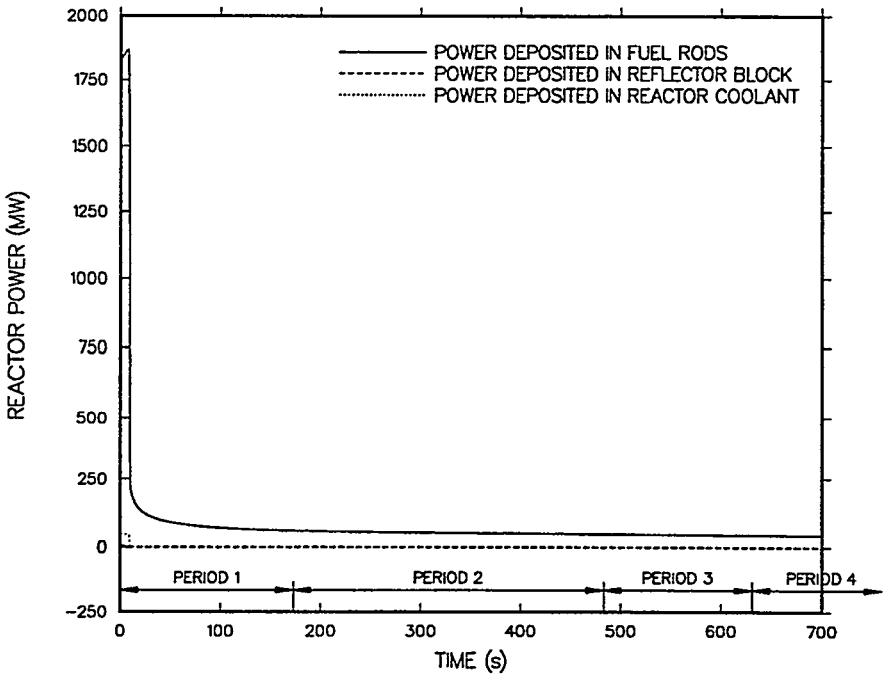

Fig. 28. Reactor power.

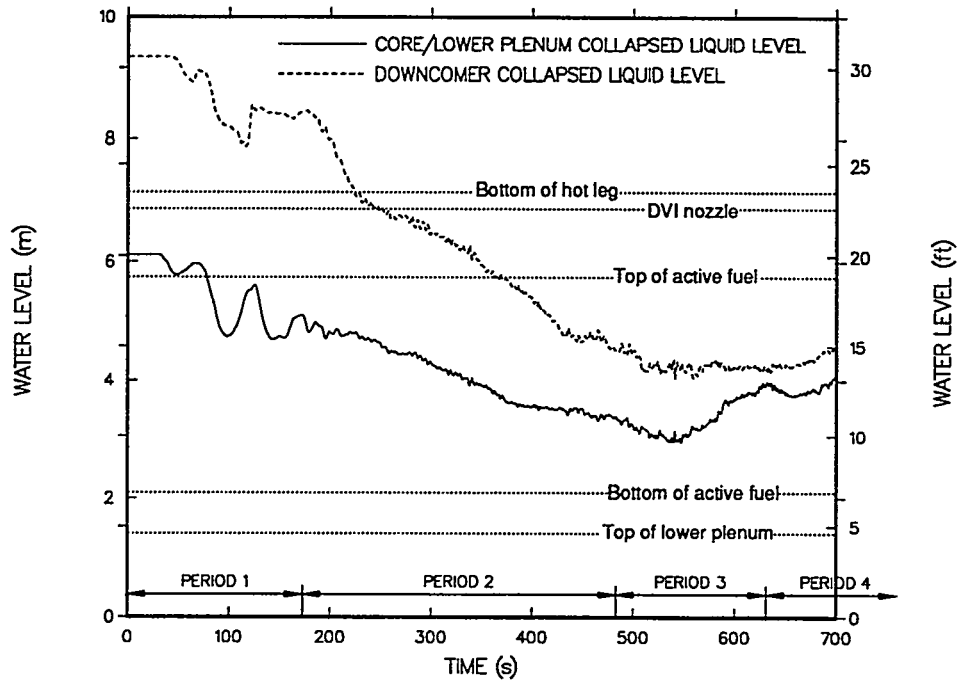

Fig. 29. Downcomer and core collapsed liquid levels.

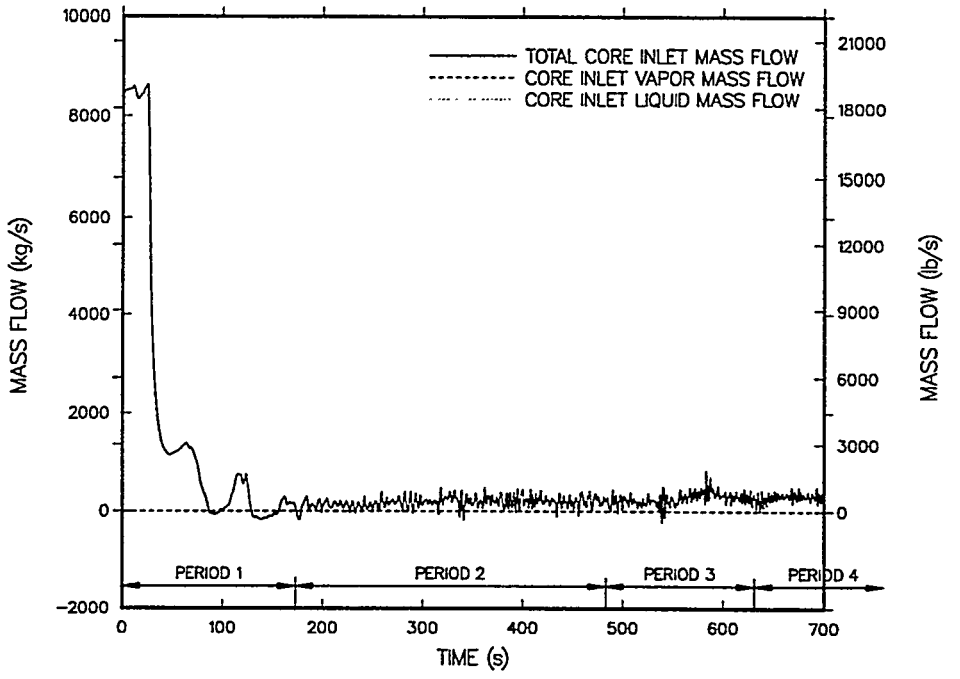

Fig. 30. Core inlet mass flow.

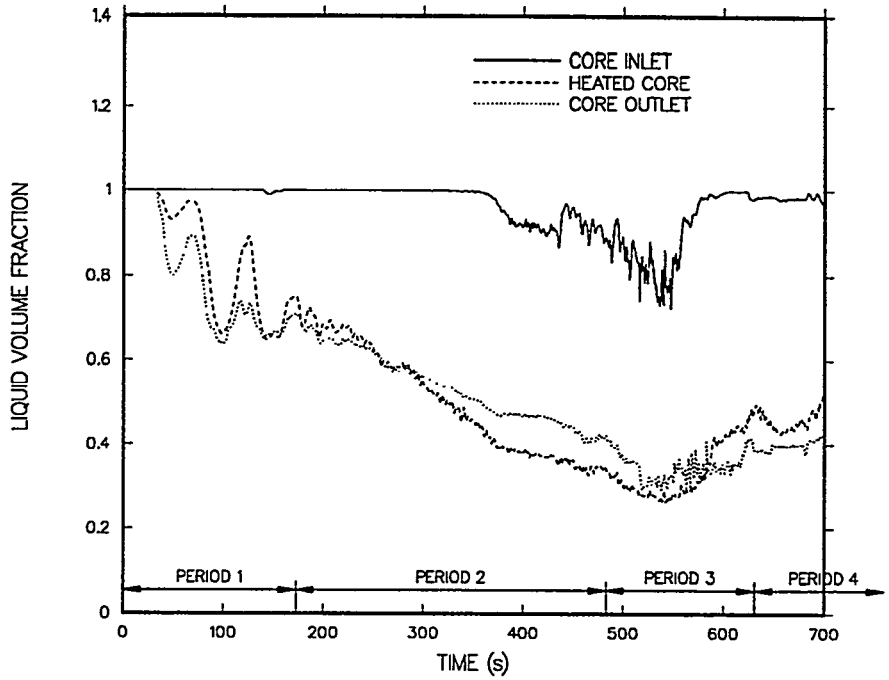

Fig. 31. Core region liquid volume fractions.

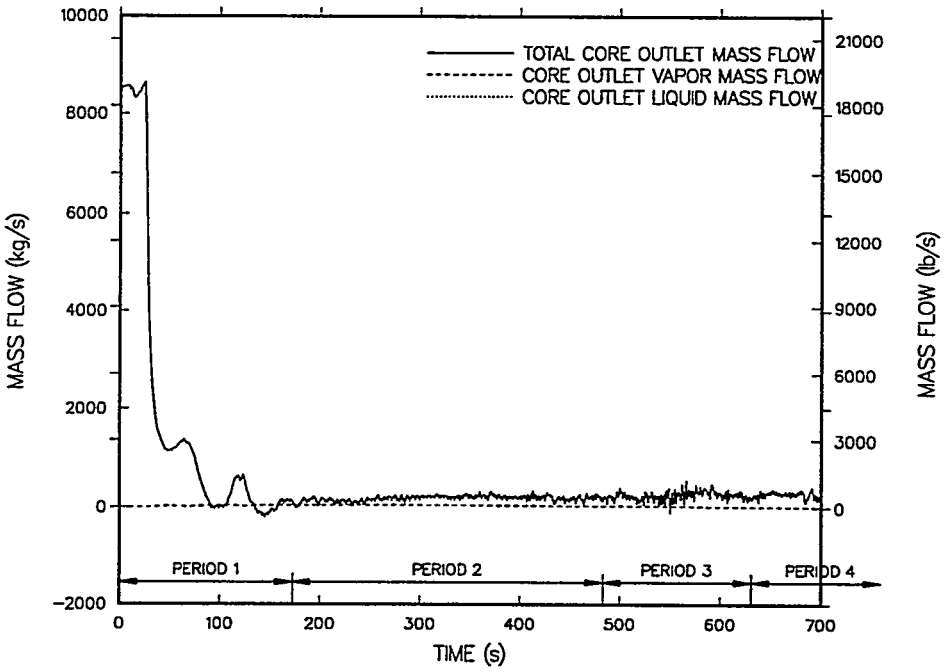

Fig. 32. Core outlet mass flows.

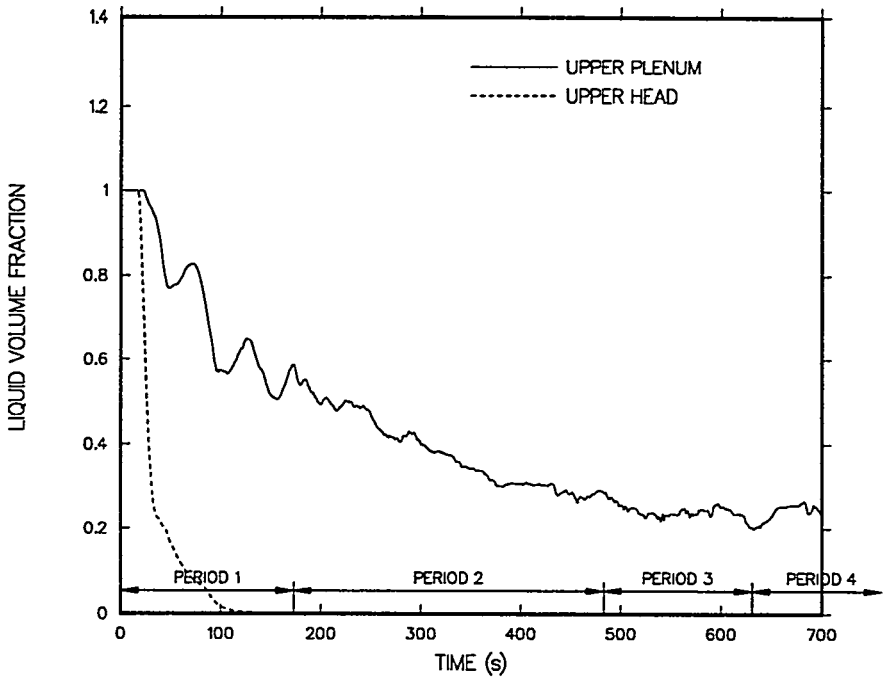

Fig. 33. Upper plenum and upper head liquid volume fractions.

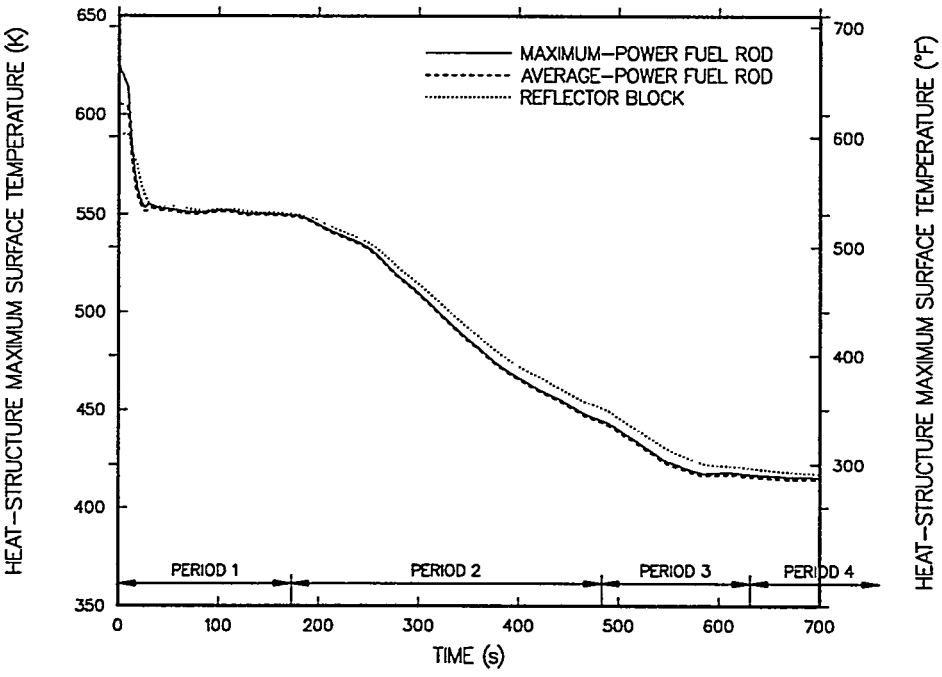

Fig. 34. Maximum cladding and reflector block temperatures.

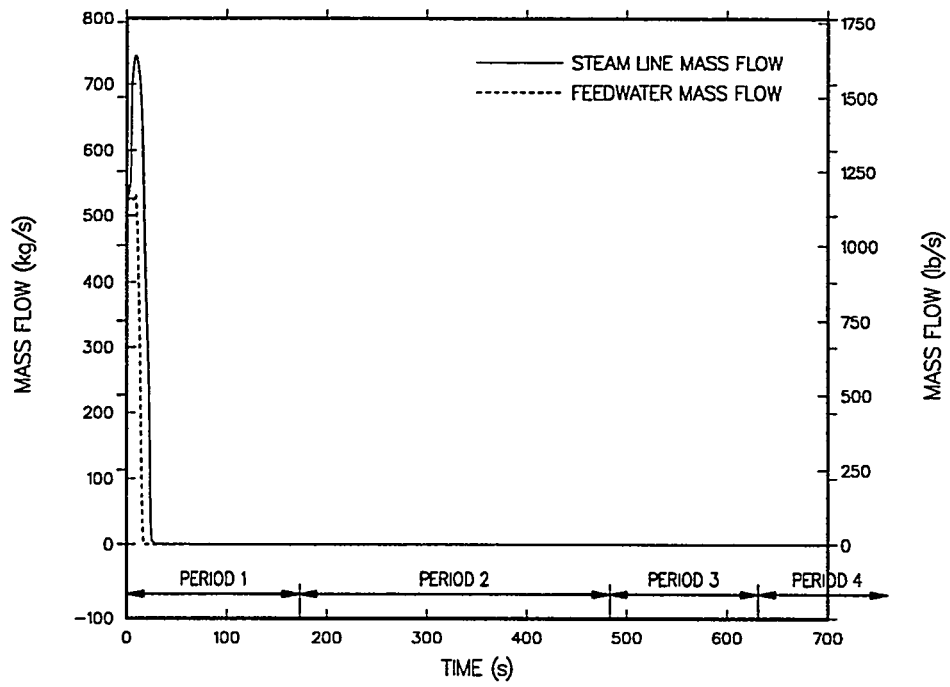

Fig. 35. Loop 1 steam and feedwater flows.

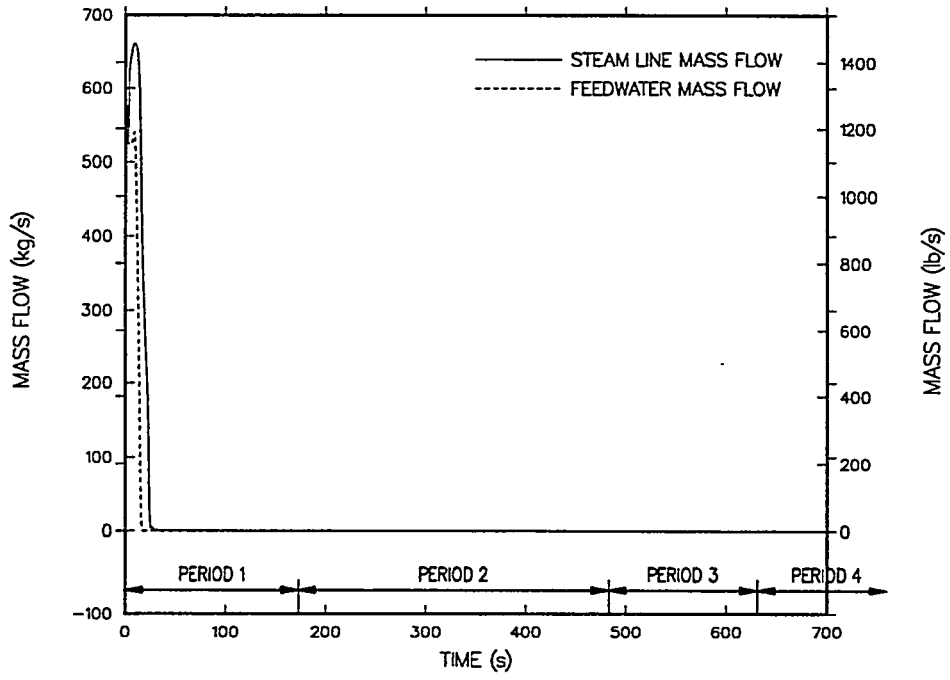

Fig. 36. Loop 2 steam and feedwater flows.

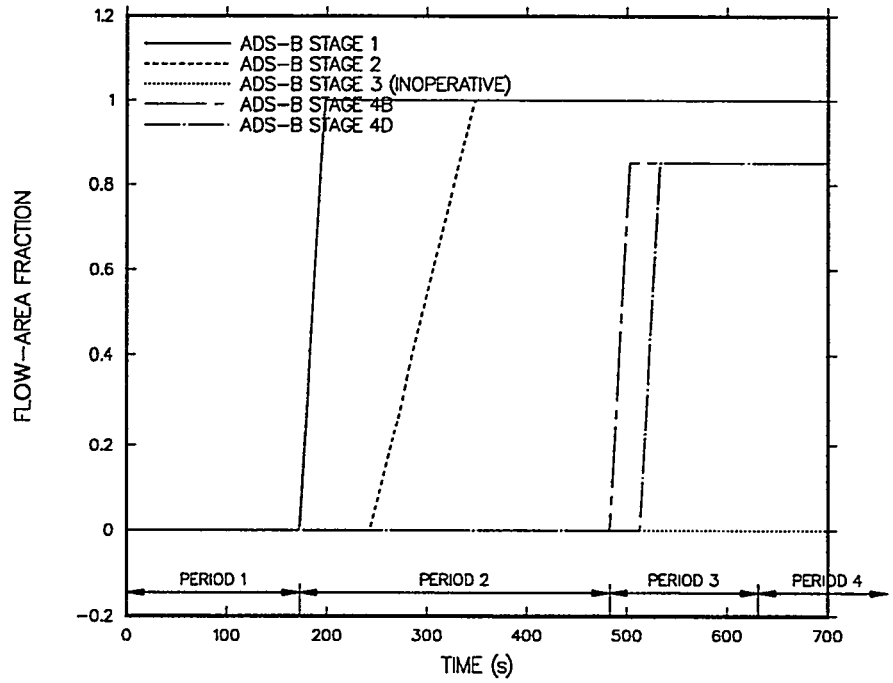

Fig. 37. ADS-B valve area fractions.

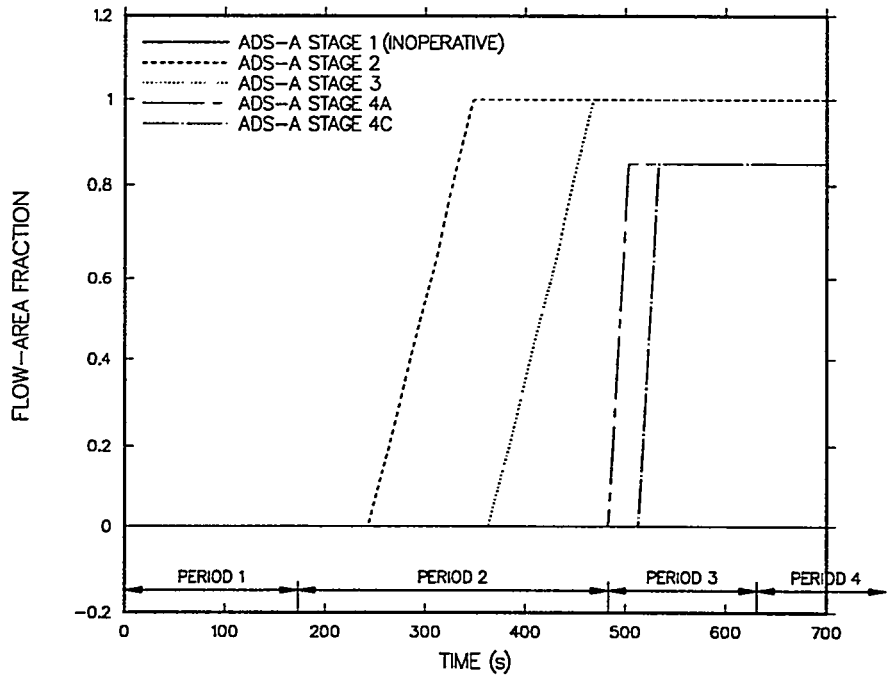

Fig. 38. ADS-A valve area fractions.

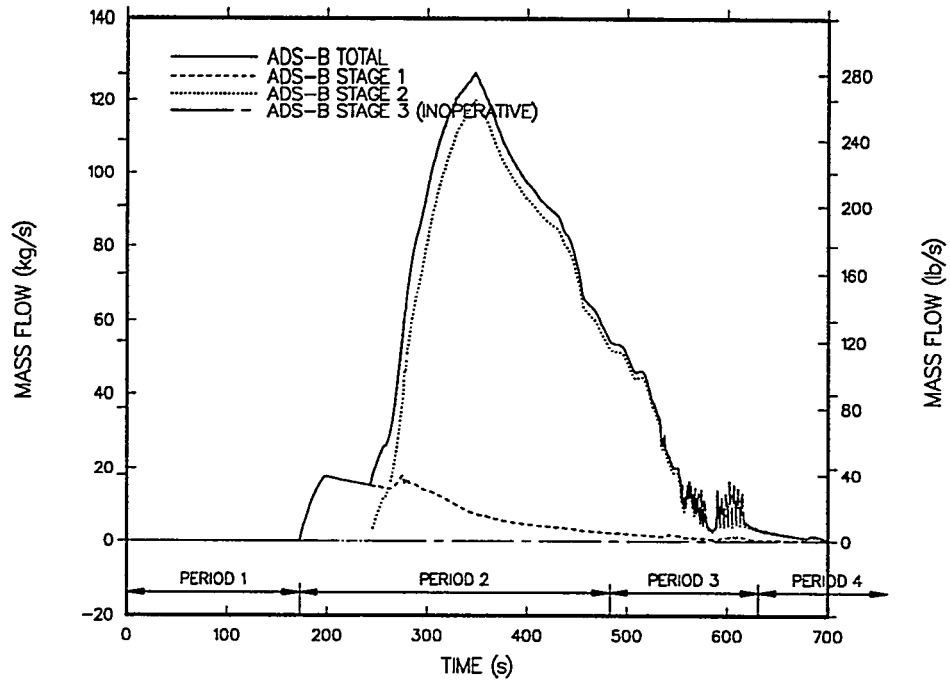

Fig. 39. ADS train B stages 1-3 mass flows.

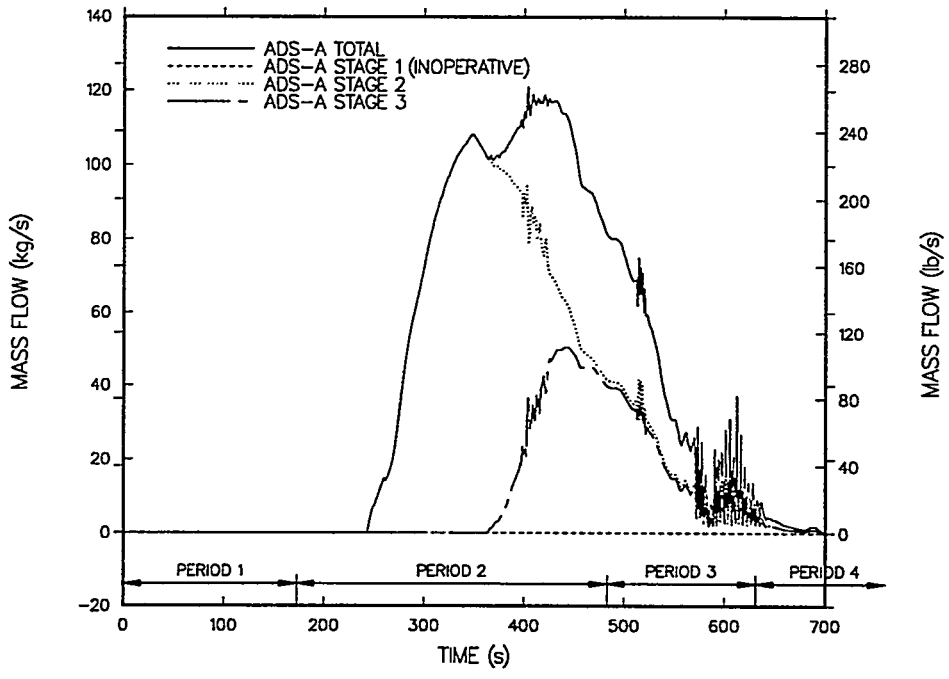

Fig. 40. ADS train A stages 1-3 mass flows.

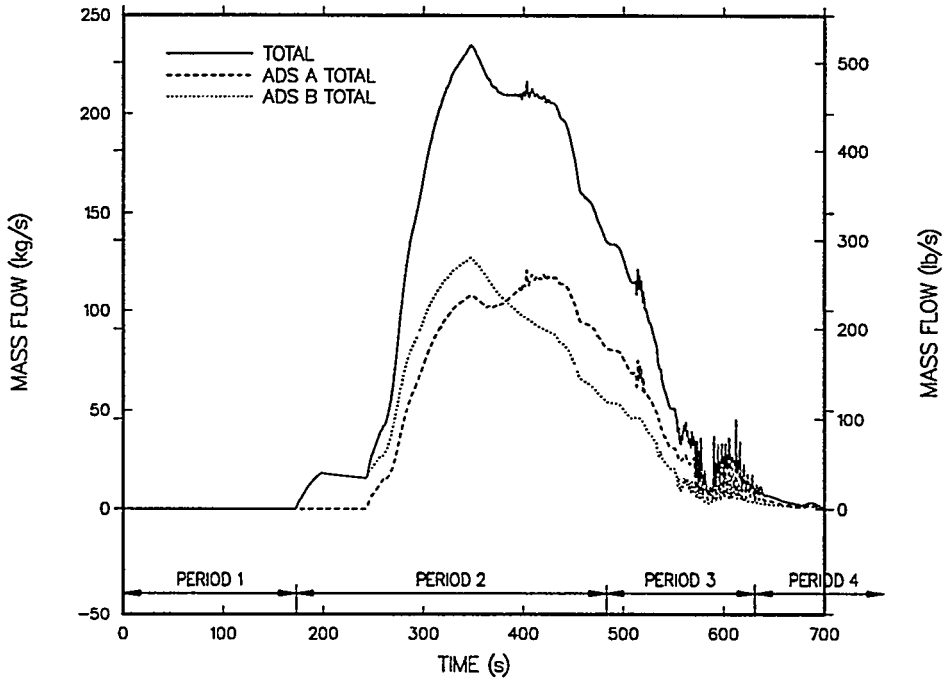

Fig. 41. Total ADS stages 1-3 mass flows.

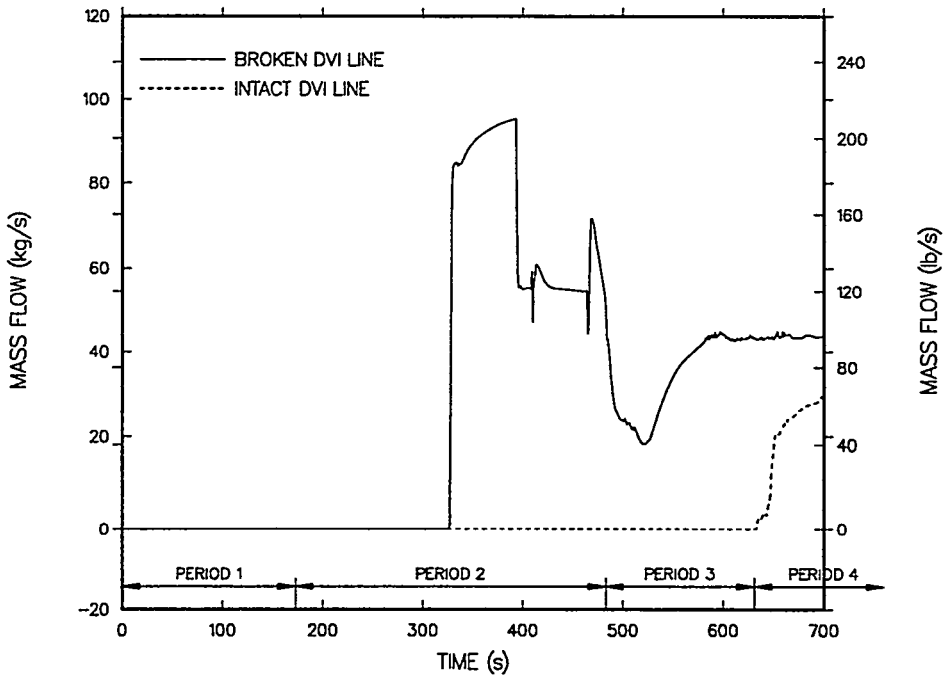

Fig. 42. IRWST drain line mass flow.

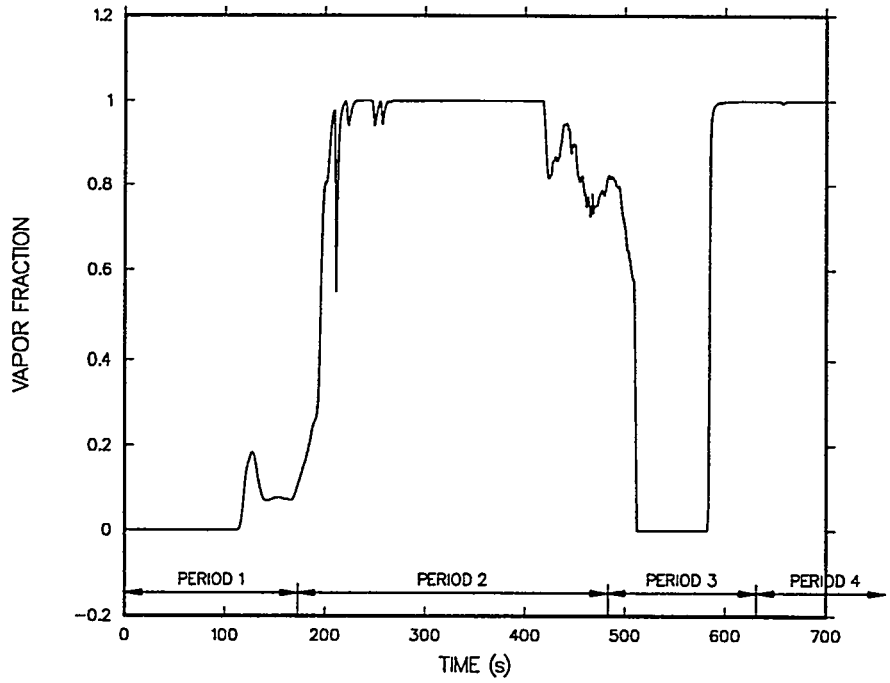

Fig. 43. Cold leg 2B PBL voiding at highest elevation.

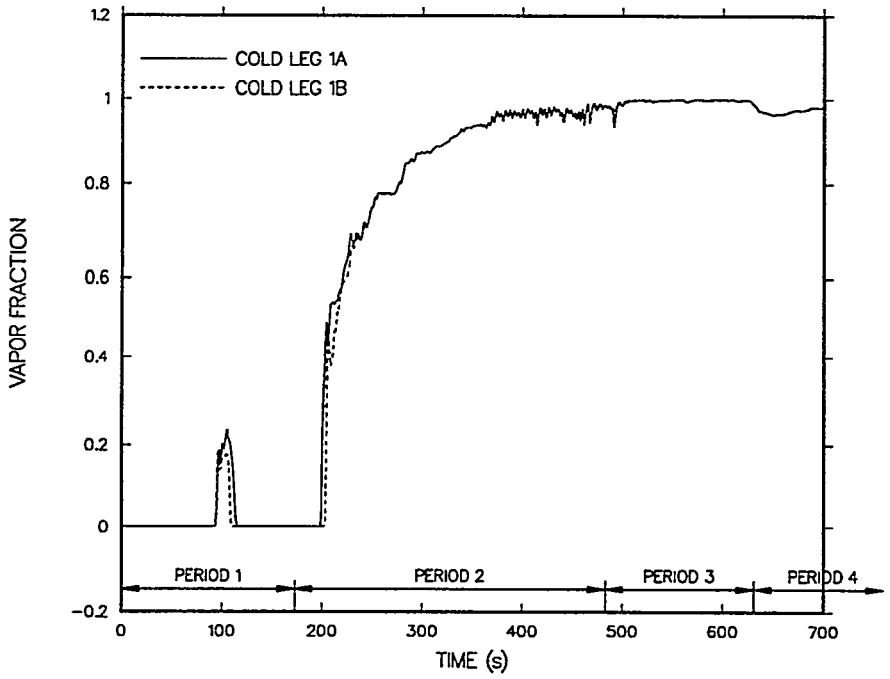

Fig. 44. Cold legs 1A and 1B voiding.

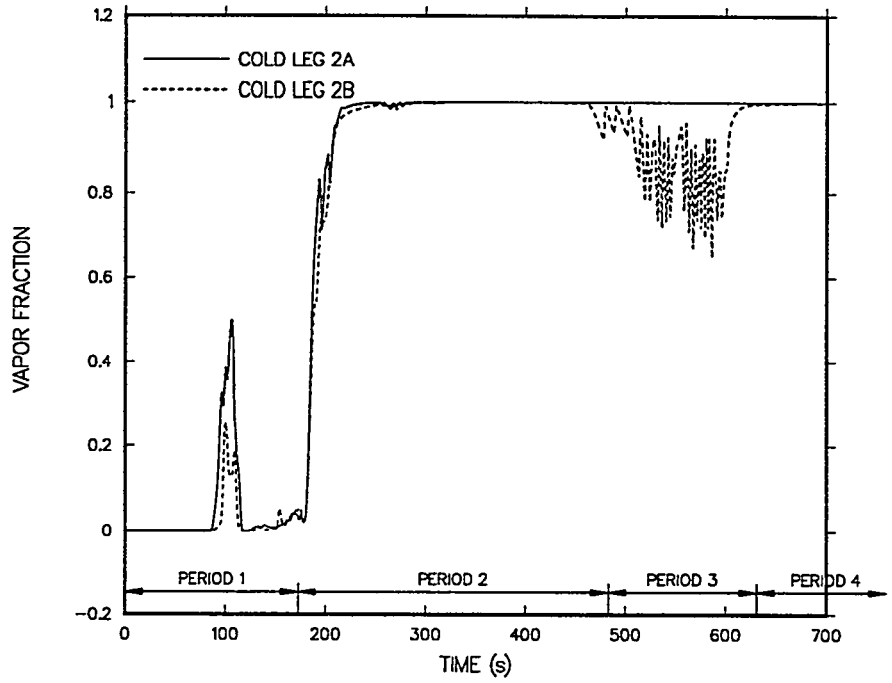

Fig. 45. Cold legs 2A and 2B voiding.

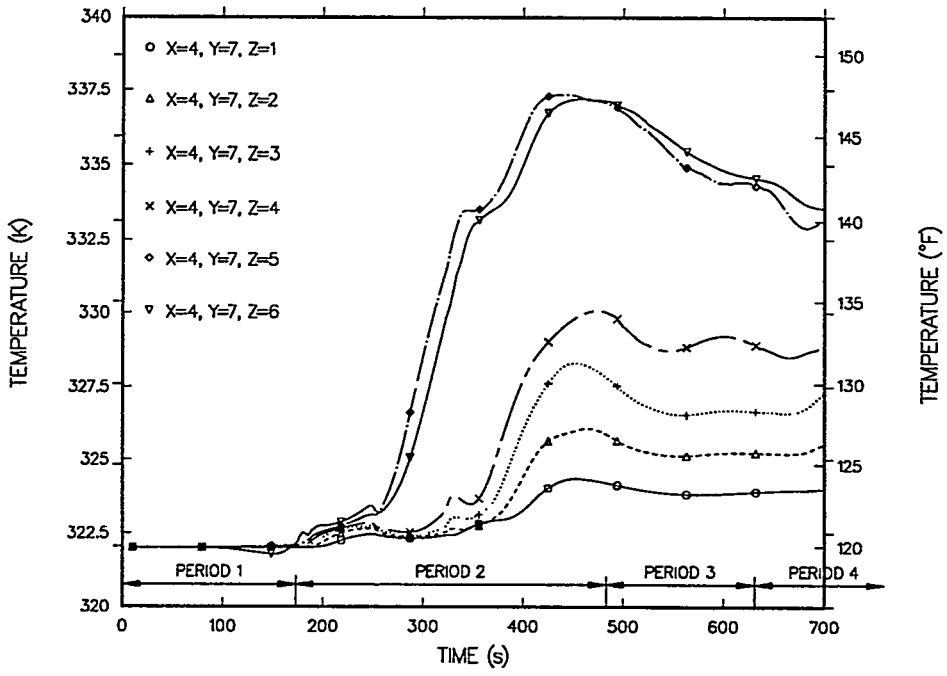

Fig. 46. IRWST liquid temperatures at sparger A.

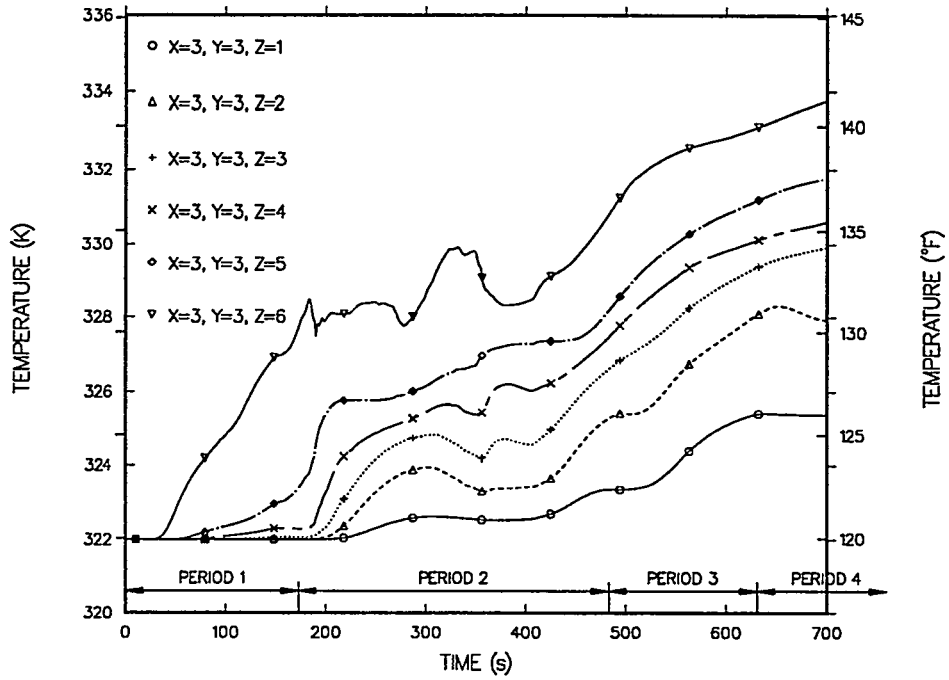

Fig. 47. IRWST liquid temperatures between the PRHRS heat exchangers.

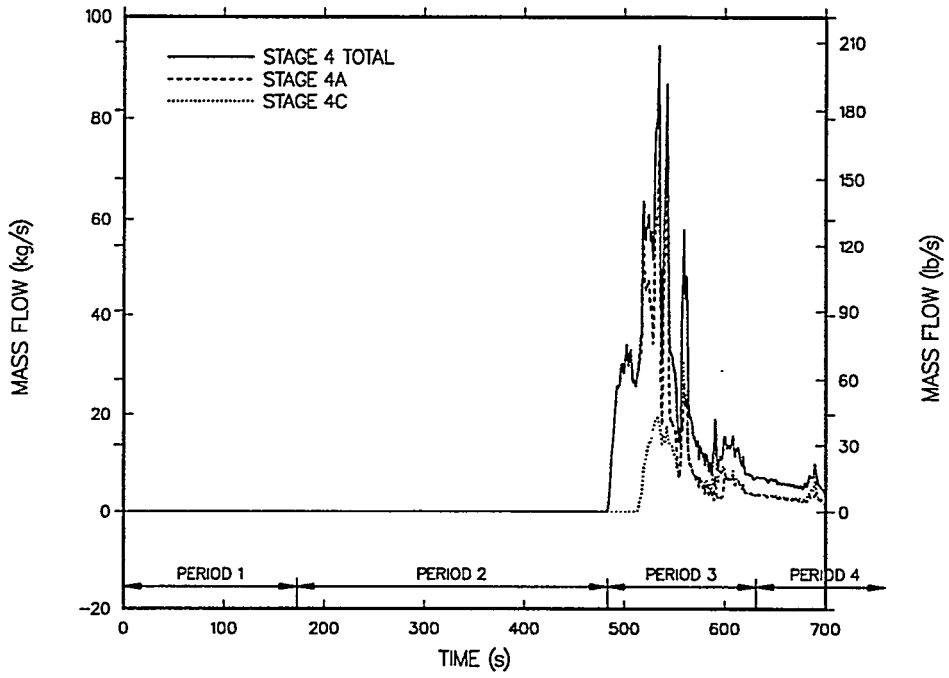

Fig. 48. ADS Stages 4A and 4C mass flows.

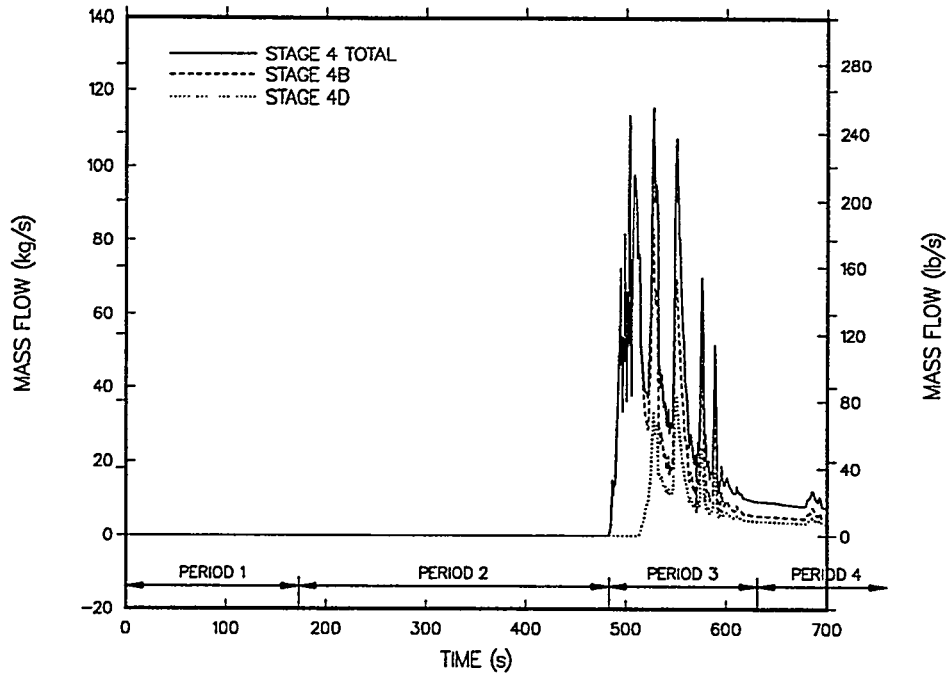

Fig. 49. ADS Stages 4B and 4D mass flows.

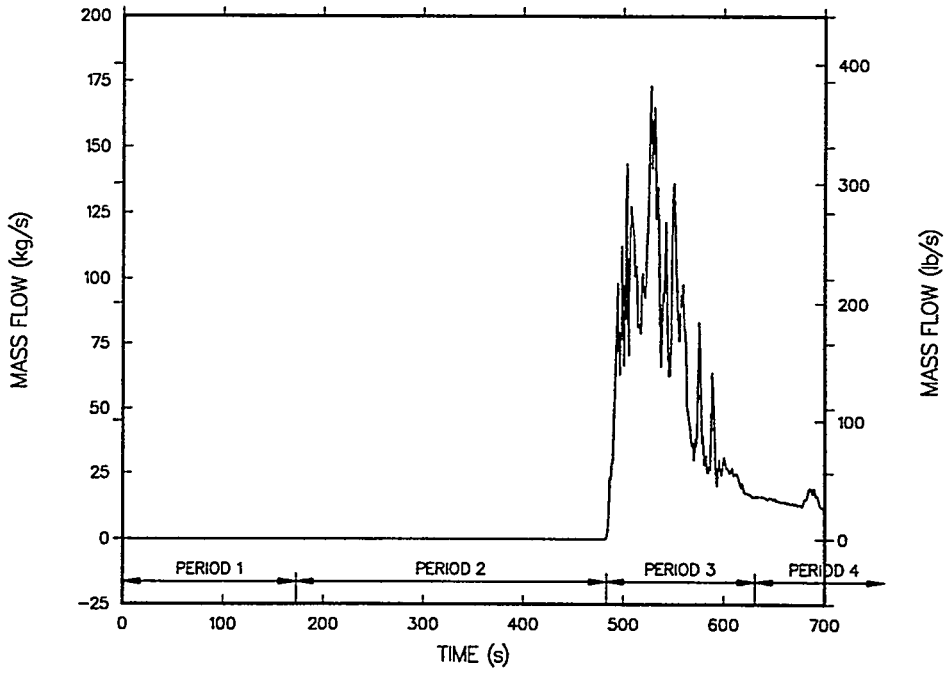

Fig. 50. Total fourth-stage ADS mass flow.